UNIVERSITY OF MANITOBA

REHABILITATION OF CRACKED CONCRETE DAMS

By

Abdulhamid Mohamed Irhouma

A THESIS

Submitted to the Faculty
of Graduate Studies
in partial fulfillment of the requirements for
the degree of

Doctor of Philosophy

Department of Civil and Geological Engineering
The University of Manitoba
Winnipeg, Manitoba, Canada

THE UNIVERSITY OF MANITOBA

FACULTY OF GRADUATE STUDIES

*****

COPYRIGHT PERMISSION PAGE

REHABILITATION OF CRACKED CONCRETE DAMS

BY

ABDULHAMID MOHAMED IRHOUMA

A Thesis/Practicum submitted to the Faculty of Graduate Studies of The University of Manitoba in partial fulfillment of the requirements of the degree of DOCTOR OF PHILOSOPHY

Abstract

This thesis addresses the rehabilitation of cracked construction joints in concrete dams which are located in severe climatic conditions. In order to measure the strength of joints between concrete materials and repaired concrete structures, when subjected to severe thermal conditions, a large scale experimental program has been implemented. This program is intended to evaluate the strength of weak concrete interfaces at different temperatures. Interfaces are weaker than the base material because of the residual strain accumulation usually caused by the differential curing histories of the two adjacent concrete layers. In addition to uniaxial specimens and wedge splitting specimens, wedge specimens cast in two stages were prepared and tested in this research program. After the splitting test, the specimens were repaired and by gluing the two halves together using different repair materials. The set-up used in the experiment includes a cold chamber where the temperature may reach -50 °C. The chamber has circular holes at the top and bottom ends to allow steel extension pipes to transmit the load. The tests are carried under crack opening displacement control at a rate of 0.05 μm/sec. The fracture parameters are extracted for low temperature as well as room temperature. In general, with repair materials under dry conditions and low temperature have a brittle behavior. Also, higher energy release rates are consistently observed at low temperature. Furthermore, specimens are found to be weaker when repaired under wet surface conditions. Finally, the effect of thermal residual stress state in the interfaces between successive lifts of concrete on the fracture parameters is also addressed as part of this research to identify the source of joint weakness.

Based on the experimental test results, recommendations are proposed to fix a dam failure. The dam in question is the Long Spruce Generation Station on the Nelson River in Northern Manitoba.

Contents

List of Figures

List of Tables

Symbols

A_n= Undamaged area of the cross-section

A= Total area of the cross-section

a= Notch depth, Crack length

a_{eff}= Effective crack length

a_{true}= True crack

a_{FPZ}= Length of fracture process zone

B= Width of the beam

C= Compliance

COD= Crack opening displacement

Cn= Normalized compliance

C_{exp}= Experimental compliance

C^{i}_{exp}= Initial experimental compliance

C^{i}_{nu}= Initial normalized numerical compliance

$CTOD$= Crack tip opening displacement

$CTODc$= Critical crack tip opening displacement

$CMOD$= Crack mouth opening displacement

C= Specific heat in J/(kg °K)

$[C]$= Specific heat matrix

c= Crack-guiding groove

d = pecimen size

d_a= Maximum size aggregate in the concrete

D= Damage parameter

E_{eff}= Effective elastic modulus

E= Young's modulus

E_c= Concrete Young's modulus

$\hat{E}$= $E_i/(1-\nu_i^2)$ =Plane strain tensile modulus of material i

F_{sp}= Splitting force

F_v= Vertical component applied load

f_t'= Direct tensile strength of concrete

FCM= Fictitious crack model

G_F= Fracture energy

G= Energy release

G_{Ic}= Mode I critical Energy release rate

h= Ligament length

K= Stress intensity factor

K_I= Model I stress intensity factor

K_{II} = Model II stress intensity factor

K_{III}= Model III stress intensity factor

K_C= Fracture toughness

k= Thermal conductivity tensor

$[K]$= Effective conductivity matrix

kt= Maximum temperature of concrete under adiabatic condition

K_e= Finite element stiffness matrix

k= Structural stiffness corditioning number

k_o= Initial Structural stiffness corditioning number

LEFM= Linear elastic fracture mechanics

M_c= Critical bending moment

M_1= Bending moment due to the maximum applied load

M_2 = Bending moment due to self weight of the beam

NLFM= Non-Linear fracture mechanics

P = Load

P_{cr}= Maximum load

q= Rate of heat generation within the control volume in W/m^3

$\{Q\}$= Effective heat flux

$\{Qe\}$= Applied heat flux

$\{Qc\}$= Convective heat transfer vector

$\{Qr\}$= Radiation vector

$\{Qi\}$= Vector of internal heat generation rates

r= Radial distance

$R(t)$= Rate of heat generation

S= Brittleness number

SIF= Stress intensity factor

t = Specimen thickness

t_n= Thickness of notched web

T= Temperature in °K, a function of the point coordinates x, y, z and the time t

T_o= Initial temperature

$\{T\}$= Matrix of nodal temperature values

$\{\dot{T}\}$= Time derivative of $\{T\}$

T= Temperature of the concrete under adiabatic condition

t= Time (hr)

v= Actuator displacement

w= Fictitious crack

w_c= Critical fictitious crack

σ_{xx}= Normal Stress component in cartesian coordinates

σ_{yy}= Normal Stress component in cartesian coordinates

σ_{zz}= Normal Stress component in cartesian coordinates

τ_{xy}= Shear Stress component in cartesian coordinates

τ_{yz}= Shear Stress component in cartesian coordinates

τ_{xz}= Shear Stress component in cartesian coordinates

θ= Angular coordinate in polar coordinate system

θ_c= Angle of crack propagation

Ω= Domain in 2D or 3D space

Γ= Surfaces on the domain Ω

u= Displacement field near the crack tip

v= Displacement field near the crack tip

w= Displacement field near the crack tip

σ_{22}= Near-tip stresses

σ_{12}= Near-tip stresses

σ_{23}= Near-tip stresses

σ_{nc}= Critical nominal stress at the crack tip

ν = Poisson's ratio

σ_N= Nominal stress at failure

λ_o= Disimilaraty constant

ε= Dtrain tensor

ε_c= Strain at maximum nominal stress

ρ= Mass density

α= Heat generation rate parameter

λ= Eigenvalue

μ_1= Shear modulus

α= Mismatched parameters

β= Mismatched parameters

Ψ= Real phase angle of the complex quantity

$\Phi = \tan^{-1}(K_{II} / K_I)$

α= Wedge angle

μ= Coefficient of friction

λ= Relative structure size$(\frac{d}{d_a})$

ACKNOWLEDGMENTS

First of all, All thanks goes to Allah almighty for the blessings and gaudiness that I receive during the easy and difficult moments of my work.

I would like to express my sincere appreciation and thanks to Professor Mohamed Laoucet Ayari for giving me the opportunity to participate in his research program, and for his guidance, encouragement, patience and enthusiastic support throughout the course of this work. My thanks go to Professor John Glanville for his continual encouragement and invaluable advices during the progress of this research program.

Thanks are extended to Professor Khaled Soudki from the University of Waterloo for reviewing the thesis as the external examiner. Also I would like to thank Manitoba Hydro for providing the financial support for this research, in particular Mr. Lorne Robinson and Mr. Terry Armstrong for their contribution to this work.

Thanks are extended to Dr. Amr Abdelrahman for his assistance during the experimental phase of this Study.

Finally, I would like to thank my parents for their love, patience and support during these years; also, the patience, love and support of my wife and my children cannot be praised enough. To them this thesis is dedicated.

Chapter 1

INTRODUCTION

1.1 Background

It is well established that many operating concrete dams present zones of extensive cracking. Such situations are unusual for reinforced and pre-stressed concrete structures, where cracking is restricted at the design level. The appearance of detectable cracks in such structures is interpreted as a structural failure, and usually as a consequence, repair measures are immediately undertaken. In the case of large structures, such as dams, a certain amount of cracking is unavoidable, and the structural analyst should guarantee the global stability of the construction even when long cracks exist. Among the primary reasons behind cracking is the seasonal thermal variation and excessive heat generation. In the northern region of Canada, structures might be subjected to seasonal surface temperature variations of more than 70°C with minimum temperature reaching - 40°C. Cracks usually occur due to the poor preparation of the horizontal interface between successive lifts of concrete, or when the time interval

between pouring lifts is longer than necessary. This results in degradation of strength and stiffness properties of the structure. Another serious problem related to cracking in dams is the combined effect of cracking and water intrusion on the mechanical behavior of concrete. The research on the mechanism of structural degradation and cracking of concrete is key for rehabilitation studies.

Successful rehabilitation of cracked concrete dams is a pressing issue which has recently captured the attention of the engineering community. Because of uncertainties related to in-situ material behavior, lack of reliable procedures used in injecting repair materials, and the unknown long term response of the concrete/repair material, proven standards for dam rehabilitation have yet to emerge.

1.2 Objectives

The main objectives of this thesis are to:

1. Identify and characterize cracking in concrete dams, when subjected to severe thermal conditions.

2. examine and obtain more information on the behavior of cracked horizontal interfaces between adjacent lifts of concrete.

3. characterize joints when rehabilitated with different types of repair materials, particularly special attention is given to the influence of low temperature and moisture condition of the concrete. Such information is important especially for repairs in cold climate areas.

4. Study the effectiveness of repair materials commonly used to seal and prevent leakage from joints.

5. Study the overall failure mechanism of concrete joints in dams operating in cold regions and the proper repair strategies based on a specific case study of joint failure.

1.3 Scope of Thesis

This research has three major components. It comprises;

1. An experimental test program is to identify the fracture characteristics of plain concrete, concrete joint in interfaces and repaired joints under room and low temperature;

2. An analytical investigations to reproduce the observed test findings using fracture mechanics concepts; and

3. An actual case study of cracked dam operating in the north region of Canada, including design of repair strategies.

1.3.1 Experimental test program

Organic materials such as epoxies and inorganic materials such as cementitious grouts, have been developed, to be injected into cracks, with different degrees of success. Cementitious materials seem to create great controversy among engineers, especially with regard to the acceptance levels of the consistency of water/cement ratio to

be used for injection. As structural and repair material, the polymers and their composites must be able to withstand high stresses under extreme service conditions. Thus a knowledge of their fracture properties, under various temperature conditions is vitally important in aiding their efficient utilization. The testing program has three consequential phases:

1.3.1.1 Phase I:

A set of sixty specimens with initial notches are tested, some of which are cast in one stage and the others are cast in two stages with 24 hours lag period between the two pours to duplicate the condition of the lifts in concrete dams. Both sets are tested at temperatures varying between 20°C and -50°C.

1.3.1.2 Phase II :

The specimens tested in Phase I, were repaired using different types of commercially available repair materials then tested at temperatures varying between 20°C and -50°C.

1.3.1.3 Phase III :

In documented cases of dam rehabilitation, the repair material fails to keep the two faces of a bonded crack together and the crack needs to be repaired again. In this phase of the experimental program, a set of twelve specimens were repaired for a second time, to study the change in the strength of the bond between the repair materials and the "re-repaired" crack surface.

1.3.2 Analytical investigation

The experimental results are numerically reproduced, the compliance method and finite element calibration analysis with the finite element program SIMEX are used in the investigation. The fracture tests were simulated numerically and, then, the calculated load (F_{sp}) versus crack opening displacement (COD) curve were compared to the experimental curve. The analysis is repeated until good agreement between calculated and experimental curve is obtained. The softening post-peak regime of the (F_{sp} *vs* COD) diagram leading to this agreement is considered to be the tensile softening response of the tested concrete.

1.3.3 Repair of cracked concrete dams

The " Long Spruce Generations Station " in the northern region of Manitoba, Canada is used as case study to propose a repair strategy. This choice is made on the light of the extension instrumentation put in place by Manitoba Hydro and the well documented failure history of its transition structure at the joints interface. A selection of grouting material is recommended to be injected with a simultaneous pre-tension anchorages at the upper part of the dam.

1.4 Thesis Organization

This research involves numerous topics which are required to be addressed to tackle the ultimate goal of concrete dam rehabilitation, such as fracture of concrete, joint behavior, concrete behavior under low temperature, etc. The body of the relevant

literature is in consequence very extensive. Hence, while the main body of the literature can be found in chapter two, specific relevant work to each key subject is referred to through out the thesis in the other chapters.

The following is a brief description of the contents of each chapter in the thesis:

Chapter 1 provides an overview of the problems being investigated, objectives, scope, and contents of the thesis.

In chapter 2, a literature review is presented. The related topics covers a wide range of topics including linear elastic fracture mechanics, non-linear fracture mechanics, damage mechanics and bi-materials interfaces mechanics.

Chapter 3 presents, the experimental program conducted at the University of Manitoba to test a total of hundred and thirty specimens (total of all tests) at different temperatures, Also described are different types of materials used in repairing concrete dams and different grouting procedures.

Chapter 4 covers, the descriptions and the observations of the tests results.

chapter 5 covers, the discussions of results and the behavior of each set of tests.

Chapter 6 presents the finite element program adapted in this thesis and also cover the comparison of numerical and experimental results.

Chapter 7 is an overview of a case study and covers the effect of ambient condition and ice loading.

Finally chapter 8 gives, conclusions and recommendations for future work.

Chapter 2

LITERATURE SURVEY

2.1 Background

Cracking is a key characteristic in the behavior of concrete structures. Even under service load, concrete and other cementitious materials normally contain numerous small cracks. The presence of microcracks and other inherent flaws and voids act as potential sources for crack propagation and fracture under externally applied loading. Hence the effect of cracking should be taken into account in predicting ultimate load capacity as well as service behavior.

In existing design methods, the tensile strength of concrete is mostly neglected. This assumption works well for concrete structures with low stresses. However, for many kinds of failure where the tensile capacity governs, a size- effect has been observed which cannot be explained either by elasticity or ultimate load theory. Such failure types are: (i) structural failure of plain concrete beams such as unreinforced concrete pipes; (ii) shear and bond failure and (iii) cracking in heavy and mass struc-

tures such as dams.

The most general cause of cracking of mass concrete is that it is initiated by restrained volume changes of the concrete. Restraint that produces tensile stresses in concrete is of concern since this may result in cracking. A uniform volume change does not produce cracking if the change is relatively free to take place in all directions. However, this rarely happens for mass concrete structures. The cracking behavior of a dam is influenced by concrete properties such as the modulus of elasticity, Poisson's ratio, tensile strength, strain capacity, creep and volume change tendencies.

In many cases non-structural cracks develop, where the safety of the dam is rarely jeopardized. On the other hand there may be numerous structural causes for cracking, such as:

1. Differential settlement.

2. Uplift water pressure along internal cracks.

3. Release of heat due to hydration process, and resulting internal thermal gradient.

4. Upstream water pressure.

The extreme situation is that cracking may cause a different behavior from that intended in design and ultimately threaten the integrity and stability of a dam.

Many contributions have been made in the last three decades to apply fracture mechanics concepts to cement, mortar, plain and structural concrete. The early application to concrete was made by Kaplan (1961). Different attempts have been made

to study the temperature effects on fracture parameters of concrete and repairing materials. Bažant *et. al.*(1988), investigated the temperature and humidity effects on fracture energy of concrete using bending specimens and eccentrically loaded compressive specimens at + 20°C to + 200°C in predried and water saturated conditions at various specimen sizes. Elices *et. al.* (1987) evaluated fracture behavior of saturated concrete at temperature ranging from 20°C to -170°C, found that the toughness of concrete increases at low temperature also the fracture energy increase in a ratio of 3 to 1. Ohlsson (1990), performed three points beam tests, with different compressive strengths at low temperature, showed an increase in fracture energy of 100-200% comparing to room temperature. An excellent collection of bibliography on this subject has been compiled by Mindess(1983), and recently a large number of research works were listed by Leger and Tinawi (1994).

2.2 Fracture of Cementitious Materials

Through various tests, and close observations, it is by now universally accepted that softening is directly tied to the ability of concrete to transmit stresses through a crack.

To examine the localized and global response of a concrete specimen subjected to a uniaxial tension imposed deformation. The concrete would at first behave elastically up to about 50 to 60% of its tensile strength, then some non-linearity appears. This non-linearity is attributed to the formation and coalescence of micro-cracks. It is assumed that those micro-cracks are uniformly distributed within the specimen. Around the peak load many of those microcracks will coalesce into a localized zone

of failure. At this point if the test was run under load control, a sudden and abrupt failure which would be typical of brittle failures. If on the other hand the test is run under displacement control, a gentle release of stresses would occur. The part away from the localized failure will unload elastically, and at the localized failure we would have a gentle decrease the tensile carrying capacity from a peak of f_t' to zero stress. It is with the localization of the deformation that strain softening is associated. While softening occurred in an uncracked concrete specimen, a crack would act as a "catalyst" for its formation due to the high stress at its tip induced by the theoretical singularity. Thus a true crack will be preceded by a "fictitious crack" or process zone which can transmit stresses across the fictitious crack, Shah (1988).

2.2.1 Concrete strain softening

Concrete softening is characterized by a stress crack opening displacement curve (and not stress-strain).

The exact characterization of the softening response should ideally be obtained from a uniaxial test of an uncracked specimen. However, it has been reported that not only are those tests extremely sensitive, but different values can be obtained from different geometries, sizes and testing machines.

Despite the lack of a widely accepted model, there appears to be wide consensus over the following characteristics:

1. A peak value equal to the tensile strength.

2. A very small residual stress at relatively large crack opening displacement.

3. There is a sharp discontinuity in the descending branch. The first part of it has been associated with (unconnected) microcracking ahead of the stress free crack, and the second part with "bridging" of the crack by aggregates.

4. The area under the curve, termed the fracture energy G_F, is a measure of the energy which needs to be spent to generate a unit surface of crack

5. Pre-peak nonlinearity is often neglected for mathematical convenience and is in practice very small compared to the post-peak inelastic behavior.

6. By analyzing numerous test data, Bažant and Oh (1983) have found that G_F may be predicted (with a coefficient of variation of about 16%) from the following empirical equation:

$$G_F = 0.0214(f_t^{'} + 127)f_t^{'2}\frac{d_a}{E_c} \tag{2.1}$$

where E_c and $f_t^{'}$ are in pounds per square inch, d_a is the aggregate size in inches.

Alternatively the fracture energy G_F can be indirectly determined through "flexural" based tests, while the uniaxial stress-crack opening displacement curve can be indirectly determined through a finite element calibration.

2.2.2 Failure modeling of concrete

Irrespective of the adopted model for cracking in concrete, methods for modeling failure are categorized into:

1. Strength of material approach;

2. Fracture mechanics approach;

3. Damage Mechanics approach.

The strength of material simply evaluates the tensile stresses around the crack tip and compares them with the tensile strength. If the tensile stresses are found to exceed the strength, then the crack is said to propagate. While such an approach has been extensively used for many years, Bažant and Cedolin (1979) were the first to point out the erroneous nature of this model. In fact it is well known that a stress singularity exists at the tip of a crack, Irwin (1957). Thus given a fine enough mesh, even an infinitesimal load would induce crack growth. As such, a fracture mechanics approach should be used. In case of fracture mechanics, two models, originally developed for metallic solids, could be adapted to concrete:

1. Linear elastic fracture model in which the inelastic zone at the crack tip is small compared to crack length. and therefore nonlinearity is not important enough to account for.

2. Nonlinear fracture mechanics in which inelastic zone size is not negligible in comparison with the crack size and other dimensions of the structure.

As such it should come as no surprise that most of the original work on fracture mechanics of concrete focused on LEFM. However it rapidly became evident that experimentally measured fracture toughness values, K_{IC}, were specimen and crack

size dependent. Hence LEFM was discarded and researchers focused on nonlinear fracture models.

In case of damage mechanics, the strength of a loaded structure is determined by the deterioration of the material caused by loading. This deterioration or damage may be described in terms of a continuous defect field.

2.3 Linear Elastic Fracture Mechanics

There are two generally accepted approaches to linear elastic fracture mechanics (LEFM). The first is based on an energy balance, Griffith (1920), whilst the second approach is based on the singular nature of the stress distribution near a crack tip, as first presented by Irwin (1957).

2.3.1 Crack tip stress and displacement

Irwin (1957) noted that in the neighborhood of the sharp crack tip, the stress components $\sigma_{ij}(i,j = x,y)$ are the same regardless of the shape of the elastic body and manner of loading. It is customary to resolve the general stress state into three elementary states which are called modes I, II and III respectively, Figure 2.1. Mode I refers to a planar symmetric state of stress which causes a crack to open, that is, the crack faces are displaced normal to their plane, Figure 2.1a. It is also referred to as the opening mode. Mode II refers to a planer antisymmetric state of stress which causes a relative displacement of the crack faces in their own plane, Figure 2.1b. It is also referred to as the in-plane shear or sliding mode. Finally, Mode III refers to as

a state of stress which causes a relative displacement of the crack faces out of their plane, Figure 2.1c. It is also referred to as the anti-plane shear or the tearing mode. The leading terms of the non-zero component of stresses and displacements field near the crack tip, Figure 2.2, can be expressed as following.

Mode I

$$\sigma_{xx} = \frac{K_I}{(2\pi r)^{1/2}} \cos\frac{\theta}{2}\left(1 - \sin\frac{\theta}{2}\sin\frac{3\theta}{2}\right) \tag{2.2}$$

$$\sigma_{yy} = \frac{K_I}{(2\pi r)^{1/2}} \cos\frac{\theta}{2}\left(1 + \sin\frac{\theta}{2}\sin\frac{3\theta}{2}\right) \tag{2.3}$$

$$\tau_{xy} = \frac{K_I}{(2\pi r)^{1/2}} \sin\frac{\theta}{2}\cos\frac{\theta}{2}\cos\frac{3\theta}{2} \tag{2.4}$$

$$\sigma_{zz} = \nu(\sigma_x + \sigma_y) \qquad \text{for plane strain} \tag{2.5}$$

$$\sigma_{zz} = 0 \qquad \text{for plane stress} \tag{2.6}$$

$$u = \frac{K_I}{8\mu}\left(\frac{2r}{\pi}\right)^{1/2}(2k-1)\cos\frac{\theta}{2} - \cos\frac{3\theta}{2} \tag{2.7}$$

$$v = \frac{K_I}{8\mu}\left(\frac{2r}{\pi}\right)^{1/2}(2k+1)\sin\frac{\theta}{2} - \sin\frac{3\theta}{2} \tag{2.8}$$

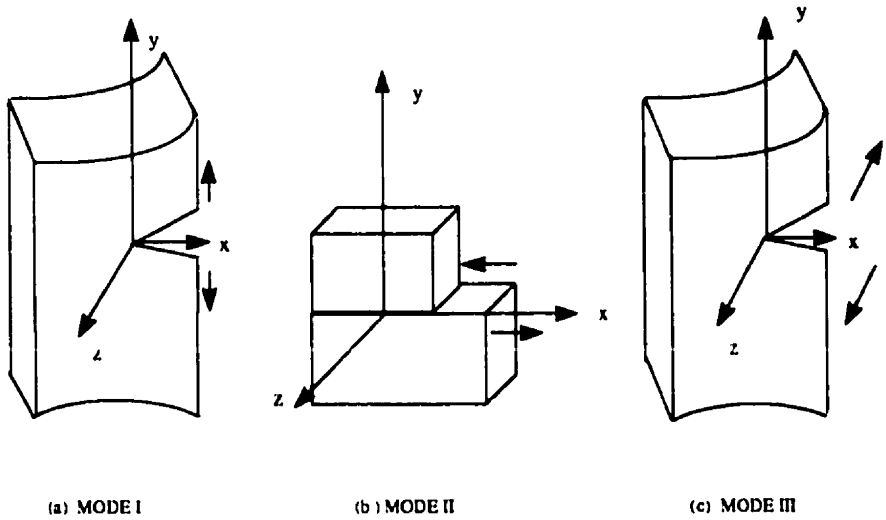

Figure 2.1: Three possible modes of deformation at a crack tip

$$w = 0 \qquad \text{for plane strain} \qquad (2.9)$$

$$w = -\frac{v}{E}\int(\sigma_{xx}+\sigma_{yy})dz \qquad \text{for plane stress} \qquad (2.10)$$

Mode II

$$\sigma_{xx} = -\frac{K_{II}}{(2\pi r)^{1/2}}\sin\frac{\theta}{2}\left(2+\cos\frac{\theta}{2}\cos\frac{3\theta}{2}\right) \qquad (2.11)$$

$$\sigma_{xy} = \frac{K_{II}}{(2\pi r)^{1/2}}\sin\frac{\theta}{2}\cos\frac{\theta}{2}\cos\frac{3\theta}{2} \qquad (2.12)$$

$$\tau_{xy} = \frac{K_{II}}{(2\pi r)^{1/2}}\cos\frac{\theta}{2}\left(1-\sin\frac{\theta}{2}\sin\frac{3\theta}{2}\right) \qquad (2.13)$$

$$\sigma_{zz} = \nu(\sigma_{xx} + \sigma_{yy}) \qquad \text{for plane strain} \qquad (2.14)$$

$$\sigma_{zz} = 0 \qquad \text{for plane stress} \qquad (2.15)$$

$$u = \frac{K_{II}}{8\mu}\left(\frac{2r}{\pi}\right)^{1/2}\left((2k+3)\sin\frac{\theta}{2} + \sin\frac{3\theta}{2}\right) \qquad (2.16)$$

$$v = \frac{K_I}{8\mu}\left(\frac{2r}{\pi}\right)^{1/2}\left(-(2k-3)\cos\frac{\theta}{2} - \cos\frac{3\theta}{2}\right) \qquad (2.17)$$

$$w = 0 \qquad \text{for plane strain}$$

$$w = -\frac{v}{E}\int(\sigma_{xx} + \sigma_{yy})dz \qquad \text{for plane stress} \qquad (2.18)$$

Mode III

$$\tau_{xz} = -\frac{K_{III}}{(2\pi r)^{1/2}}\sin\frac{\theta}{2} \qquad (2.19)$$

$$\tau_{xy} = \frac{K_{III}}{(2\pi r)^{1/2}}\cos\frac{\theta}{2} \qquad (2.20)$$

$$\sigma_{xx} = \sigma_y = \sigma_{zz} = \tau_{xy} = 0 \qquad (2.21)$$

$$w = \frac{K_{III}}{\mu}\left(\frac{2r}{\pi}\right)^{1/2}\sin\frac{\theta}{2} \qquad (2.22)$$

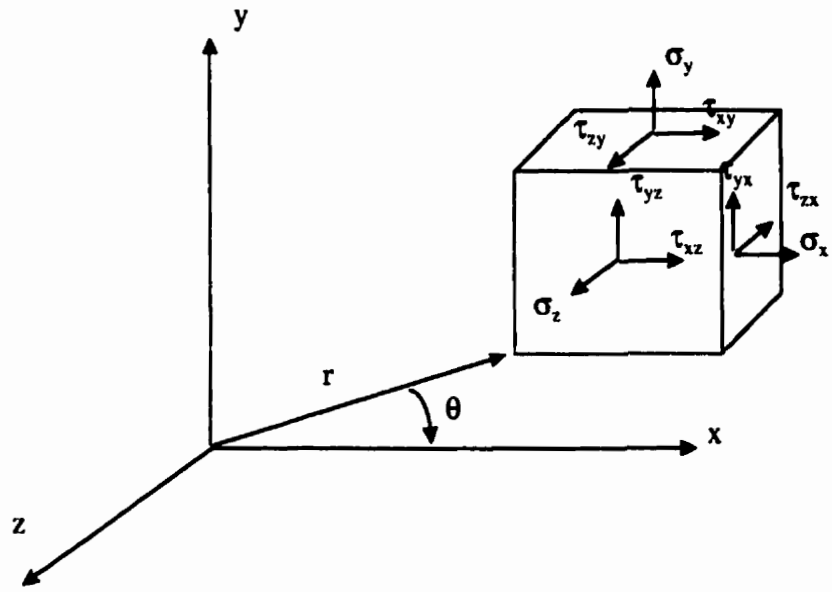

Figure 2.2: Coordinate system and stress components ahead of a crack tip

$$u = v = 0 \tag{2.23}$$

where u, v and w are the displacement components in x, y, z directions, ν is Possion's ratio, θ is the angle with respect to the horizontal crack plane, μ is the shear modulus, $k = 4 - 4\nu$ for plane strain, $k = (3 - \nu)(1 - \nu)^{-1}$ for plane stress and K is known as the stress intensity factor.

2.3.2 Stress intensity factor(SIF)

As mentioned above, the concept of stress intensity factor was introduced by Irwin (1957), and can be defined as a scaling factor, denoted by the symbol K, used in linear-elastic fracture mechanics to describe the strength of the singular field at the

tip of a crack of known size and shape. The stress intensity factor can be represented numerically as,

$$\begin{bmatrix} K_I \\ K_{II} \\ K_{III} \end{bmatrix} = \lim_{r \to 0, \theta \to 0} \sqrt{2\pi r} \begin{bmatrix} \sigma_{22} \\ \sigma_{12} \\ \sigma_{23} \end{bmatrix} \tag{2.24}$$

where $\sigma_{22}, \sigma_{12}, \sigma_{23}$ are the near-tip stresses;

K_I, K_{II}, K_{III} are the stress intensity factors representing

2.3.3 Fracture toughness

One of the underlying principles of fracture mechanics is that unstable fracture occurs when the stress intensity factor at the crack tip, K, reaches a critical value, K_C. For Mode I deformation, the critical stress intensity factor for fracture instability is designated by K_{IC}. K_{IC} represents the inherent ability of a material to withstand a given stress field intensity at the tip of a crack and to resist progressive tensile crack extension. Thus, K_{IC} represents the fracture toughness of a particular material, whereas K_I represents the stress intensity ahead of a sharp crack in any materials. Some of the methods used to evaluating K_{IC} are presented in the following section.

2.3.4 Test methods

Different types of specimen have been used for the evaluation of the fracture toughness, K_{IC}, and the critical strain energy release rate for mode I, G_{IC}, for concrete

and cement materials. The wide variety of specimen forms is partly due to the fact that unlike metallic materials, no standard specimens are recommended for the determination of fracture mechanics parameters of cementitious materials. The same holds true for the experimental procedure in such a test. It is noteworthy that a wide discrepancy of results is observed in experiments on hardened cement paste in which different experimental techniques were used. Thus, generally, caution is recommended when comparing fracture mechanics parameters obtained by using different specimen forms. It has till now not been checked how various non-elastic effects influence the results of particular tests. For example the effect of creep of cement paste at the crack tip may be different in tests with different specimen forms. It has to be accepted further that the microcrack formation ahead of the crack tip is strongly influenced by experimental conditions. The most important specimen geometries and the relevant methods of evaluation are described, below.

1- Notched beam specimen

One of the most commonly used specimen types for K_{IC} or G_{IC} evaluation is the notched beam loaded in three point or four point bending, Figure 2.3. The advantages of the notched beam are its economic fabrication and its relatively simple testing procedure. The notches are fabricated by inserting thin foils into the specimen mould or by saw cutting into a hardened specimen. When performing a test, a gradually increased load is applied to the notched beam until a stress level is reached which results in crack propagation. Dependent on the notch depth and the stiffness of the material and of the loading frame, the resultant load-displacement diagrams exhibit

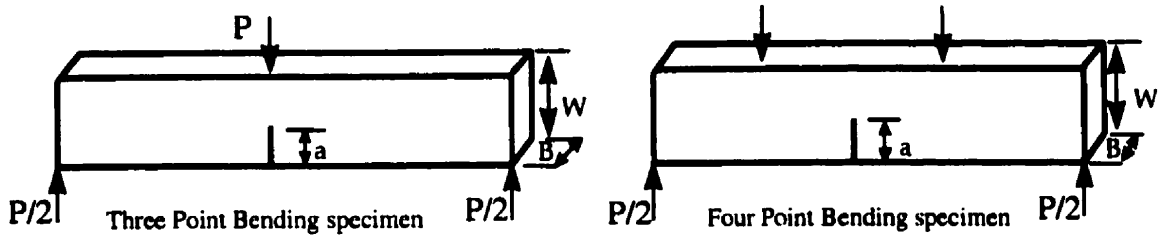

Figure 2.3: Notched beam loaded in 3 and 4 point bending

catastrophic, semi-stable or stable fracture.

Assuming a beam of cross-section b×w and of crack length a and denoting the critical nominal stress at the crack tip by σ_{nc}, the fracture toughness can be given by:

$$K_{IC} = \sigma_{nc}\sqrt{\pi.a}f(a/w) \tag{2.25}$$

$$\sigma_{nc} = \frac{6M_c}{B(w-a)^2} \tag{2.26}$$

where M_c is the critical bending moment = $M_1 + M_2$;

M_1 is the bending moment due to the maximum applied load;

M_2 is the bending moment due to self weight of the beam;

a is the notch depth;

w is the depth of the beam; and

B is the width of the beam.

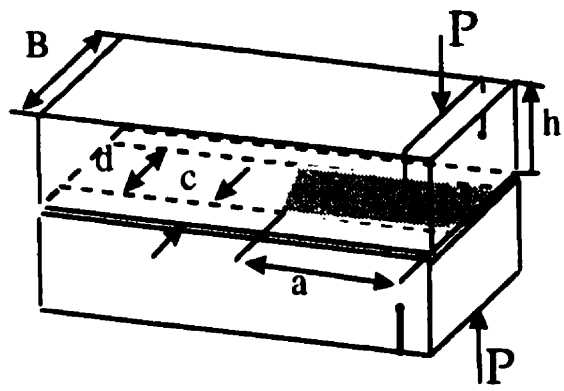

Figure 2.4: Double cantilever beam specimen

2- Double cantilever beam specimen

The double cantilever beam method has been used by several investigators because it has the advantage that crack growth can be analyzed over a range of crack lengths, Figure 2.4. The specimen has the form of a long prism with two crack guiding grooves cut symmetrically along its length. At one end there is a notch acting as a crack starter joining the grooves at one end. The crack is propagated by mechanically separating the ends of the two cantilevers. As for any other method, there are several equivalent expressions for the critical stress intensity factor, K_{IC}. The most commonly used the expression proposed by Mai (1979).

$$K_{IC} = \frac{2\sqrt{3}P_{\max}a}{(Bd)^{1/2}h^{3/2}}\left(1 + 0.7(h/a)\right) \tag{2.27}$$

where h is the beam height, d is the web width, c is the crack-guiding groove, B is the beam width and a is the notch length.

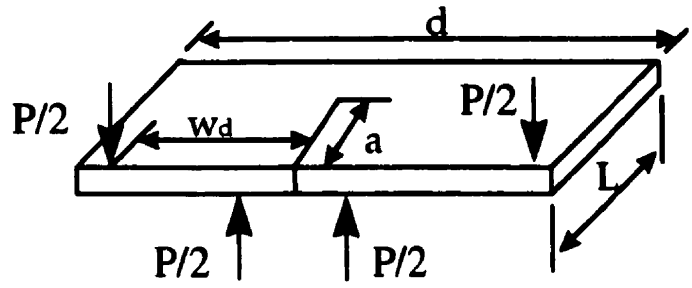

Figure 2.5: Double torsion beam specimen

3- Double torsion beam specimen

In the double torsion beam, the stress intensity factor at the notch depends only on the load and on the specimen dimensions and not on the crack length. In the experiment the test specimen is loaded by torsional forces, Figure 2.5, and the stress intensity factor is given by the following formula, Ziegeldorf (1983):

$$K_I = P_{\max} . \mathrm{w}_d . \sqrt{\frac{3(1+\nu)}{\mathrm{w} t^3 t_n}} \tag{2.28}$$

where w_d is the loading width, ν is Poisson's ratio, t is the thickness, w is the width and t_n is the thickness of notched web.

4- Compact tension specimen

It is one of the most widely used methods in fracture toughness testing of metallic materials, see Figure 2.6. The compact tension test specimen is subjected to a critical stress intensity factor calculated using the formula

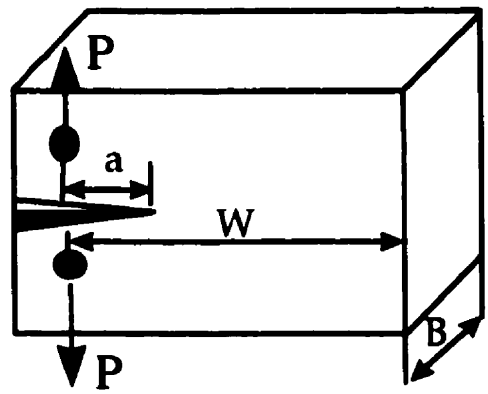

Figure 2.6: Compact tension specimens

$$K_{IC} = \frac{P_{\max}\sqrt{a}}{wB}.F(a/w) \tag{2.29}$$

where $F(a/w)$ is a function of geometry.

Based on the compact tension test, the splitting wedge test was proposed by Linsbauer (1985). Brühwiler and Wittmann (1990) recommended a test procedure, which is discussed in Chapter IV. Rossi *et. al.* (1991) used the wedge splitting test on three structural concretes with different size of aggregate for both cylindrical and cubical specimens. Saouma *et. al.* (1991) used wedge splitting specimens to evaluate fracture properties of concrete with different sizes and shapes of aggregates. They reported that values of fracture toughness are independent of aggregate sizes and specimen size if certain minimum dimensions are exceeded but depend on the type of aggregate. Bažant *et. al.* (1990) tested a series of geometrically similar wedge splitting specimens of maximum cross-sectional dimension of 6 ft and applied the size effect law to obtain the fracture toughness corresponding to extrapolation to still much longer sizes.

2.3.5 Damage and crack assessment

Fracture mechanics is based on the realistic assumption that the materials contain defects which constitute the nuclei of fracture initiation. Designing a structure free of crack initiation is physically unrealistic since the initial cracks can develop during casting or service life. There are several types of non-destructive tests (NDT) used to detect the cracks in concrete structures. Four of these tests that are widely used are briefly discussed below.

2.3.5.1 Acoustic emissions monitoring

Acoustic emissions is one of the most promising methods of fracture process zone detection. This method is based on using the transient elastic waves which are generated by the rapid energy release from localized sources in the concrete due to cracking processes. Ultrasonic pulses are used to detect these waves, the time they travel through the surface of the concrete being detected by piezoelectric transducers. This technique was used by Maje and Shah (1988) to determine the volume orientation and type of microcrack. In term of the fictitious crack model, Izumi *et. al*(1986) approximated the size of the process zone. Saouma (1991a) used the acoustic emissions (AE) techniques as a quantitative aid to his work in splitting wedge tests, and according to his observation, the material response was evaluated as, (1) large AE burst or continuous activity, interpreted as crack extension or aggregate-matrix bond failure, and (2) little or low AE activity, indicating micro-cracking associated with the formation of the process zone.

2.3.5.2 Ultrasonic

This method is based on the transmission of ultrasonic waves through the material by transducers. Metallurgical defects and surface boundaries reflect the incident pulse which is monitored on an oscilloscope. The ultrasonic pulse measurement does not lead to a geometrical description of the damage zone, and there is uncertainty about the results provided by this method, Maje and Shah (1985) .

2.3.5.3 Photoelastic method

Photoelastic techniques were used by different researchers to study crack localization, crack branching and crack opening, but the results from this method were not able to define a fracture process zone, Shah (1985).

2.3.5.4 Scanning electron-microscopy

This method has been used extensively to study microcracking in concrete, the observed results varying from research to another. Diamond and Benture (1985) were among the few researchers who applied the method extensively to study microcracking, and concluded that "While the subdivision and branching seem to occur near the tip zone in the concrete examined, in some respects reminiscent of what is expected in a process zone, there is no physical distinction corresponding to separate lengths of (straight, open crack) behind a crack tip and (process zone micro-cracking) ahead of a crack tip."

2.3.6 Measurement of fracture parameters

In this section, the key parameters that require to be established from test results are addressed. These parameters are, effective Young's modulus, effective crack length and stress intensity factor

2.3.6.1 Load, displacement and strain control tests

Three types of control are usually used to measure material and structural response when a specimen is subjected to uniform tension: tension load, displacement and strain control. In load control, the machine cross head applies increasing load on the specimen by means of a load cell. In this case and when the load increases the tensile strength, a sudden brittle failure occurs, that is, sudden release of energy. In the case of stroke (displacement) control, the machine cross head applies increasing displacement to the specimen instead of increasing load. For concrete (softening) material, there will be a post-peak response with slow decrease in stress, in another words, increase in displacement and decrease in stress, and this leads to the gradual release of strain energy. The last type of control, strain gage or a clip gage, is usually used to provide feedback measurement to the test equipment. In the present work a clip gage located at the mouth of the crack and on the bearing axis provides the specimen response.

2.3.6.2 Effective Young's modulus

The Young's modulus can be determined using the ACI's approximate equation

$E = 57000\sqrt{f_c}$, experimentally through compressive cylinder tests or indirectly

from the specimen compliances, by using the slope of the load - COD curve.

$$E_{eff} = Cn/C_{exp} \tag{2.30}$$

where, E_{eff} is the effective elastic modulus,

Cn is the normalized compliance, and

C_{exp} is the experimental compliance.

2.3.6.3 Effective crack length

As the measurement of the exact crack length cannot be done, an effective crack length a_{eff} is usually used. The effective crack considered should be longer than the true crack and shorter than the true crack plus the fracture process zone.

$$a_{true} \leq a_{eff} \leq a_{true} + a_{FPZ} \tag{2.31}$$

The major drawback of this approach is that it can, at best, provide an estimate for crack length.

2.3.6.4 Stress intensity factor

The SIF can be derived using the compliance. From the compliance method, the energy release to extend a crack by (da) is as follows,

$$G = 1/2Pdu \tag{2.32}$$

$$u = CP \tag{2.33}$$

$$G = (1/2)(P^2/B)(\partial C/\partial a) \tag{2.34}$$

Where G is the energy release, P is the load, C is the compliance, B is the thickness, u is the point load displacement, and a is the crack length. G can be obtained experimentally. Also,

$$G = K_I^2/E' \tag{2.35}$$

where, $E' = E/(1-\mu^2)$ for plain stress, K_I is the stress intensity factor and can be obtained from equations (2.34) and (2.35) as follows:

$$K_I = \left(\frac{E' P^2\, \delta C}{2B\, \partial a}\right)^{1/2} \tag{2.36}$$

2.4 Non-linear Fracture Mechanics

Kaplan (1961) was the first to apply the theory of linear elastic fracture mechanics (LEFM) to concrete. During the last fifteen years some researchers expressed doubts regarding the application of LEFM to normal size structural components, and they tend to favor some form of non-linear fracture mechanics based models.

One of the most important models of nonlinear fracture mechanics and among the most widely used in finite element analysis is the fictitious crack model (section 2.4.2), In this model, a process zone (fictitious crack) is assumed in front of the crack tip, and ahead of the true or physical crack. One of the characteristics of this zone is that the stress decreases from tensile strength of concrete at the tip of the fictitious crack to zero at the tip of the physical crack. Its main disadvantage lies in omitting certain effects, especially during the stage of microcrack development when the crack is not yet localized, but still spread over a certain volume.

2.4.1 Crack models

Fracture toughness of concrete evaluated according to the conventional LEFM principles are found to be size dependent. The observed size effect has been attributed to the formation of a nonlinear fracture process zone around the crack tip. The nonlinear fracture process zone is assumed to consist of innumerable microcracks tending to coalesce into a macrocrack and across which considerable traction still exists owing to the bridging of aggregates as well as roughness and the tortuous pattern of cracking. The stress field ahead of the crack tip, instead of being dependent on the stress intensity factor is found to be dependent on the deformational characteristics of the nonlinear fracture process zone. The size of this zone is found to be considerably large, sometimes of the same magnitude as the size of the specimen itself. Fracture of concrete cannot be adequately described by classical LEFM principles, unless the size of the fracture process zone is so small compared to the structural dimensions that

it can be treated as a point, which is the case in dams. It is becoming increasingly recognized from various recent studies that fracture mechanics principles are applicable to concrete provided a finite nonlinear zone at the fracture front is taken into account. When tested under stroke control the stress-strain diagram of concrete in tension is found to have a descending branch in the post-peak region, from which it follows that the simplest idealization for concrete can be as a bi-linear softening material. Recognizing this behaviour several theoretical investigations have been carried out incorporate nonlinear fracture process zone and the effect of slow crack growth, and their dependence on size. This has led to the development of several analytical models which can be broadly classified as nonlinear models with strain softening and modified LEFM models.

2.4.2 Hillerborg fictitious crack model, (FCM)

Hillerborg (1976) proposed the fictitious crack model for predicting how the fracture zone affects crack propagation and the fracture process for plain concrete and similar materials. The fracture process zone is treated as a fictitious crack with bridging stresses as shown in Figure 2.7 and is characterized by a softening stress displacement relation. The crack is assumed to propagate when the maximum principal stress at the crack tip reaches the limiting tensile strength which then falls to zero at once, but to decrease with increasing width of the fictitious crack w, for that part of the crack, where $w < w_c$ where w_c is the critical width. When $w > w_c$ the fictitious crack gets converted into a real crack. The fictitious crack, in reality, corresponds to

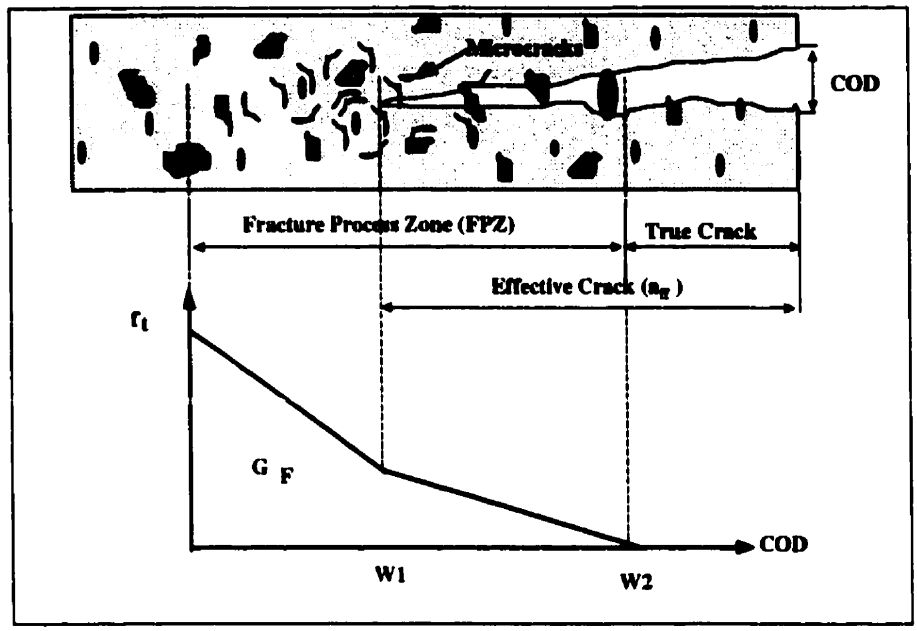

Figure 2.7: Hillerborg's fictitious crack model

a microcracked zone with some remaining ligaments for stress transfer. As this stress transferring crack is not a real one but fictitious, the model is known as the fictitious crack model. As there is a stress to be overcome in opening the crack, energy is absorbed. The amount of energy absorbed per unit crack area in widening the crack from zero to w_c is:

$$G_F = \int_o^{wc} \sigma(w)\, dw \tag{2.37}$$

which is the area under the curve (σ, COD) and is known as fracture energy.

2.4.3 Jenq and Shah's model

Jenq and Shah (1985) proposed a two-parameter fracture model to include the non-linear slow crack growth in the pre-peak region using the elastic crack tip opening

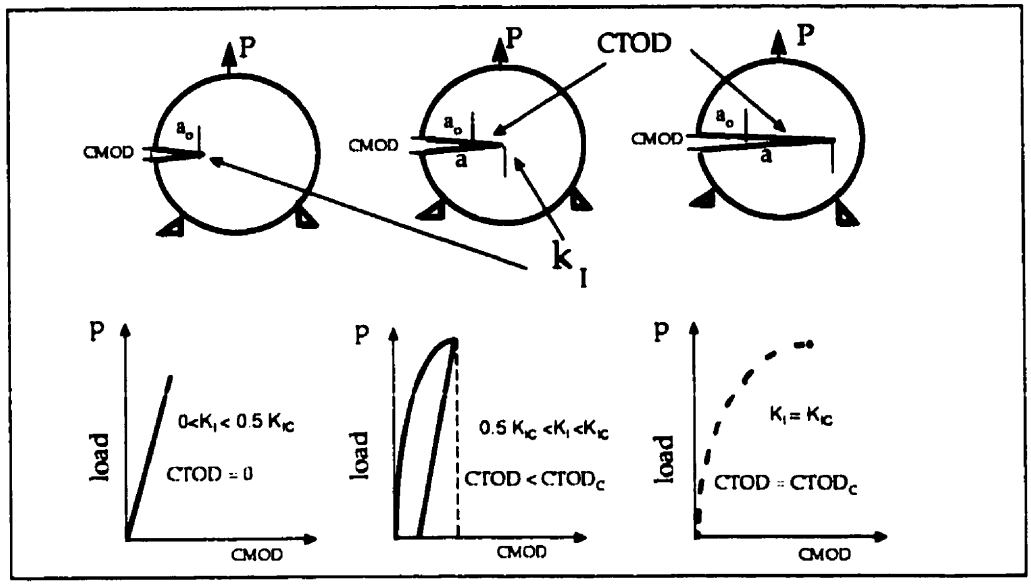

Figure 2.8: Fracture resistance stages of plain concrete

displacement ($CTOD$) to dictate the critical effective crack extension. Figure 2.8 explains the model and shows that the load-$CMOD$ curve is linear up to about one-half of the maximum load (P_{cr}). In this case K_I (mode I stress intensity factor) is less than 0.5 K_{IC}, where K_{IC} is the critical value of K_I. During this stage the $CTOD$ is zero, as predicted by LEFM. In the nonlinear region of Figure 2.8 slow crack growth (process zone formation) occurs and a significant inelastic deformation takes place, which is the critical point. In this case the value of $K_I = K_{Ic}$ and $CTOD = CTODc$, and any further crack growth may occur at a steady state value of K_{IC}. The propagation of the crack depends upon the rate of loading, the geometry of specimen and the method of loading. Also, the model is found to be independent of the size of the material and their properties.

2.4.4 Bažant's size effect law

The capacity of cementitious materials is known to depend on the size of specimens tested in the laboratory. Such dimensional influence is known to be as "the size effect". A well published law proposed in the literature was proposed by Bažant (1984). This law will be presented next and will be used in chapter six to fit the test results represented in chapter five.

The size effect law was stated by Bažant as follows: the maximum nominal stress decreases as the inverse of the square root of the size.

$$\sigma_N = \frac{B f_t'}{\sqrt{1 + \frac{d}{\lambda_o d_a}}} \tag{2.38}$$

where

σ_N = nominal stress at failure

f_t' = direct tensile strength of concrete

d = specimen size

d_a is the maximum aggregate size in the concrete

λ_o and B are constant when geometrically similar specimens are considered.

Equation 2.38, expresses the self-similarity properties of fracture of brittle heterogeneous materials. The geometrical constants B, λ_o are determined by statistical linear regression of test data. For structure of a small size relative to the size of aggregate, the value $d/\lambda_o d_a$ can be neglected, and the nominal stress σ_N will be given by

$$\lim_{d \to 0} \sigma_N = B f_t' \tag{2.39}$$

which is governed by the classical strength of material (SOM) criterion, Figure 2.9. For a very large concrete structure such as dams, the asymptotically approaches the size effect of linear elastic fracture mechanics, i.e., the equation governed by linear elastic fracture mechanics (LEFM). Equation 2.38 will be reduced to:

$$\lim_{d \to \infty} \sigma_N = \frac{B f_t'}{\sqrt{\frac{d}{\lambda_o d_a}}} \tag{2.40}$$

2.4.5 Carpinteri brittleness number

Carpinteri (1986) developed the so called brittleness number to accommodate failure caused by both classical strength of material (SOM) and fracture collapse in terms of (LEFM). The number is dimensionless, and depends upon the fracture toughness K_{Ic},

$$S = \frac{K_{Ic}}{f_t' \sqrt{d}} \tag{2.41}$$

Where f_t' is the tensile strength; S is the brittleness number and d is a characteristic of the specimen (or structure) geometry. For large value of S, in another

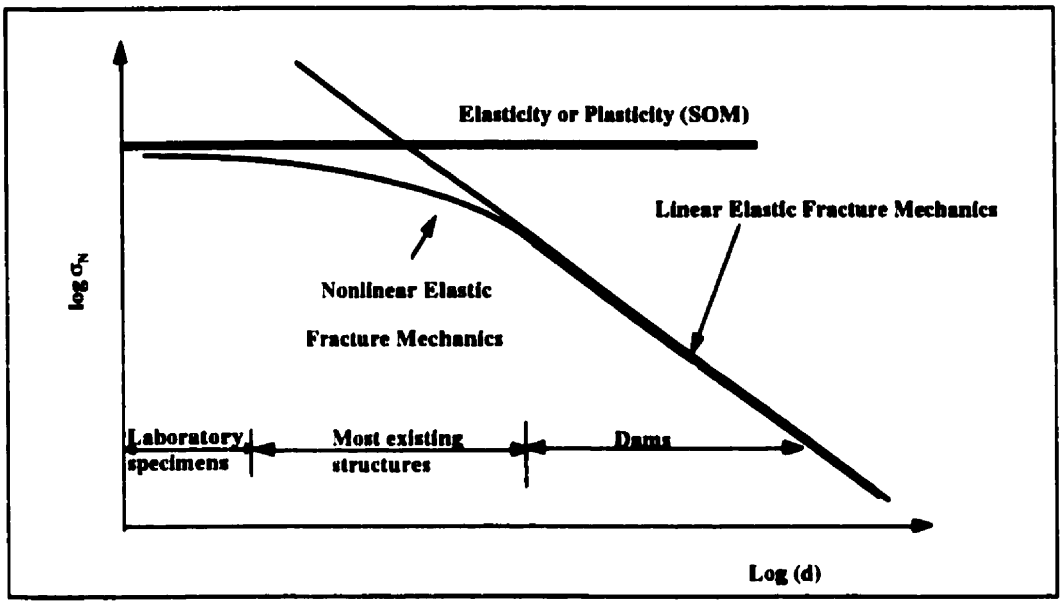

Figure 2.9: Bažant's size effect law

words small specimen dimension(d), SOM satisfies the interpretation of the test, and fracture mechanics play no role. On the other hand when the value of S is small, that is, large value of specimen dimension(d), fracture mechanics is valid, and (SOM) does not give reliable results. Brittle fracture occurs if $S < S_o$, and the value of S_o depends upon the type of test under consideration.

2.5 Damage Mechanics

Damage corresponds to irreversible degradation of the cohesion of the material under internal and/or external straining. This may lead to failure of an elementary volume. The main difference between damage and fracture mechanics, Figure 2.10, can be stated as:

1. In damage mechanics, the strength of a loaded structure is determined by the deterioration of the material caused by loading. This deterioration or damage may be described in terms of a continuous defect field.

2. In fracture mechanics, the strength of a loaded structure is determined by the severity of a single defect such as a sharp crack. The medium around the crack is assumed to be mechanically intact. A more realistic assessment of the behavior of a loaded structure may be obtained by combining these two approaches.

2.5.1 Damage characterization with Uniaxial States of Stress

Under uniaxial state of stress, the damage theory can be characterizes by a scalar parameter, D, which denotes the concentration of microcracks existing in an elementary volume of the material:

$D = 0$ corresponds to the intact material without deterioration; it is the reference state.

$D = 1$ corresponds to the failure of an elementary volume of the material.

$1 - D$, in the uniaxial state, can be expressed as the fractional area of undamaged material.

$$1 - D = \frac{A_n}{A} \tag{2.42}$$

where A_n = undamaged area of the cross-section

A = total area of the cross-section

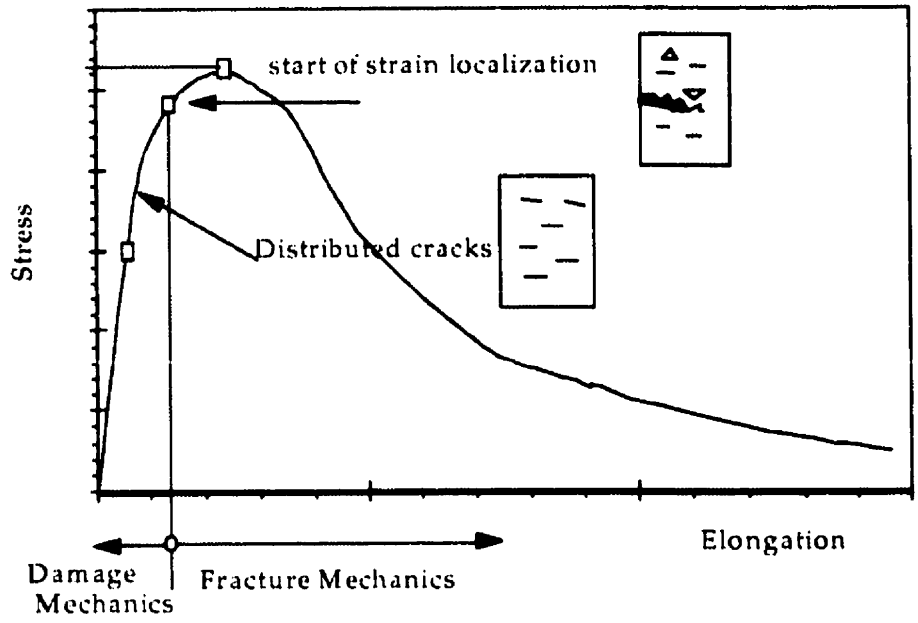

Figure 2.10: Stages of crack propagation in concrete under uniaxial tension

$(A - A_n)$ = the damage area of the cross-section

$$D = \frac{A - A_n}{A} \tag{2.43}$$

An effective net stress σ_n acting on the undamaged material can be defined as:

$$\sigma_n = \frac{\sigma}{1 - D} \tag{2.44}$$

for $D = 1$, $\sigma_n \rightarrow \infty$.

2.5.2 Thermodynamic interpretation of the damage parameter

The damage parameter D has been considered by Lemaitre and Chaboche (1978), cited in Wittmann, (1983), as one of the hidden thermodynamic variables, responsible for irreversible processes. These variables are called hidden because they do not appear in the thermostatic analysis of a continuum. They remain constant during reversible thermostatic transformations.

2.5.3 Damage parameter measurement

The damage parameter, D, can be measured during loading cycles. The stress-strain relation for decreasing load may be described as follows:

$$\frac{d\sigma}{d\varepsilon} = \frac{d}{d\varepsilon}\left(E_n\ (1-D)\varepsilon\right) \tag{2.45}$$

$$= \frac{dE_n}{d\varepsilon}(1-D)\varepsilon + E_n(1-D) - E_n\varepsilon\frac{dD}{d\varepsilon} \tag{2.46}$$

Since damage is assumed to be irreversible, we may write the unloading case:

$$\frac{dD}{d\varepsilon} = 0 \tag{2.47}$$

Further more we assume that the net modulus of elasticity is a material property which yields:

$$\frac{dE_n}{d\varepsilon} = 0 \tag{2.48}$$

hence :

$$\frac{d\sigma}{d\varepsilon} = E_n(1 - D) \tag{2.49}$$

$$D = 1 - \frac{1}{E_n}.\frac{d\sigma}{d\varepsilon} \tag{2.50}$$

If E^* is the mean slope of an unloading branch of the $\sigma - \varepsilon$ diagram then

$$D = 1 - \frac{E^*}{E}\ , \tag{2.51}$$

where E is the initial value of Young's modulus.

2.5.4 Application of damage theory

Mazars's model (1980)

This model describes the stress-strain curve of concrete under uniaxial tension.

Before peak load: $\varepsilon < \varepsilon_c$, where the net stress $\sigma_n = E\varepsilon$, and $D = 0$, after peak load $\varepsilon > \varepsilon_c$ where the net stress :

$$\sigma_n = \frac{\sigma}{1 - D} \tag{2.52}$$

the damage is given by:

$$D = 1 - \frac{\varepsilon_c(1 - A_1)}{\varepsilon} - A_1 e^{(B_1(\varepsilon_c - \varepsilon))} \tag{2.53}$$

and nominal stress:

$$\sigma = E(1 - D)\varepsilon \tag{2.54}$$

where ε_c is the strain at maximum nominal stress and A_1, B_1 are constants which can be determined experimentally.

Also Løland (1980) derived his model where he differentiates between phases in modeling the $\sigma - \varepsilon$ curve in uniaxial tension, this model takes into account the fact that the descending branch of the $\sigma - \varepsilon$ curve is size-dependent.

2.6 Interface Fracture Mechanics

In the past three decades considerable attention has been directed towards studying the mechanical behavior of interfacial regions, where defects usually exist in the form of voids or cracks. The objective of interface fracture mechanics is to define a property, that is, toughness, that characterizes the fracture resistance of the interfaces. Williams(1959) investigated the geological problem dealing with fault lines along the interface between two layers of rock strata and can be applied to joints, owing to faulty jointing techniques. It was discovered for the first time that the stresses possess an oscillating character of the type $r^{-1/2}\sin(\cos)\epsilon \log r$, where r is the radial distance from the crack tip and ϵ is a function of material constants. In the case of a homogeneous material the local stress behavior is given in the order of $\sigma \approx r^{\lambda-1} = r^{-1/2}$, and λ is

an eigenvalue of the form $\lambda = n(integer) - 1/2 + i\epsilon$ for plane strain or plane stress. Erdogen (1963) treated the problem of two semi-infinite elastic planes with different properties bonded along the real axis and subject to loads at infinity. The bond contains some cavities which are idealized as cracks, and his solution is considered as an extension of the Westergaard solution which is restricted to homogeneous planes. England (1965) studied the two-dimensional problem of a crack under constant pressure between dissimilar materials and found that an apparent solution to the problem does not satisfy a necessary physical condition, as it implies wrinkling and overlapping of the crack surface near the crack tip. The problem was later extended by Sih & Rice (1965). In (1988) Sih and Rice applied complex variables integrated with the eigenfunction - expansion technique, Williams (1959) to solve the problem of bonded dissimilar elastic planes containing cracks along the bond, solution being given in closed form for a number of extensional problems. To avoid the stress oscillation, Atkinson (1977) used three layer interface models, where the jump discontinuity in the material properties was eliminated. Comninou(1977) tried to solve this inconsistency by applying the frictionless crack face contact model. In this model there is only one independent eigenfunction and the leading order solution can be written as follows:

$$\sigma_{xx} = \frac{-K_{II}^c}{\sqrt{(2\pi r)}} \frac{1}{2(K+1)} \left((2K+5)\sin\frac{\theta}{2} + \sin\frac{5\theta}{2}) \right)$$

$$\sigma_{yy} = \frac{-K_{II}^c}{\sqrt{(2\pi r)}} \frac{1}{2(K+1)} \left((2K-3)\sin\frac{\theta}{2} + \sin\frac{5\theta}{2} \right) \qquad (2.55)$$

$$\sigma_{xy} = \frac{-K_{II}^c}{\sqrt{(2\pi r)}} \frac{1}{2(K+1)} \left((2K+1)\cos\frac{\theta}{2} + \cos\frac{5\theta}{2} \right)$$

The near-tip mixed mode is determined by the asymptotic solution itself. However, some argued that the general belief is that the resolution to this has to come from a more realistic modeling of the interfacial region of the bonded materials. The traditional open crack tip as formulated by Williams(1959) shows arbitrary constants K_I and K_{II}, so that the near-tip mode-mix cannot be defined as the asymptotic solution alone. The leading term of the solution for the open crack tip model can be written as:

$$\sigma_{xx} = \frac{1}{\sqrt[4]{2\pi r}} \left(K_I \left(3\cos\frac{\theta}{2} + \cos\frac{5\theta}{2}\right) + K_{II}\left(-7\sin\frac{\theta}{2} - \sin\frac{5\theta}{2}\right) \right)$$

$$\sigma_{yy} = \frac{1}{\sqrt[4]{2\pi r}} \left(K_I \left(5\cos\frac{\theta}{2} - \cos\frac{5\theta}{2}\right) + K_{II}\left(-\sin\frac{\theta}{2} + \sin\frac{5\theta}{2}\right) \right) \tag{2.56}$$

$$\sigma_{xy} = \frac{1}{\sqrt[4]{2\pi r}} \left(K_I\left(-\sin\frac{\theta}{2} + \sin\frac{5\theta}{2}\right) + K_{II}\left(3\cos\frac{\theta}{2} + \cos\frac{5\theta}{2}\right) \right)$$

Consider a seminfinite free crack lying along the interface between two homogeneous isotropic half-planes, with material 1 above and material 2, Figure 2.11. Here, plane deformation in an isotropic bimaterial is considered. A bi-material is a composite made of two homogeneous materials for which continuity of traction and displacement across interfaces are maintained. With the interface on the x-axis, let E_1, μ_1, ν_1 be the Young's modulus, shear modulus, and Poisson's ratio, respectively, of material 1. Similar quantities, E_2, μ_2 and ν_2 for material 2 are also defined. Dundurs (1969) has observed that for interface cracks the material properties, and in particular the ratio of Young's moduli, play an important role in the behavior of fracture. In the

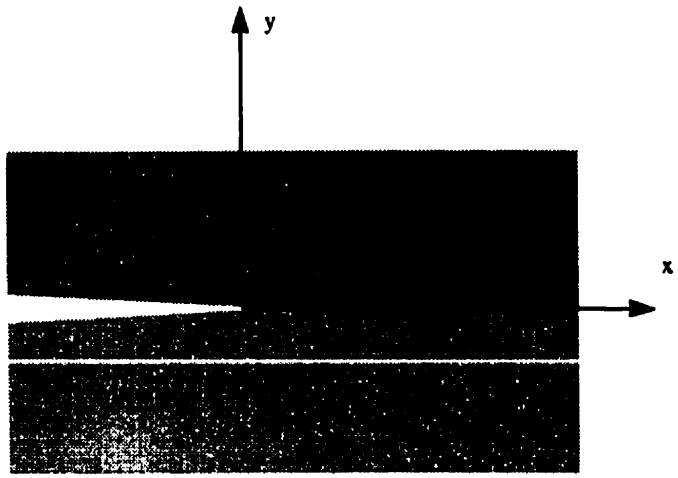

Figure 2.11: Crack tip geometry and convention

simplest case of two bonded materials, where both are homogeneous and isotropic, the Young's moduli are constant, and therefor the discontinuity jump exists at the interface. With such a discontinuity it is well known that the stress state around the crack tip exhibits an oscillation, and that a wide class of plane elasticity problems for bimaterials depend on two non-dimensional combinations of the Young's modulus. For plane strain, Dundurs introduced mismatched parameters:

$$\alpha = \frac{\hat{E}_1 - \hat{E}_2}{\hat{E}_1 + \hat{E}_2} \tag{2.57}$$

and

$$\beta = \frac{1}{2}\frac{\mu_1(1-2\nu_2) - \mu_2(1-2\nu_1)}{\mu_1(1-2\nu_2) + \mu_2(1-2\nu_1)} \tag{2.58}$$

where, for $\hat{E}_i = E_i/(1-\nu^2) = 2\mu/(1-\nu)$ for i =1,2, the parameter measures the relative stiffness of the two materials. The parameter causes the linear crack-tip stress and displacement fields to oscillate, Rice (1988). Note that both α and β vanish when dissimilarity between the elastic properties of the materials is absent, and α and β change signs when the materials are switched. For convenience, an average stiffness, E^*, is defined as

$$E^* = \frac{1}{2}\left(\frac{1}{\hat{E}_1} + \frac{1}{\hat{E}_2}\right) \tag{2.59}$$

for plane problems, the normal and shear stresses of the singular field acting on the interface at a distance r ahead of the tip can be written in the compact complex form

$$\sigma_{22} + i\sigma_{12} = \frac{K}{\sqrt{2\pi r}} r^{i\varepsilon} \tag{2.60}$$

where $K = K_1 + iK_2$ = the stress intensity factor at the interface, $i^2 = -1$ and the oscillation index $*$ depends on

$$\varepsilon = \frac{1}{2\pi} \ln\left(\frac{1-\beta}{1+\beta}\right) \tag{2.61}$$

The parameter $*$ brings in some complications that are not present in the theories of elastic fracture mechanics of homogeneous bodies. The associated crack-opening displacement components at a distance r behind the crack tip, is given by:

$$\delta_2 + i\delta_1 = \frac{8k}{E^*(1+2i\varepsilon)\cosh \pi\varepsilon}\left(\sqrt{\frac{r}{2\pi}}\right) r^{i\varepsilon} \tag{2.62}$$

for the case where $\beta = 0$ (i.e., $\varepsilon \neq 0$), one can define

$$K\hat{E}^{\varepsilon i} = |K|e^{\Psi i} \tag{2.63}$$

Note that $\left|\hat{E}^{\varepsilon i}\right| = 1, \left|K\hat{E}^{\varepsilon i}\right| = |K|$ and Ψ the real phase angle of the complex quantity $K\hat{E}^{\varepsilon i}$. When $\beta = 0$, K_1 and K_2 measure the normal and shear traction singularities on the interface ahead of the crack tip with the standard definition for the stress intensity factors. With $\beta = 0$, the phase angle is defined as

$$\hat{\Psi} = \tan^{-1}\left(\frac{K_2}{K_1}\right) \tag{2.64}$$

here, $\hat{\Psi}$ measures the relative effect of mode II and mode I on the interface. The case in which $\hat{\Psi} = 0°$, corresponds to pure mode I, and $\hat{\Psi} = 90°$, corresponds to mode II conditions.

The energy release rate G per unit length of extension of the crack at an interface is related to the stress intensity factors with an Irwin-type relation:

$$G = \frac{|K|^2}{E^* \cosh^2 \pi\varepsilon} \tag{2.65}$$

where $|K|^2 = K_1^2 + K_2^2$, and $\cosh^2 \pi\varepsilon = 1/(1-\beta^2)$. If both $\hat{\Psi}$ and G are defined, one can establish a fracture toughness curve, or Gc-$\hat{\Psi}$, for an interface. In linear

elastic fracture mechanics, the Gc-$\hat{\Psi}$, curve is the property of the given interface in the sense that, in principle, it is independent of the specimen geometry and the loading system. However, in general, the toughness curve is clearly dependent on the nature of the interface such as the roughness of the free surface before bonding and the bonding history, and the environment such as temperature.

For any interfacial crack problem, the complex number K will have the form,

$$KL^{\varepsilon i} = YT\sqrt{L^{\Psi i}} \tag{2.66}$$

where T is an applied traction on the structure, L is a relevant length describing the geometry, Y is a dimensionless real positive number and $\hat{\Psi}$ is the phase angle of $kL^{\Psi i}$. Both Y and $\hat{\Psi}$ depend on the geometric and loading details of the structure. The effort to establish the relationship between the applied load and K given in the above equation is referred to as a K-calibration for the structure, Wang (1990). With a K-calibration for a given structure, the loading amplitude G can be calculated from equation 2.65. Also, the loading phase angle may be calibrated by

$$\hat{\Psi} = \Psi + \varepsilon \ln(\frac{\hat{L}}{L}) \tag{2.67}$$

where L = the length used in the K-calibration; and $\hat{E}$= the fixed length, used in defining the loading phase angle $\hat{\Psi}$. The selection of $\hat{E}$ is somewhat arbitrary, Rice (1988), as long as a fixed length is used for reporting data in conjunction with

the toughness curve. The preceding discussion provides a theoretical insight into the interface fracture problem and defines the major parameters involved. For a quantitative assessment of the fracture toughness of a given interface, the development of appropriate physical models is necessary.

2.7 Fracture of Concrete Dams

Cracking frequently occurs and numerous dams in the United State and in Europe have shown disturbing signs of extensive cracking. Because of human and economical consequences of a dam failure, dams with signs of cracks are thoroughly investigated

In many cases non-structural cracks develop, where the safety of the dam is rarely jeopardized. On the other hand there may be numerous structural causes for cracking, such as:

1. Differential settlement.

2. Uplift water pressure along internal cracks.

3. Upstream water pressure.

4. Release of heat due to hydration process, and resulting internal thermal gradient.

The first three points are out of the scope of this thesis, so only thermal loading induced crack will be discussed.

2.7.1 Thermal cracks

Thermal cracking is quite usual in concrete dams, particularly in those constructed in regions with severe climate. In some cases the length of thermal cracks amounts to 100 m and higher. Cracks, cause serious problems during operation, and call for expensive and labor-intensive repair. The effect of thermal cracks on the response of structures and their stability under operating conditions can be investigated by applying adequate analytical and experimental methods. To assess thermal stresses and therefore potential cracking, it is required to solve the heat conduction problem as a coupled or decoupled problem. Chappell and Ingraffea (1981) reported the first fracture mechanics based analysis of a dam. In their investigation of the Fontana dam, cracking was attributed to thermal loading. Saouma *et. al* (1987) studied thermal cracking in roller compacted concrete (RCC) dams where the anisotropic nature of the RCC material was emphasized. Leger *et. al* (1993) and Leger *et. al* (1994) have studied the behavior of joints in dams when subjected to thermal loads.

2.6.1.1 Mechanism

During hydration the cementitious binder produces heat. The concrete temperature increases as long as the rate of heat development exceeds the rate of heat loss to the surrounding environment. With the increase in temperature there is increase in volume of the concrete. When the concrete later cools, it will contract. During the temperature rise the deformation of the concrete is small, because at early ages the concrete is relatively plastic, and thus the compressive stress induced by any restraint

in the structure will be small. During cooling, the modulus of concrete is higher, and therefore restraint can cause tensile stresses which can lead to crack initiation.

2.6.1.2 Restraint

Restraint can be divided into internal and external restraint. Internal restrains are caused by unequal temperature development in the structure,which in practice cannot be avoided. At early age, the core will usually be warmer than the surface. This can lead to surface cracks during the heating phase. Cracks may sometimes close and sometimes heal. External restraint is caused by the foundation or adjacent monolitcly which try to stop the thermal movements of the young concrete. There can be restrains against both elongation, contraction and bending. For the case of dams, external restraint can form cracks through the structure during the cooling period.

2.6.1.3 Heat conduction

Heat conduction is governed by the well-known Fourier law,

$$C_p\rho\frac{\delta T}{\delta t} = \frac{\delta}{\delta x}(k_x\frac{\delta T}{\delta x}) + \frac{\delta}{\delta y}(k_y\frac{\delta T}{\delta y}) + \frac{\delta}{\delta z}(k_z\frac{\delta T}{\delta z}) + q \quad \text{over } \Omega, \tag{2.68}$$

where ρ is the mass density;

T is the temperature in ^{o}K, a function of the point coordinates x, y, z and the time t;

C is the specific heat in J/(kg ^{o}K);

k is the thermal conductivity tensor;

q is the rate of heat generation within the control volume in W/m^3.

The boundary conditions on surfaces Γ_1 and Γ_2 on the domain Ω may be of the form;

$$T = T_o \qquad \text{on } \Gamma_1 \tag{2.69}$$

and / or

$$k_x \frac{\delta T}{\delta x} + k_y \frac{\delta T}{\delta y} + k_z \frac{\delta T}{\delta z} = q \qquad \text{on } \Gamma_2 \tag{2.70}$$

simulating thermal exchange between concrete and environment. If the finite element method is used for discretization, the governing matrix equation referred to as semi-discrete statement is obtain by:

$$[C]\{\dot{T}\} + [K]\{T\} = \{Q\}, \tag{2.71}$$

where $[C]$ is the specific heat matrix,

$[K]$ is the effective conductivity matrix,

$\{T\}$ is the matrix of nodal temperature values,

$\{\dot{T}\}$ is the time derivative of $\{T\}$,

$\{Q\}$ is the effective heat flux and is given by:

$$\{Q\} = \{Qe\} + \{Qc\} + \{Qr\} + \{Qi\} \tag{2.72}$$

where,

$\{Qe\}$ is the applied heat flux,

$\{Qc\}$ is the convective heat transfer vector,

$\{Qr\}$is the radiation vector, and

$\{Qi\}$ is the vector of internal heat generation rates.

The most important factor in modeling the thermal behavior of mass concrete is the internal heat generated by hydration of cementing materials. During hydration, concrete temperature increases as long as the rate of heat development exceeds the rate loss to the surrounding environment. The increase of temperature leads to an increase in the structure's volume, and during cooling it contracts. For mass concrete structures, an adiabatic heat of hydration test allows for reasonably accurate temperature predictions. The adiabatic temperature is given by

$$T = kt(1 - e^{-\alpha t}) \tag{2.73}$$

where T is the temperature of the concrete under adiabatic condition; kt is the maximum temperature of concrete under adiabatic condition; α is a parameter which presents a heat generation rate; and t is time (hours). Multiplying the above equation by the specific mass of concrete $(Cp.r)$, we obtain the amount of heat generated per unit volume as,

$$Q(t) = (Cp.r)T(t) = kCp.\rho(1 - e^{-\alpha t}) \tag{2.74}$$

The rate of heat generation can then be found by differentiating equation (2.7) with respect to time. That is,

$$R(t) = \alpha k C p . \rho \, e^{-\alpha t} \tag{2.75}$$

2.8 Finite Element Formulations

2.8.1 Modeling aspects of cracks in concrete materials

There are two basic approaches to modeling cracks, "Discrete Models" and "Smeared Models". Discrete Models describe a crack as a geometric discontinuity, and the Smeared Models describe the crack behavior at the constitute level, and treats a cracked solid as if they are stiff continuous domains.

2.8.2 Discrete crack concept

This approach suffered from two drawbacks. First, it implies a continuous change in nodal connectivity of the finite element method; and second, the crack is constrained to follow a predefined path along the element edge. As a result this model proved to be impractical. In the late seventies the discrete crack concept appeared again, Ingraffea and Saouma (1981), successfully eliminating the drawbacks through the use of interactive computer graphics, automatic remeshing and bandwidth minimizers. The discrete crack concept was used successfully with fracture mechanics based decision in the analysis of dams by Saouma *et. al* (1987) and Ayari (1988). The advantage of

using the discrete crack model specially with interface elements and a singular crack tip element have been summarized in the ACI 446 report, ACI committe 446 (1997):

1. Mesh regeneration associated with crack propagation, and direction change, can be accomplished automatically. This eliminates one of the greatest criticisms of the discrete crack approach.

2. The formation of discrete cracks is therefore viewed as a problem of changing geometry rather than as in the smeared crack approach, a change in properties.

3. As the interface forms, a graphical representation of the geometric discontinuity that develops, is automatically obtained by the altered mesh.

4. Interface elements are a natural way of describing the crack and are consistent with the fictitious crack model.

5. Interface elements are economical in that the crack is modeled with the minimum number of degrees of freedom.

2.8.3 Smeared crack concept

This approach was first introduced by Rashid (1968). In this approach crack behavior is modeled through non-linear constitutive behavior. With this continuum approach, the local discontinuities are distributed over some tributary area within the finite element stiffness matrix,

$$K_e = \int B^T D\, B\, d\Omega \tag{2.76}$$

The prime setback of this approach is that it would tend to spread the crack formation over the entire structure and, therefore, be incapable of predicting localized fracture formation. Also there is spurious mesh sensitivity. The advantage of using the smeared crack model specially with interface elements and a singular crack tip element have also been summarized in the ACI 446 report, ACI committe 446 (1997):

1. Remeshing is not required.

2. Distributed damage and cracking have been observed in reinforced concrete structures.

3. Tortuosity of cracks can be modeled more readily using the smeared crack approach.

4. In the case, where parallel cracks in concrete are densely and uniformly distributed, such cracks are well represented by the smeared crack model with a minimum crack band width equal to the actual spacing of the parallel cracks.

Figure 2.12 shows simulations performed by different researchers. Area and Ingraffea (1982) used a discrete approach with remeshing technique. Softening and aggregate interlock were taken into account. A fixed smeared crack model was used by De Borst (1986). De Borst claimed that an excellent match with the experimentally found load-displacement curve was obtained. However, there is a doubt about this claim, since for wrong crack pattern the load-displacement curve cannot be correct. Rots (1991) adopted a smeared crack approach with the removal of elements to overcome stress-locking effects. The cracks follow the mesh lines, which results in

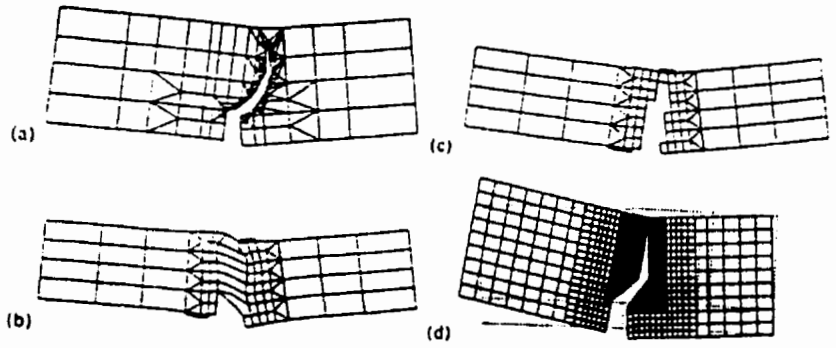

Figure 2.12: Crack patterns observed by (a) Area & Ingraffea , (b) DeBorst , (c) Rots and (d) Alfaiate

the wrong crack pattern. Alfaiate *et. al.* (1992) used a discrete crack approach with a pre-defined crack.

2.8.4 Finite Element For Interface

2.7.4.1 Analysis of non-linear joints

The problem of cracks at a bi-material interface has been of interest for the past 25 years. Various analytical methods were used, such as the eigenfunction expansion method, integral equations, method of dislocations and various complex function expansions. Most of these methods are difficult to apply in addition to possibly not being able to solve the non- linear problem associated with power law hardening materials, or other non- linearities.

The interface crack model in concrete is derived from a nonlinear material formulation, and, therefore, a finite element analysis with this material formulation involves

a system of nonlinear equations. Such a system can be solved, for instance, by the Newton-Raphson method. To exploit the full Newton-Raphson method a tangent stiffness matrix would have to be computed at each iteration. The incremental tangent stiffness matrix for the proposed material formulation can be computed from an incremental stress-displacement constitutive relationship.

2.7.4.2 Interface elements

In finite element analysis, situations arise where discontinuous behavior occurs between elements. Examples are interfaces between bimaterials and joints or fractures in the material, such as joints between lifts of concrete dams.

Various methods have been proposed in the past. The discontinuous behavior at the interface has been modelled using constraint equations or by connecting elements with each other by discrete springs. Other workers have treated the joint/interface as a quasi-continuum of small thickness, that is, by using continuum finite elements which contain planes of weakness.

Special joint finite elements have been developed by Goodman (1968), Ghaboussi *et al.*(1973), Figure 2.13. Most of the applications are in two dimensions (plane stress, plane strain), although some three-dimensional analyses have been reported.

2.8.5 Summary

In this chapter, a wide range of topics included linear elastic fracture mechanics, non-linear fracture mechanics. and interface fracture mechanics which are related to

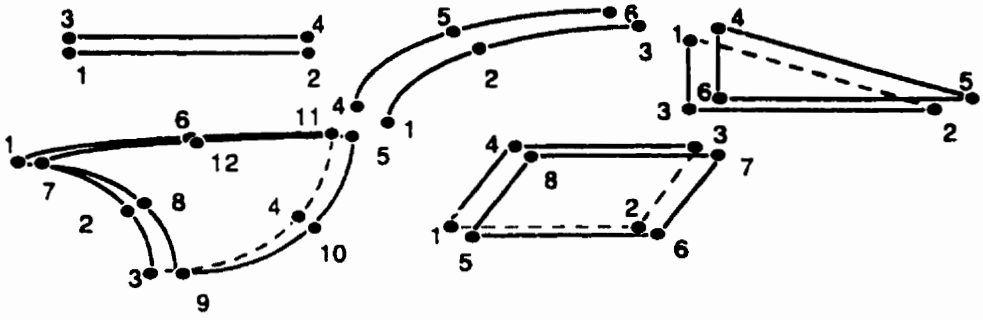

Figure 2.13: Interface element numbering

this research program were described. The experimental tests used for conducting fracture mechanics parameters by different investigators were explained. Finally, the two different approaches for modelling cracks were discussed.

The parts of the literature which will be used in this thesis include linear elastic fracture mechanics which is used only for the finite element analysis of large concrete structurs such as dams, non-linear fracture mechanics, where nonlinear model needs to be used for the finite element analysis of lab size concrete specimens, also bi-materials interface formulation which will be used for the analysis of repair specimens.

Chapter 3

EXPERIMENTAL PROGRAM

3.1 Introduction

This study was undertaken to examine and obtain more information on the fracture behavior of a repaired cracked horizontal interface between two successive lifts of concrete using different types of repair material, particularly on the influence of low temperature and moisture condition of the concrete. Such information is important especially for repairs in cold climate areas.

The experimental program is divided into three phases of testing:

• Phase I: A set of 60 specimens were tested, some of which were cast in one stage and the remainder cast in two stages, Table 3.3 with a 24 hours period between the two casts. Both sets are tested at temperatures varying between 20°C and -50°C.

•Phase II : The specimens tested in phase I were repaired using different types of repair materials and then tested at temperatures between 20°C to -50°C.

•Phase III : Ten specimens of phase III, were repaired for a second time, to study

if there is any change in the strength in the vicinity of the interface crack.

Before the test program started, six specimens were used as a pilot test to obtain the appropriate loading rate, also to avoid any problem in the setup.

3.2 Material Characterization

3.2.1 Introduction

This section provides the necessary background on the characteristics of concrete joints, also described are different types of materials and procedures used in repairing cracks and debonded concrete joints in dams.

3.2.2 Concrete Joints

Joints are a necessary part of any large construction where dimensional changes within the structure are likely to occur. This is particularly true for concrete dams where as a result of the nature and behavior of the construction material, they may suffer cracking to a greater or lesser degree unless joints are provided to control these problems. Such cracking can frequently extend throughout the shorter horizontal dimension of a section thus providing a passage for the leakage of water.

The development of strength in concrete is due to the hydration of the cement and slag, and pozzolanic reactions in the mixture as well as impregnants such as sulphur and polymers, where applicable, during which process considerable heat is generated, followed by cooling and drying of the material. The net result is contraction of the

concrete, which leads to the development of stresses which obviously become more severe the larger the mass of concrete cast monolithicallies. Even though modern technology has introduced techniques for reducing the effects of heat of hydration and of drying, some contraction will always occur and it is necessary to divide the concrete structure into blocks so that the contraction within each block will be within tolerable limits.

Construction procedures and sequence may also lead to the development of large stresses, as for example in the case of double curvature concrete dams where the casting of intermediate blocks at a later stage can lead to the development of high vertical cantilever stresses in the initial blocks.

Periodic thermal variations may be large and can thus give rise to large stresses which cause cracking. Especially where dams are located in severe climates, the seasonal difference in ambient temperature may be high as 70°C with minimum temperatures in the region of -45°C. The provision of joints to accommodate this type of movement caused by temperature changes is therefore also necessary.

When the horizontal interface between two successive lifts of concrete has not been properly prepared, or there has been a long interval between lifts, a good bond between the two casting construction lifts may not occur and leakage of water can take place in this area.

To minimize the effects of both heat of hydration and relative movement, concrete dams are cast in alternate blocks or monoliths so that as much of the contraction as possible can take place before the intermediate or filler blocks are poured.

3.2.3 Repair Materials

3.2.3.1 Introduction

A variety of different repair materials are widely used to fill cracks in different types of concrete structures. The grouts used tend to be based on portland cement, silicates, chemical, polyurethanes or resins. The choice of grout depends on a number of factors, namely the grain size of the grout, which depends upon the viscosity, pot-life, bleeding and wash-out resistance of the grout mix, the condition of the crack, if it is active or passive dry or wet, and on water pressure and whether water is running with the crack.

3.2.3.2 Types of repair materials

1- Epoxy resins Since epoxies came on the market in the 1930's, they have been widely used in repairing concrete. There are thousands of epoxy resins. Epoxy resins are immiscible in water and there is a clear boundary between the resin and any water it displaces. In clean cracks, bond strengths can exceed the tensile strength of the concrete but in real cracks such as those occurring in dams there is no such think as a clean dry crack. Epoxy and polyester systems are normally Newtonian fluids before hardening, where the rate of shear is proportional to the shear stress. The viscosity can be varied over a wide range but has to be relatively high if high strength is required. Also high viscosity resins require high grouting pressure. In the case of repairing cracks in concrete dams, ultra-low viscosity epoxy is required, but only a few fall into this category and the data list physical performances under

normal conditions only. A research program for comparison purposes was carried out by Manitoba Hydro's Research and Development (1993) to evaluate eight epoxy resins for suitability for use in the field. It was concluded that, additional testing is required to ensure field requirements are met.

2- Polyester resins These materials are cheaper than epoxies. However, because they shrink on hardening, they pull away from the face of the crack and so may not be as reliable if bond is required. To reduce shrinkage, polyester resins with inert fine grained fillers are used.

3- Polyurethane foam is a mixture of two liquids which are pumped into the crack. A solid foam results from the mixture, which can accommodate considerable movement. Hydraulic pressure in the crack can prevent or limit development of the bubbles.

4- Cement based grouting materials Cement-based grout, being a rigid brittle material with no guarantee of bond to all sides of a void, cannot be expected to develop high tensile strength. Cementitious grouts can efficiently penetrate cracks larger than 0.3 *mm* wide. In using cementitious grouting, only high speed high-shear rate mixers should be used to ensure that individual cement particles are separated from one another.

Many grouting applications involving large fissures also include smaller fissures which are not easily penetrated by conventional cementitious materials. In such circumstances, grout formulations are adjusted during grouting operations and may

include eliminating various materials from the grout formulation, as well as substituting microfine cements for cements for conventional portland cements. According to Houlsby (1990), the suitability of various cement grouting materials, to penetrate narrow fissures may be evaluated by using the following formula:

$$\text{Grouting Ratio (GR)} = \text{fissure width}/d_{95}\ \text{(grout)}$$

where d_{95} reflects type of grout. Satisfactory grouting results can be consistently obtained with stable cementitious grout mixes for site conditions. When GR<5, it becomes increasingly difficult to obtain satisfactory grouting results. Grout penetration into narrow fissures can be facilitated by selecting grouting materials to accommodate various site conditions.

Research has shown that penetration of grouting fluids into fine fissures is proportional to the cube power of the fissure width (w^3). As a results of this relationship, penetration of fine fissures may be significantly enhanced at various water/cement ratio by selecting finer cements in accordance with site conditions. For grouting projects which involve filling large fissures and voids, the use of stable grouts formulated with locally-available portland cements are recommended. Where grouting operations are performed under water-filled conditions, cohesive, thixotropic, water-repellent grout formulations prepared with low water /cement ratio are preferred. In the case of placing cementitious grout into flowing water conditions, the use of special thixotropic agents are used to obtain a rapid gelation of the grout in order to resist dilation and minimize the extent of grout washout. Under extreme grouting conditions involving high water velocities and short flow paths, it may be necessary to combine the use of

cementitious grout and water-activated resins to obtain very fast setting cementitious grouting materials.

5- Chemical grouting This is usually a chemical substance mixed with water in a wide range of proportions to form a strong film, gel or foam according to the mix design requirements of the application. This capability makes chemical grouting ideal for use as a remedial waterstop. The form of the final product, whether it is film, gel or foam, is controlled by the ratio of water to the final product. One of the disadvantages is that each crack case is unique. So it needs highly experienced personal who can choose the correct mixture for the specific case.

6- Latex membrane Geomembranes are very low permeability membrane liners and barriers used with geotechnical engineering related material so as to control fluid migrations in a man-made project, structure or system. The term liner applies when a geomembrane is used as an interface or a surface revetment. The term barrier is usually reserved for the cases where the geomembrane is used inside an earth mass. Geomembrane is a generic term which has been proposed to replace many terms such as: synthetic membranes, plastic liners, flexible membrane liners, impermeable membranes and impervious sheets.

Geomembranes should not be confused with geotextiles. Geotextile refer to textiles (fabrics) used in geotechnical engineering. Geomembrane are designed to have a permeability as low as possible. In other words, geotextiles allow or conduct fluid flow, while geomembranes restrict fluid flow. A geotextile is often used in conjunction

with the geomembrane to provide protection against puncturing.

In dam applications geomembranes come in rolls, each roll being long enough to cover the height of the upstream face where it is to be installed, thus avoiding horizontal welds. Various configurations of geomembranes have been used to provide impervious synthetic barriers in dams particularly in Europe, for the last three decades. In general, membranes are either placed within an embankment or rockfill dam as part of the impervious core or at the upstream face of embankment, rackfill and concrete gravity dams. Also, the main requirement for a suitable membrane is to be waterproof, have sufficient strength/ductility, have an acceptable life time, have an acceptable history, have test and design data available and to lay relatively without expensive equipment.

Application of geomembrane, have been reported by Koerner (1986), some of the geotechnical application of geomembrane in earth dams, concrete dams, spillway capacity etc. Geomembranes are used to rehabilitate concrete, masonry, rockfill, gravity, concrete dams, as well as reservoirs and canals.

7- Shotcrete Shotcrete is a method that involves the premixing of binder and aggregates, which are then fed into a special mechanical feeder metering the premixed materials into a hose. The mix is jetted from the hose's nozzle at high velocity onto the concrete surfaces.Prior to applying shotcrete, the surfaces must be prepared by cleaning out defective concrete using pneumatic picks or by very high pressure water jetting. The thickness of the shotcrete will be determined by the engineer to meet the requirements of loading, durability and impermeability. The shotcrete can be

reinforced with a mesh of either steel or glass reinforced plastic (GRP). In dam repair, shotcrete must be dense and durable and anchor bars should be used to secure the new shorcrete to the existing concrete.

3.2.4 Grouting procedures

3.2.4.1 Water pressure testing

Water pressure testing includes investigative procedures which are performed for various stages of each grout hole prior to grouting. Appropriate grout formulations can be selected for specific stages to be grouted depending on the water pressure test results.

3.2.4.2 Grout monitoring equipment

Electronic flow measuring and pressure recorders are recommended for all major grouting projects. The availability of instantaneous grouting data and indications of dynamic trends are useful in achieving optimum results.

3.2.4.3 Multiple hole grouting

Multiple hole grouting techniques can improve grouting productivity when substrate conditions restrict grout flow rates. Improved grouting performance may also result from increasing the connection time to each grout hole.

3.2.4.4 Refusal techniques

The application of long duration refusal techniques is recommended (i.e. maintaining zero flow at maximum grouting pressure) at the conclusion of each grouting operation. Improved grouting results are achieved when grouting materials have been allowed sufficient time to undergo the pressure filtration phenomenon.

3.3 Test material characteristics

3.3.1 Concrete mixes

Concrete was mixed using aggregates from two different sites (limestone and crashed granite). For each mix, six standard 15 cm x 30 cm cylinders were used to the determinate the concrete material properties. The water/cement ratio was about 0.4 and the cement content was $400kg/m^3$. The mix proportions by weight were 1(portland cement): 2.9 (course aggregate) : 1.7 (fine aggregate). Rehobnilt 1000 super-plastisizier with 3 liter/m^3 was used to increase the workability. The nominal specified compressive strength of concrete was found to be 20 MPa after 3 days. The tests were conducted according to ASTM C39-86. The elastic modulus as well as the tensile strength of concrete were also evaluated at the first day of testing based on ASTM C469-87a and C496-90, respectively.

The compressive strength and tensile splitting strength for each concrete mix were determined for each wedge-splitting specimen. The average compressive strength of concrete cylinders was 33 MPa at the day of testing. The dimensions of the wedge

splitting (ws) specimens tested in the experimental program are shown in Figures 3.2 and 3.3.

3.3.2 Repair materials

Two types of commercial epoxies and one ultra fine cement were used in this study, these being referred to as epoxy-K, epoxy-W and fine-cement respectively. The two epoxies, have a viscosity between 150-200 poise at room temperature and a specific gravity between 1.1 and 1.6. The ultra fine cement was prepaired with a 0.5 water/cement ratio with 2.5% (of the weight of the fine cement) plasticizer. The three repair materials were applied to the broken surfaces of the specimens, the halves were clamped and left for seven days to cure in a special curing room. Also small load cells were used to measure the amount of clamping force applied to the repaired specimens.

•EPOXY K: is a two component, low viscosity, high modulus material. It has a 2:1 (by volume) mixing ratio and employs special colorants for contrasting component color. Primary applications include the structural repair of cracks and delaminations in concrete, masonry, stone and wood. Filling of voids in porous and honeycombed concrete and grout, adhesive bonding of steel plates (external reinforcement) and anchoring bolts dowels and rebar into concrete or rock.

•EPOXY W: is a two component, low viscosity, high modulus material. The resin to hardener mix ratio is 5:1 by volume and employs special colorants for contrasting component color. Primary applications include the structural repair of cracks and delaminations in concrete, masonry, stone and wood.

• ULTRA FINE CEMENT: is a brittle gray solid powder material with a specific gravity of 3 and solubility in water at 20°C less then 1%. The powder is mixed with water/cement ratio of 1:2 with 2.5% superplastizier by weight of cement.

3.3.3 Specimen preparation

In phase I, the specimens are cast according to two procedures. They were cast from a single mix or cast in two stages whereby one half is poured and left to cure for a period of 7 hours. The concrete surface is then roughened by sandblasting, and loose material and dust are removed by air jet and subsequently, the second half is poured the following day. A total of sixty specimens of two basic sizes, Figure 3.16, small (S) and large (L) were tested at temperatures varying between room and -50°C, Figures 3.10 and 3.11 are a photograpic representation, with initial crack sizes equal to 100 *mm* or 200 *mm*. Table 3.2 summarizes phase I experimental program.

Phase II, a total of 60 specimens were tested 40 specimens were repaired using epoxies repair materials and 20 specimens were repaired with ultra-fine cement, Figures 3.12 and 3.13 are a photograpic representation. The specimens were tested at room temperature and - 50°C in dry and water saturated condition, with initial crack sizes equal to 100 *mm*. The specimens were left for at least seven days inside cure room before test takes place. Table 3.3 summarizes phase II experimental program. Ten specimens were re-repaired using ultra-fine cement; and epoxy K and were used for testing in phase III.

3.4 Splitting Wedge Test

The cube and drilling core wedge splitting test, Figure 3.1 (only the cube specimen was used in this program), was developed at the University of Technology, Vienna, and involves the testing of a number of drilled core samples. Such samples have, of course, limited diameters and to overcome the special problem associated with the application of fracture mechanics Bažant developed the size effect relationship shown in Figure 2.9. In the Bažant's model, the nominal strength at failure is given by:

$$\sigma_n = cf_t'/(1 + d/d_o)^{1/2}$$

where f_t' = strength parameter. The factor 1 becomes insignificant within the value of $(1 + d/d_o)^{1/2}$ for large concrete specimens and the relationship can be simplified as follows:

$$\sigma_n = cf_t'(d/d_o)^{1/2} \tag{3.1}$$

In linear elastic fracture mechanics the fracture toughness is given by

$$K_{IC} = \sigma_n(a\pi)^{1/2}F(a/d) \tag{3.2}$$

$$K_{IC} = cf_t'(ad_o\pi)^{1/2}F(a/d) \tag{3.3}$$

or

$$K_{IC} = cf_t^{'}(d_o)^{1/2}F(a/d) \tag{3.4}$$

the above expression is further reduced to,

$$K_{IC} = 1/(B)^{1/2}F(a/d) \tag{3.5}$$

This equation can now be used to obtain values of K_{IC} for values of $d \rightarrow \infty$. Tests carried out on dam drilling cores having diameters between 200 and 300 mm provide fracture energy values G_F between 174 and 257 $N/m^{3/2}$. This leads to calculations of fracture toughness K_{IC} of concrete in dams between 2 and 3.5 MN/m . This shows the major strength of the above model, which is its ability to extrapolate experimental results obtained from laboratory-size specimens to predict failure of geometrically similar structures.

The setup of the wedge splitting test is presented in Figures 3.5 and 3.6. First a specimen is prepared by casting a groove and a notch. The specimen is placed on a linear roller support, which is fixed on the lower plate of the testing machine. Two massive loading devices both equipped with rollers, are placed on the top of the specimen as shown in Figures 3.4 and 3.9. A stiff steel profile with no identical wedges is fixed at the upper plate of the testing machine. The actuator is then moved so that the wedge enters between the rollers on each side, see Figure 3.5. The dimensions of the groove and the notch are chosen so that the crack propagates in the vertical direction; the specimen is split into two halves. During test, the applied load F_v

(vertical component) and the crack opening displacement (COD) are measured. The splitting force F_{sp} is the horizontal component of the force acting on the rollers. It is calculated taking the wedge angle α into consideration.

$$F_{sp} = \frac{F_v}{2\tan\alpha} \tag{3.6}$$

The above equation can be applied in the case where the coefficient of friction μ is smaller than 0.5%. The manufacture of the roller bearing give values ranging between 0.1% and 0.5%. To reduce friction, rollers with a coefficient of friction 0.3% were used, and the wedge surface was carefully polished and Teflon sheet was used. In the case where the coefficient of friction is larger than 0.5%, the coefficient of friction μ has to be taken into consideration and the splitting force is given by following expression

$$F_{sp} = \frac{F_v}{2\tan\alpha}\left(\frac{1-\mu\tan\alpha}{1+\mu\cot\alpha}\right) \approx \frac{F_v}{(1-\mu\cot\alpha)(2\tan\alpha)} \tag{3.7}$$

or

$$F_{sp} = \frac{1}{2\tan\alpha}\frac{F_v}{(1+\mu\cot\alpha)} \tag{3.8}$$

The COD was measured by means of a clip gage, that is fixed at the level where the splitting force acts on the specimen, at the axis of the rollers. The test stability (i.e. no sudden drop of load) was checked by means of a load-time plot. The tests were carried out by monotonically increasing of the displacement of the actuator of the testing machine. During the test, not only the splitting F_{sp}-COD curve, and the vertical force F_v-vertical actuator displacement u-curve recorded. The fracture

energy, G_F, is obtained from the area under the splitting force F_{sp} versus COD curve by the projected fracture area, also the energy can be calculated from the area under the vertical force F_v versus u curve. Theoretically the above two area should be equal, but larger energy values are determined from the F_v versus u curve were because it includes contribution of the testing machine and test-setup displacements.

3.5 Experimental Test Setup

A schematic representation of the test setup is illustrated in Figure 3.7 and Figure 3.8 is a photograpic representation. It mainly consisted of a cold chamber which could easily achieve and maintain a temperature of up to - 50°C. The chamber was mounted on a mobile table to provide easy access in and out of the MTS machine. The cold chamber has circular holes at its top and bottom ends, in order to allow steel extension pipes with outside diameter of 168 *mm* and wall thickness of 14 *mm* to pass through. The upper extension pipe was welded on one end to a 19 *mm* thick plate, and the other end was welded to a steel pipe cap. A hole of 76 *mm* diameter was threaded into the pipe cap where a matching threaded high alloy steel rod of the same diameter was used to connect the pipe cap to a load cell. Load cell rings were used to tighten and untighten the upper grip system. The lower plate of the MTS machine was removed, and the pipe cap was welded to a 89 *mm* thick plate using 25 *mm* size fillet weld. This plate was then gripped using the hydraulic grip system of the MTS machine. In addition, a plate was welded to the top of the extension pipe. This plate had a total of eight threaded holes with 19 *mm* diameter. Eight ASTM A325 19 *mm* diameter

structural bolts were used for this connection.

3.6 Test Procedure

The specimens were tested under crack opening displacement (COD) control; subjected to a constant COD rate of 0.05 $\mu m/sec$. All specimen were tested according to the following procedure: as soon as the peak load was reached, the specimen was unloaded then reloaded to a COD value twice that of the first peak load and unloaded again. Subsequently, unloading and reloading was performed with gradual increase of COD value each time. The loading rate in the post-peak softening regime was increased to 3 times that of the pre-peak region. The test was terminated once the specimen was completely fractured, Figure 3.14 is a photograpic representation, which normally occurred at a load level less than 1.0 KN. The load-COD, load-stroke and load-time diagrams were displayed during testing on the computer monitor. The test duration time was from 3 to 7 hours; depending on the specimen size.

3.7 Measurements

The data acquisition system has a 48 channel capacity, a sampling rate of 40 samples per second and a data scan 7000 digital card of 16 bit resolution at a range of 10 volts ± 0.3 $m.volt$, was used to record the data. A software "Labtech Notebook" was used to store the data at a rate of 1 sample per second. The load and stroke of the cross head of the machine were recorded. The deformation was monitored on both sides

of the specimens, the COD was also measured, with the help of two MTS clip gages one in each side.

Table 3.1: Specimens dimensions

Type	H	W	t	s	D	a	h	Number
Small	300	300	200	60	30	100	200	48
Large	600	600	300	90	60	200	400	12

Table 3.2: Test program Phase I

Number of specimens	Specimen type	Temp. deg. C	Aggr-egate	Crack depth(mm)	Stength MPa	Casting type
6	S	room	local	100	30	half
6	S	room	site	100	30	half
6	S	-50°C	local	100	30	half
6	S	-50°C	site	100	30	half
6	S	-30°C	local	100	30	half
6	S	-20°C	local	100	30	half
6	S	-05°C	local	100	30	half
6	S	room	local	100	30	full
4	L	room	local	200	30	half
4	L	-50°C	local	200	30	half
4	L	room	local	200	30	full

Table 3.3: Test program Phase I, II,III

Phase	Description	No. of specimens	Dimen-sions	Agg. type	Temp. deg. C	Surface condition
(I) No repair	with joint	6	large	l-stone	-50 & 20	
		6	small	gravel	-50 & 20	
		36	small	lime stone	-50 to 20	
	without joint	6	large			
		6	small		-50 & 20	
(II) with repair	epoxy-K	10	small		-50 & 20	wet
		10				dry
	epoxy-W	10				wet
		10				dry
	ultra-fine cement	10				wet
		10				
(III) Re-repair	epoxy k	5	small		-50 & 20	dry
	f-cement	5				

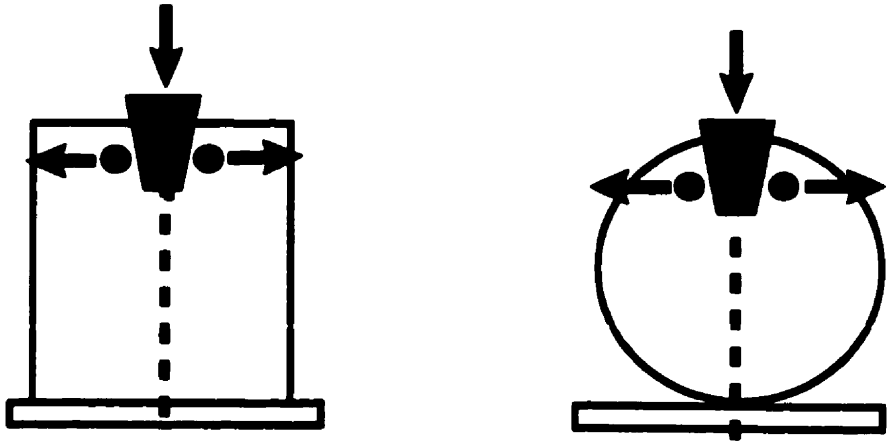

Figure 3.1: Cube and drilling wedge-splitting test

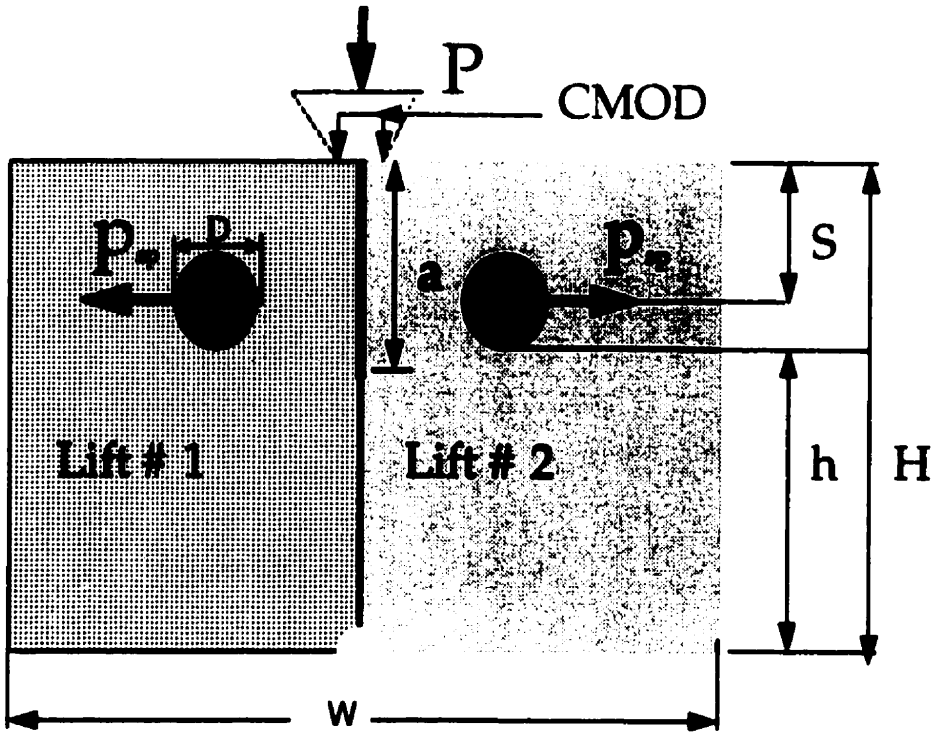

Figure 3.2: Specimen geometry for phase (I)

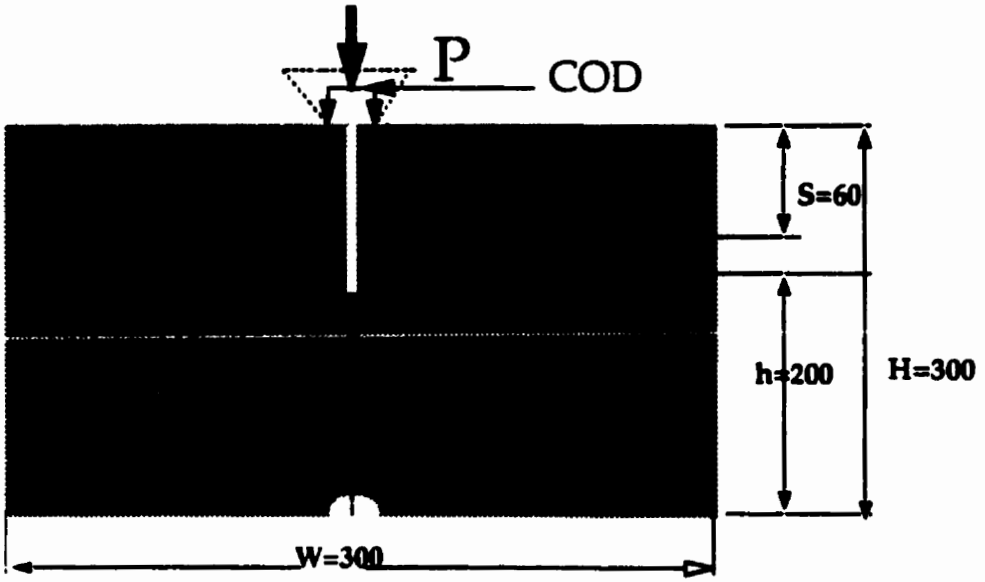

Figure 3.3: Specimen geometry for phase (I I)

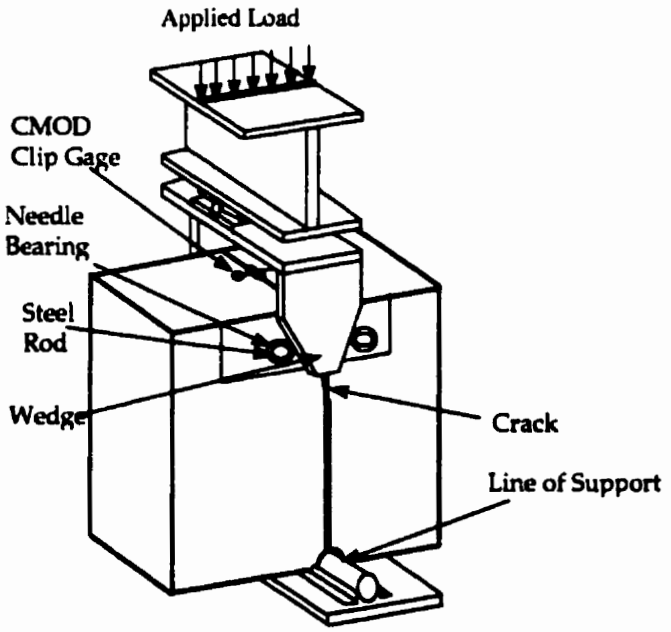

Figure 3.4: Wedge splitting test specimen setup

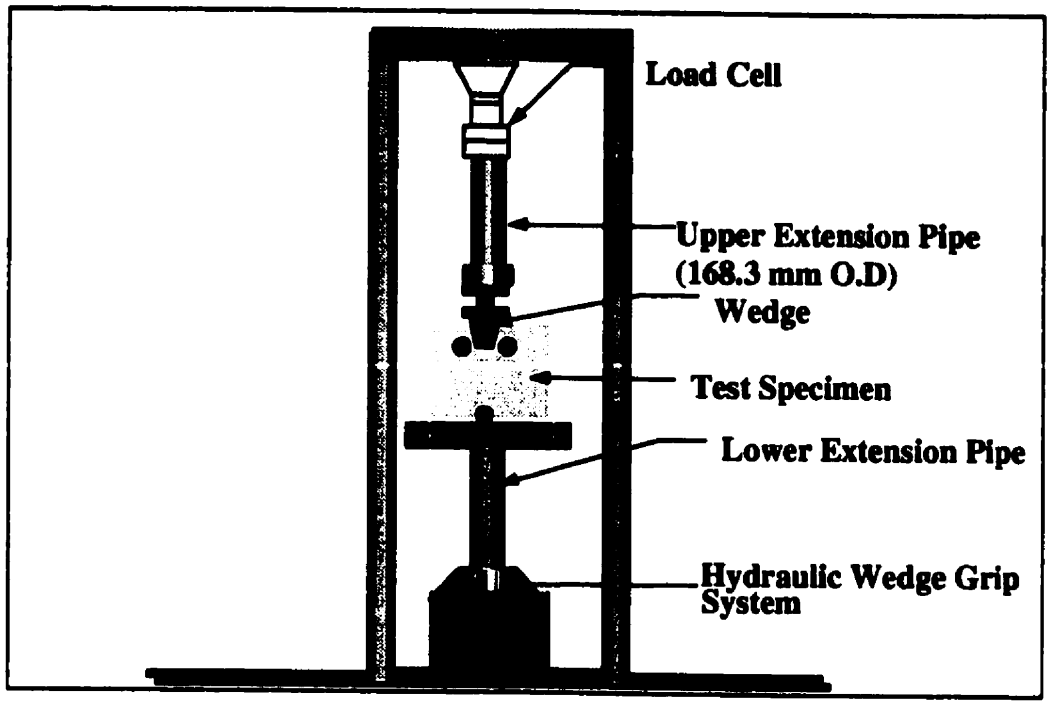

Figure 3.5: Test setup at room temperature

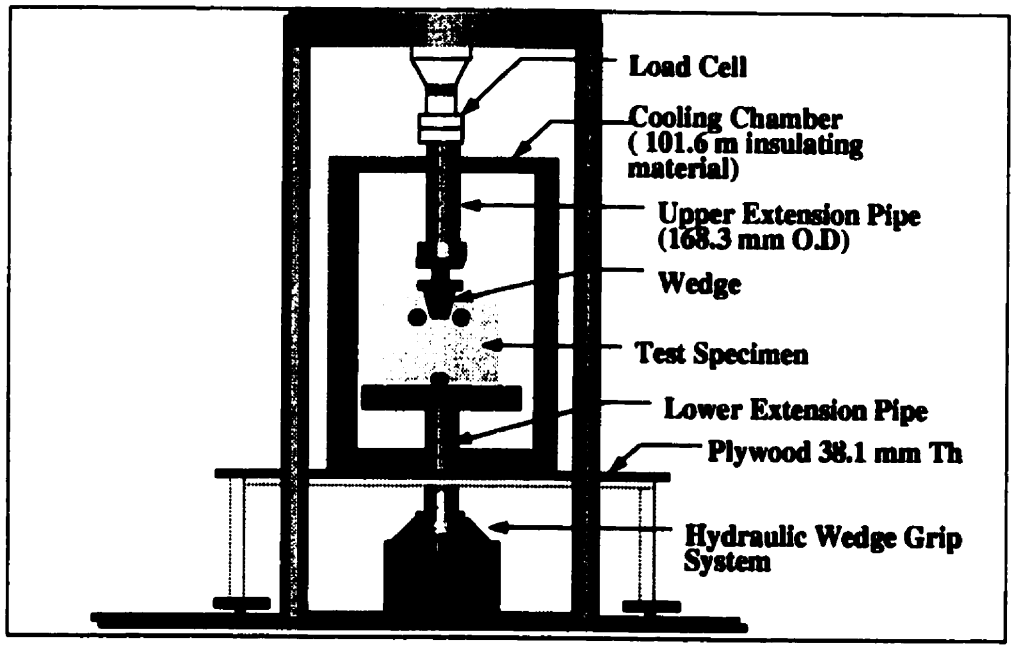

Figure 3.6: Tset setup at low temperature

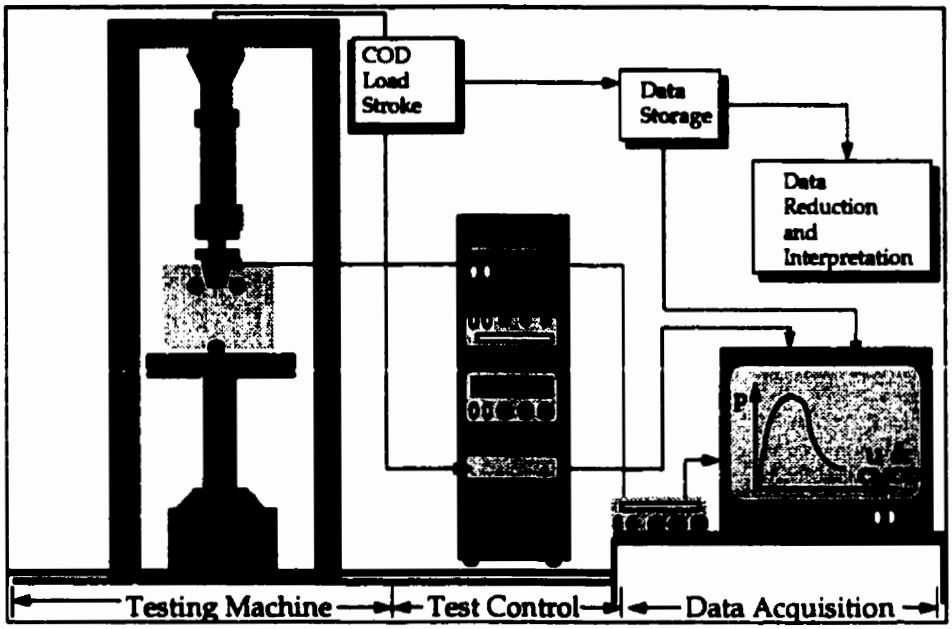

Figure 3.7: Schematic of the test setup

Figure 3.8: Test setup

Figure 3.9: Loading device

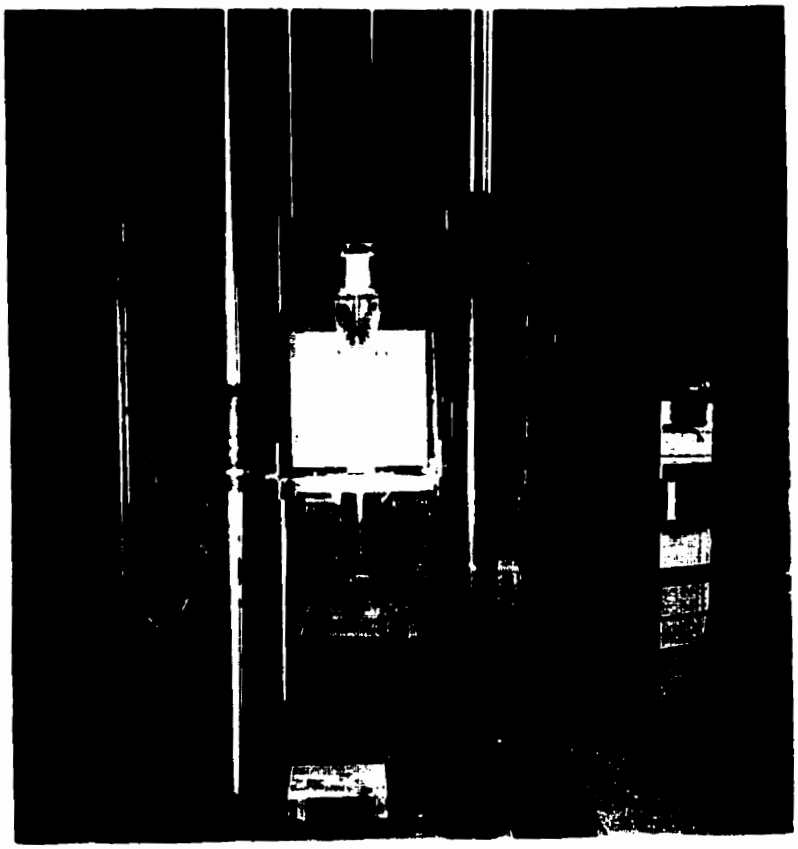

Figure 3.10: Loaded specimen at room temperature

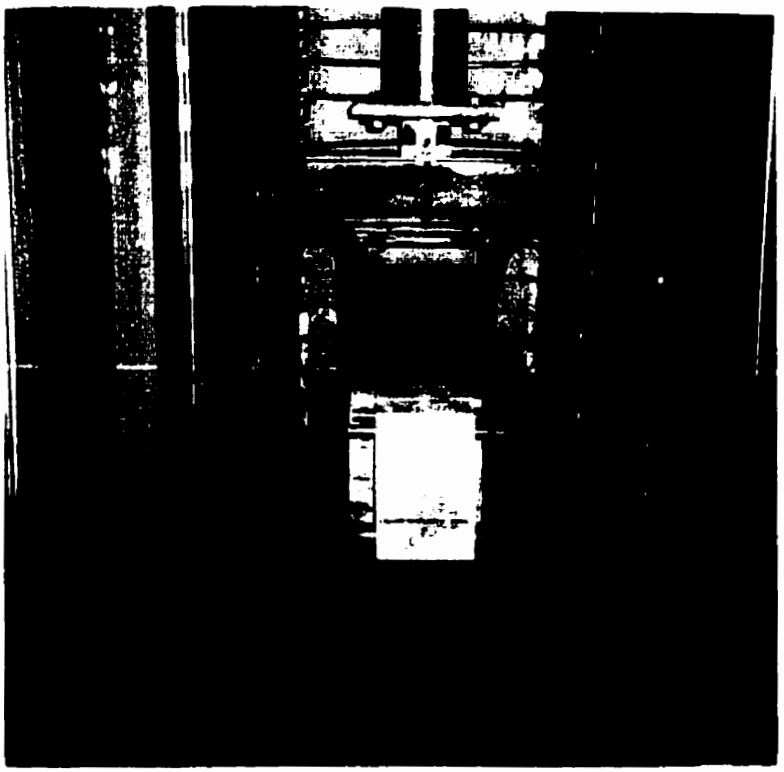

Figure 3.11: Loaded specimen at low temperature

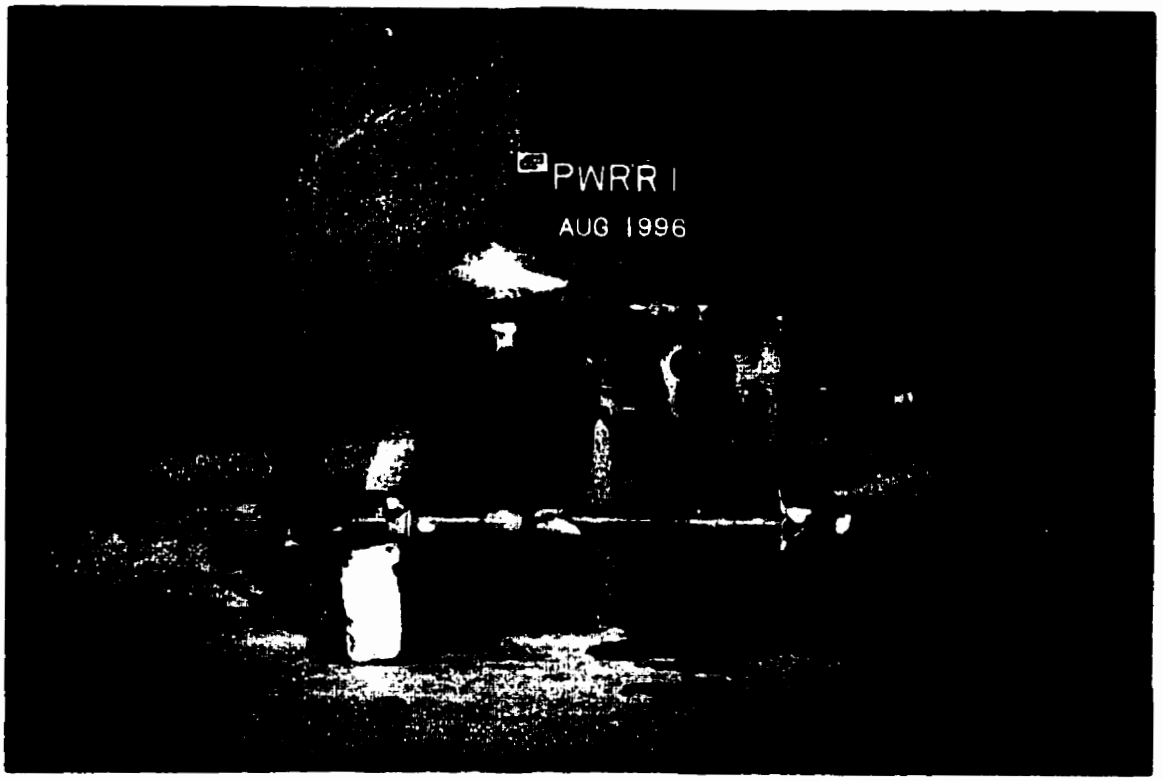

Figure 3.12: Repaired specimen using ultra-fine cement

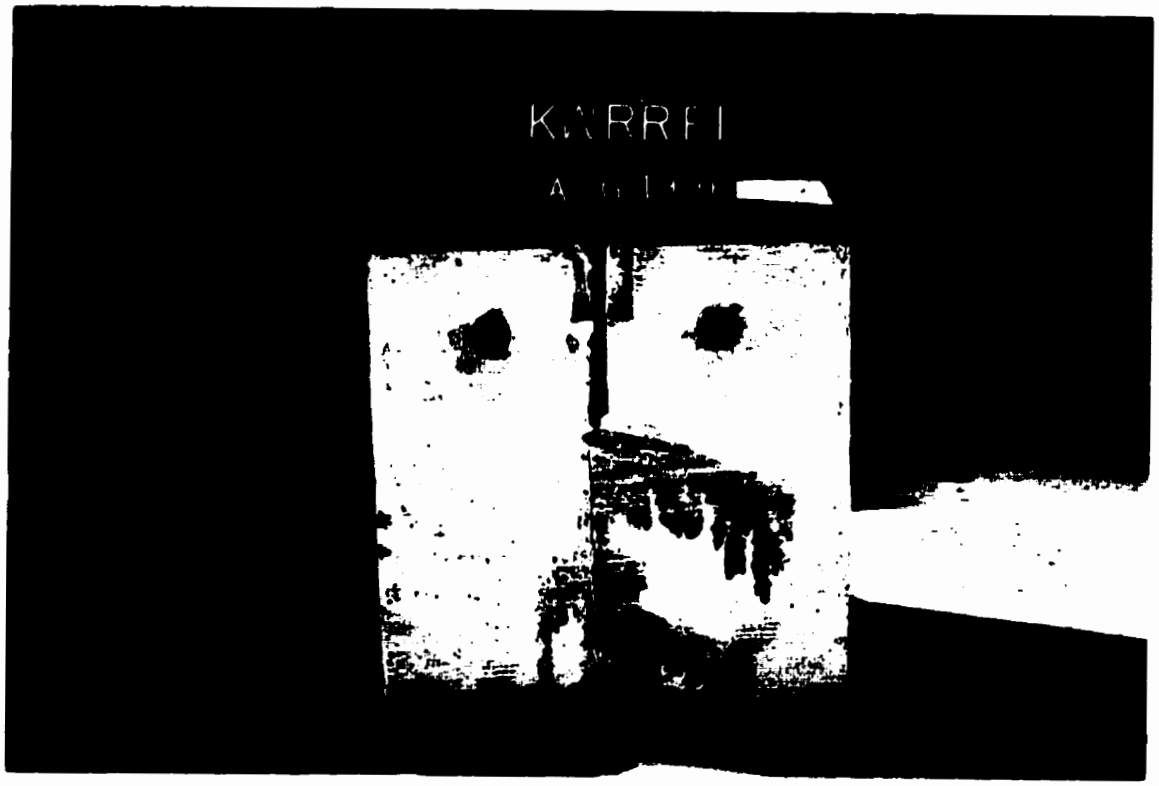

Figure 3.13: Repaired specimen using epoxy

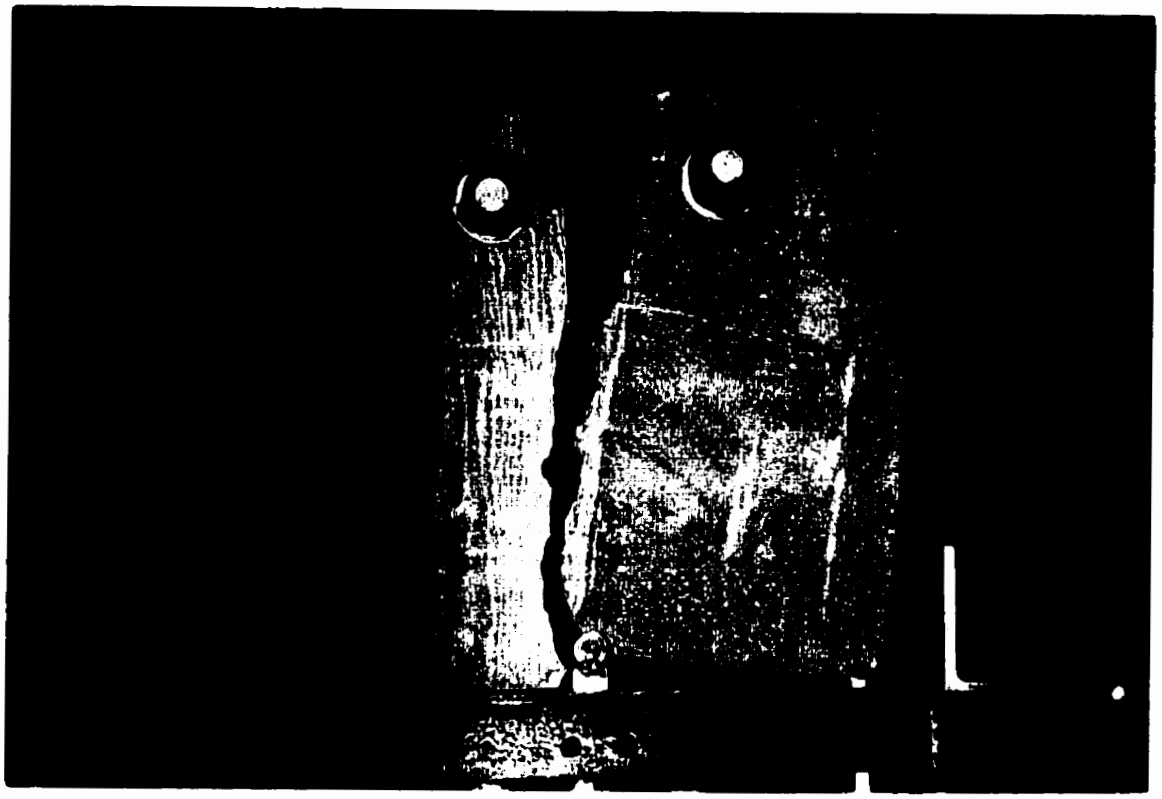

Figure 3.14: Specimen under testing

Figure 3.15: Crack monitoring

Figure 3.16: Tested specimens

Chapter 4

TEST RESULTS

4.1 Introduction

This chapter represent the descriptions and the observations of the tests results. The discussions of those results and the behavior of each set of tests will be covered in chapter six. The energy necessary to split the specimens into two halves is represented by the area under the F_{sp}-COD curve divided by the projected fracture area.

A typical F_{sp}-COD curve representative of the (ws) specimen is presented in Figure 4.1. In the F_{sp} - COD curve, both linear and non-linear responses in the ascending prepeak branch and a descending postpeak branch can be observed. The fracture toughness K_{IC} is evaluated using the compliance method, with an effective crack length that is larger than the true crack length and shorter than the true crack length plus the fracture process zone. Before the test program started, six specimens were used as a pilot test to obtain the appropriate loading rate, also to avoid any problem in the setup.

4.2 Results of Phase I

4.2.1 Description

The central focus of this part of the experimental program is to identify the effect of residual strain accumulation in the vicinity of adjacent concrete layers due to differential curing histories. Wedge splitting specimens, cast in one and two stages are tested at room and low temperatures. In addition, the size effect is studied using two different sizes of specimens. Also, two types of aggregate (limestone and crashed granite) were used to study the effect of aggregates.

4.2.2 Specimens with joints

Small specimens

A total of eighteen tests were performed for this test series. The first six specimen were used as pilot tests to determine the appropriate crack opening displacement (COD) rate which produces a stable test, and to observe if there are any problems related to the setup. Because of the different rates used in the first six specimens, the results from those tests were ignored.

Six specimens were tested at room temperature. From Figure 4.2, linear behavior of the F_{ps}-COD curve was observed until approximately 80% of the maximum load was reached, with an average splitting force value of 11 KN. The loading rate in the postpeak softening regime was increased to 4 times that of the prepeak region. The test was terminated once the specimen was completely fractured, which normally

occurred at a load level of less than 1.5 KN. The F_{ps}-COD, load versus vertical displacement and load versus time curves were displayed during testing on the computer monitor.

Six other specimens were tested at -50°C, Figure 4.3 shows a typical response of such specimens. The same behavior as the specimens tested at room temperature were observed, with a maximum splitting force of average value 26.3 kN. A more brittle behavior was observed at low temperature. Also, the postpeak softening regime has the same behavior as the room temperature one, with complete splitting of the specimens occurring at a load level of less than 2.5 KN. The loading rate in the postpeak softening regime was increased to five times that of the prepeak region.

Twelve specimens were tested at different temperatures, Figures 4.4 and 4.5. These temperatures lay in the range between -50°C and room temperature, (- 5, - 20 and -30 °C). These sets of tests were carried out to determine the gradual effect of the temperature.

Also another six specimens with different aggregate types, Figure 4.6 and Figures 4.27-4.28 are a photograpic representation, were used to study the aggregate effect on the fracture properties. In all of the above tests, the crack propagated along the interface of the joint.

Large specimens

These tests were carried out to study the size effect. Eight specimens were tested, four for each temperature. At room temperature, Figure 4.7, linear behavior of the F_{ps}-COD curve was observed until the load reached 75-85% of its maximum value,

with an average splitting force of 28 KN. The loading rate in the postpeak softening regime was increase to 3 times that of the prepeak region. The test was terminated once the specimen was completely fractured, which normally occurred at a load level of less than 2 KN. The same behavior was observed at low temperature (-50 °C), Figure 4.8, with nonlinearity starting around 60-70% of the maximum load, at a value of 64 KN. A complete splitting of the specimens occurred at a load level of less than 3 KN. The loading rate in the postpeak softening regime was increased to three times that of the prepeak region.

4.2.3 Specimens without joints

Small specimens

A total of twelve specimens were tested under this test series, six of which were tested at room temperature. Typical response is shown in Figure 4.9. In all tests, the initial linear elastic response is followed by pre-peak non-linearity at about 80% of the maximum load. The test has a maximum average splitting force of 14.7 KN.

A softening part where the crack gradually propagates with increased displacement up to three times that of the prepeak region, and reduced load follows. The test was terminated once the specimens were completely fractured, Figures 4.25-4.26.

Six specimens were tested at -50°C. Typical response is shown in Figure 4.10. The same behavior as room temperature specimens was observed with considerable increase of strength. The test has a maximum average splitting force of 27.7 KN and a maximum applied load of 14.7 KN. The loading rate in the postpeak softening

area was increased to five times that of the prepeak region with complete fracture at a load level of less than 2.5 KN.

4.2.4 Stiffness degradations

The stiffness of the specimen decreases with each loading cycle. If the relative stiffness k/k_o, Figures 4.11 and 4.12, is plotted versus the total deformation which has been reached on the envelope curve, a very steep decline in stiffness can be seen. At a total deformation of 20 μm the stiffness is only 30% of its original value. Various stages can be distinguished from the curves: elastic elongation of the specimen, small crack opening, elastic unloading and crack closure. From the slope of the lines it can be said that in each cycle the cracked zone increase in length and that the crack faces no longer match.

4.3 Results of Phase II

4.3.1 Description

This part of the experimental program was to examine and obtain information on the fracture behavior of repaired cracks at the horizontal interface between two adjacent lifts of concrete using different types of repair material, particularly on the influence of low temperature and the moisture condition of concrete. Such information is important especially for repairs taking place in cold climate areas. The same test procedure used in phase I was followed..

4.3.2 Dry condition

In all tests, the initial linear elastic response is followed by pre-peak nonlinearity. This is caused by the formation of microcracks ahead of the macrocrack. A post-peak part where the crack gradually propagates with increase displacement and reduced load. Table 4.2, represent the average amount of fracture energy released.

Epoxy-K

A dark purple color of the surface represents a strong bond of the dry condition. The same behavior as the previous tests was observed. In the case of room temperature the pre-peak nonlinearity starts at approximately 90% of the maximum load. The maximum average splitting force is 25 KN, see Figure 4.13. At -50°C, Figure 4.14, the maximum average splitting force reached a value of 33 KN. The load rate in the postpeak softening regime was increased to four times in the case of low temperature and to three times in the case of room temperature testing.

Epoxy-W

A yellow color of the surface represent a strong bond of the dry condition, Figure 4.32. Similar behavior was observed as with epoxy K. The pre-peak nonlinearity starts at approximately 80% of the maximum load. In the case of room temperature, the maximum average splitting force is equal to 22 KN. At -50°C, the maximum average splitting force was 29 KN. The load rate in the postpeak softening regime was increase to three times in the case of low temperature, Figure 4.15, and to five times in the case of room temperature, Figure 4.16.

Ultra-fine cement

In the ultra fine cement, strong bond has a green color after failure and a weak bond has scattered green spots. There was no difference observed between the behavior of ultra fine cement in case of dry and wet conditions, Figures 4.17-4.18 and Figure 4.30 is a photographic representation. In both cases, and when the load dropped to approximately 40-45% of its maximum value, no more cycles was needed and slow crack propagation was observed.

4.3.3 Wet condition

In the wet condition specimens were kept immersed under water for 24 hours before taken out and repaired. A total of thirty specimens were repaired in this test series. The $F_{sp} - COD$ curve was linear up to approximately 90% of the maximum load, followed by pre-peak nonlinearity. The amounts of fracture energy released are given in Table 4.2.

Epoxy-K

The distinctive light purple color on the surface points to a weak bond, Figure 4.31. At low temperature, the bond becomes quite strong. In room temperature, the bond showed a decrease in strength. The pre-peak nonlinearity starts at approximately 65% of the maximum load. The maximum average splitting force of 11.3 KN in the case of room temperature. At -50°C, the maximum average splitting force has a value of 41 KN. The load rate in the postpeak softening regime was increased to five times

in the case of the low temperature, Figure 4.20, and up to 3 times in the case of room temperature, Figure 4.19.

Epoxy-W

The bond is weak and has a white/yellow color. At low temperature, the bond becomes weak and has a crispy layer which is difficult to remove using a water jet. Also, this layer is weak under tension load (if removed in a direction normal to the surface). The pre-peak nonlinearity start at approximately 85% of the maximum load, Figures 4.21 and 4.22. The maximum average splitting force of 11 KN in the case of room temperature. At -50°C. the maximum average splitting force has a value of 2.3 KN. At room temperature and after the third cycle, theF_v-COD curve was dropping slowly and crack opening displacement was increased up to 4 mm where a complete failure occurred.

4.4 Results of Phase III

A total of twelve specimens were cleaned and re-repaired using ultra fine cement and epoxy K. All specimens were tested at room temperature. Both materials showed decreasing strength with considerable variation in the results, Figure 4.23. Ultrafine-cement behavior were characterized by one cycle failure, i.e., the test needs just one cycle to be completed with no sudden failure occurring.

4.5 Figures

Table 5.1: Results of phase I

Specimen size	Casting type	Temperature deg. C	Maximum load (kN)	Max. split. load (kN)	Fracture energy (N/m)
small	full	room	7.9	14.7	231
small	full	- 50	22.8	42.5	341
small	half	room	6.1	10.9	95
small	half	- 50	14.1	26.3	155
large	half	room	14.83	27.7	113

Table 5.2: Results of phase II

Repair material	Condition	Temperature deg. C	Maximum load (kN)	Load (kN) Max. split.	Fracture energy(N/m)
epoxy K	dry	room	13.5	25.2	125
epoxy K	dry	-50	-	-	-
epoxy K	wet	room	8.4	15.7	174
epoxy K	wet	-50	17.6	36	209
epoxy W	dry	room	11.9	22.2	135
epoxy W	dry	-50	14.5	27	-
epoxy W	wet	room	5.8	10.9	77.5
epoxy W	wet	-50	2.15	4.1	47.5
f-cement	dry	room	2.52	4.7	44.2
f-cement	dry	-50	2.41	4.5	23
f-cement	wet	room	2.62	4.9	42.7
f-cement	wet	-40	2.2	4.1	25.5

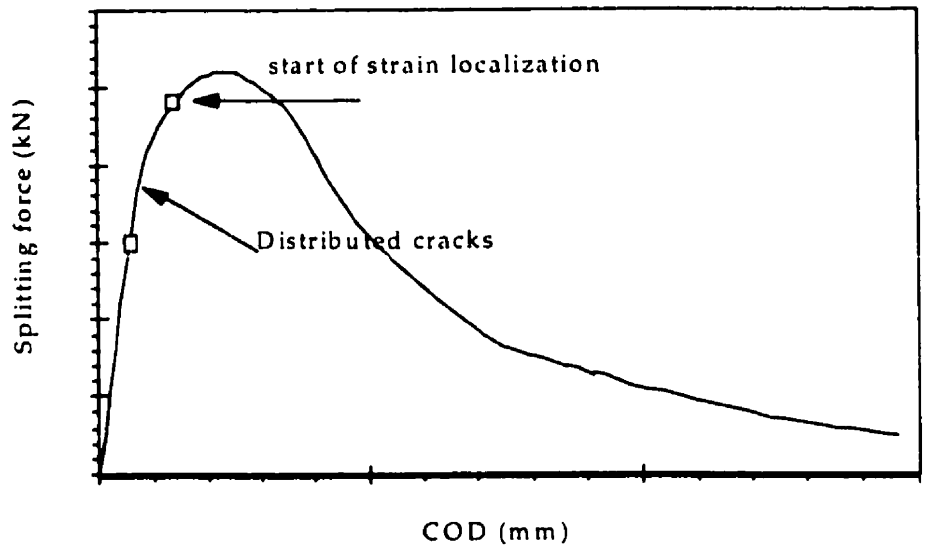

Figure 4.1: Typical splitting force versus COD curve

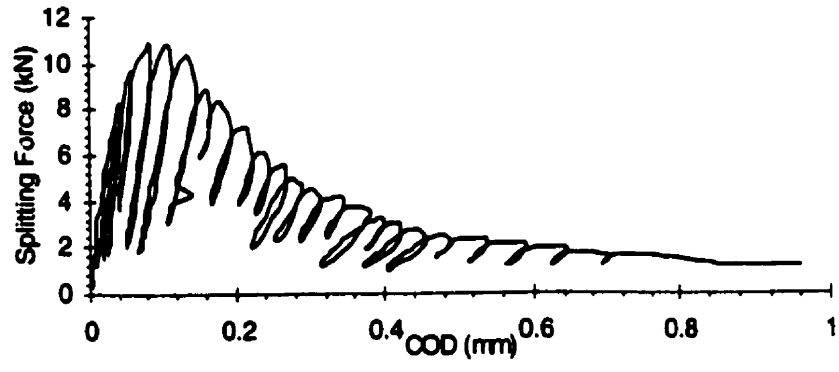

Figure 4.2: Response of specimen cast in two blocks at room temperature

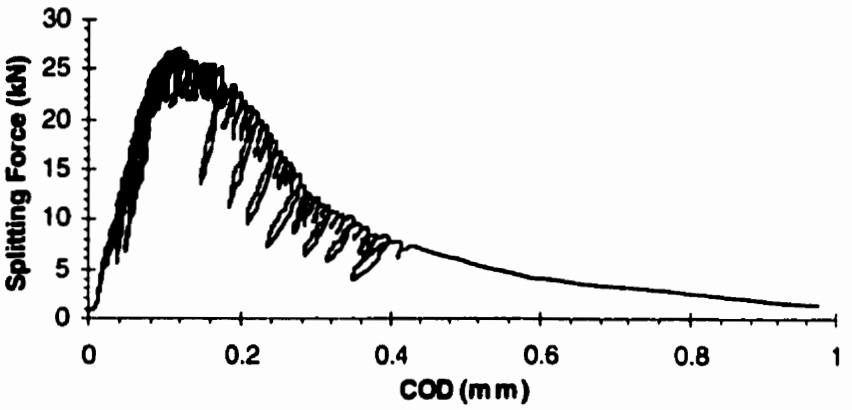

Figure 4.3: Response of specimen cast in two blocks at - 50 °C

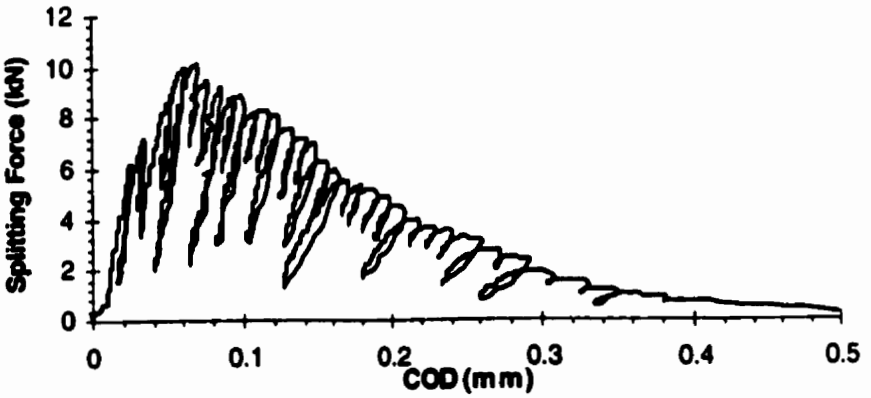

Figure 4.4: Response of specimen cast in two blocks at -5 °C

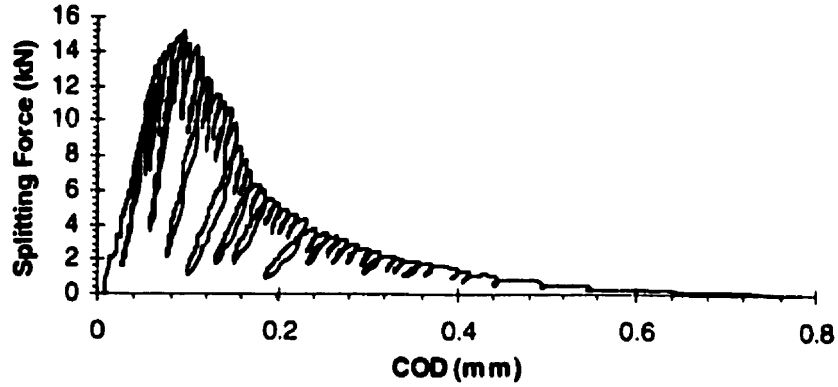

Figure 4.5: Response of specimen cast in two blocks at -20 °C

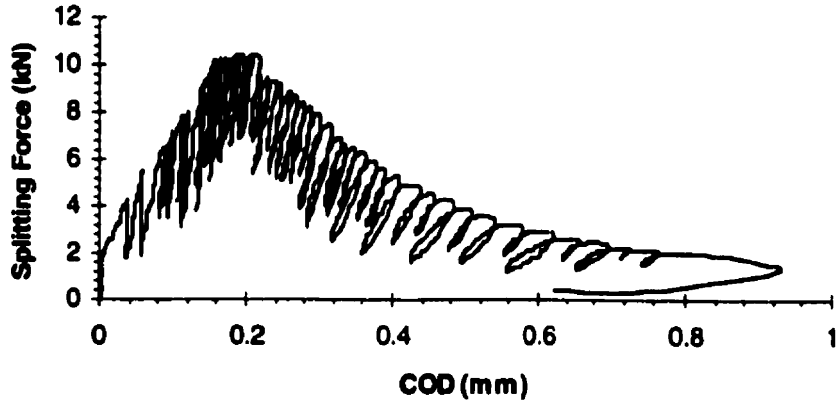

Figure 4.6: Specimen with site aggregate at room temperature

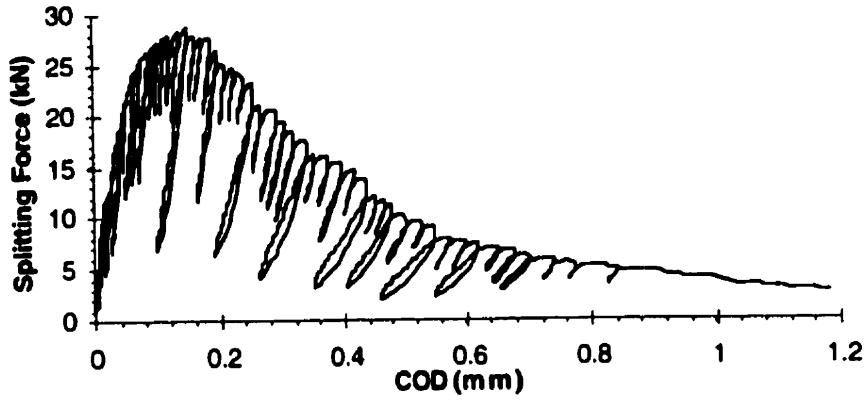

Figure 4.7: Response of large specimen cast in two blocks at room temperature

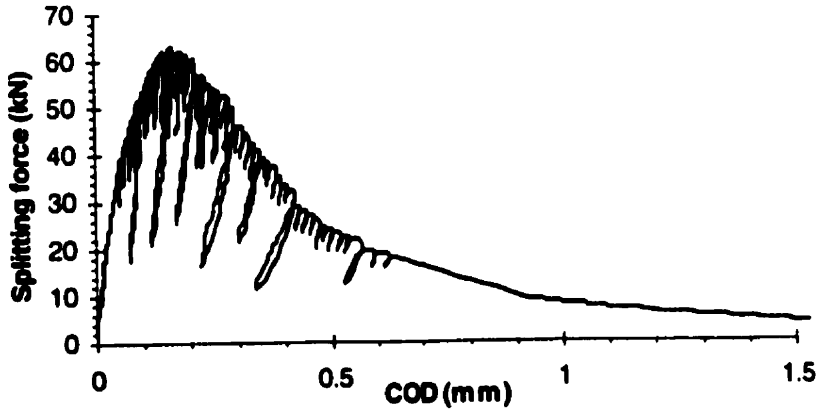

Figure 4.8: Response of specimen cast in two blocks at -50 °C

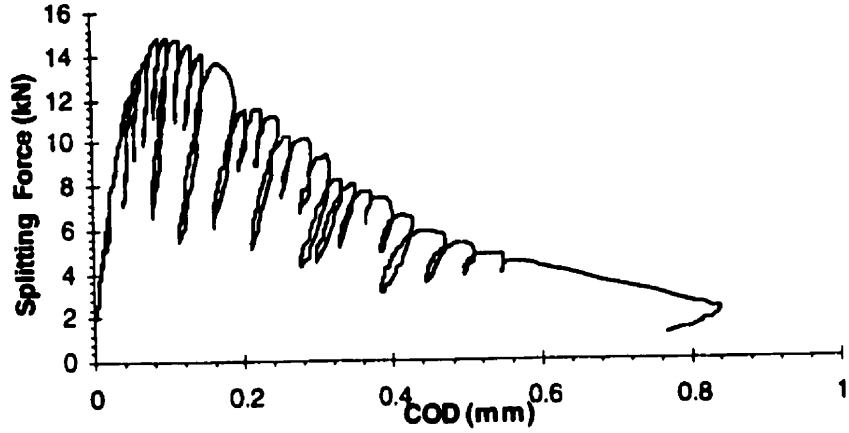

Figure 4.9: Response of specimen cast in one block at room temperature

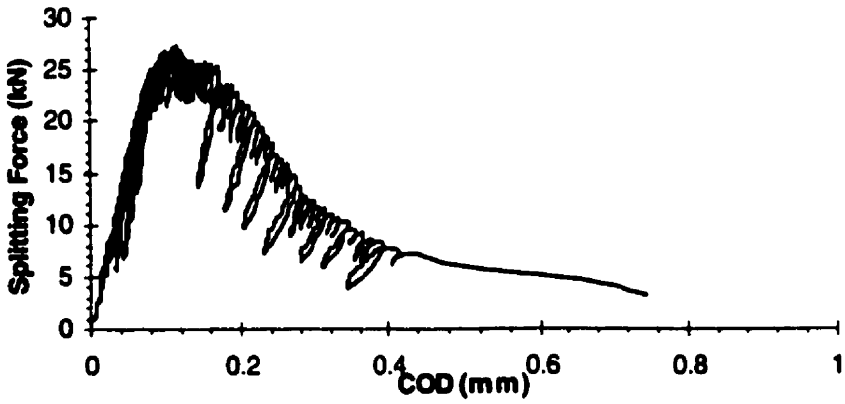

Figure 4.10: Response of specimen cast in one blocks at -50 °C

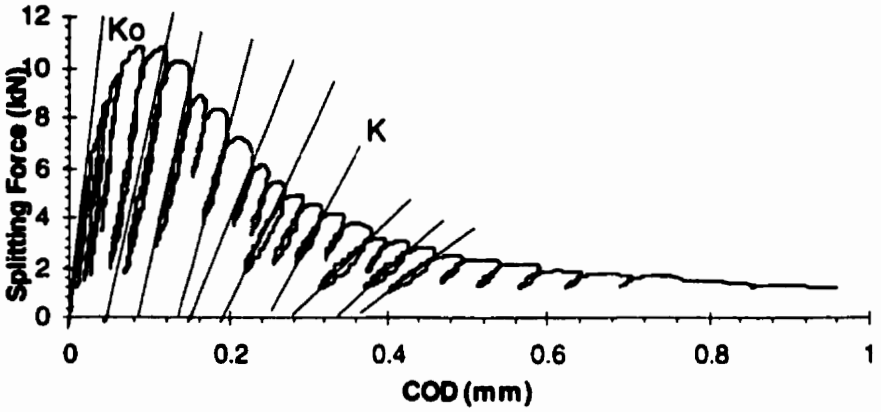

Figure 4.11: Stiffness degradation

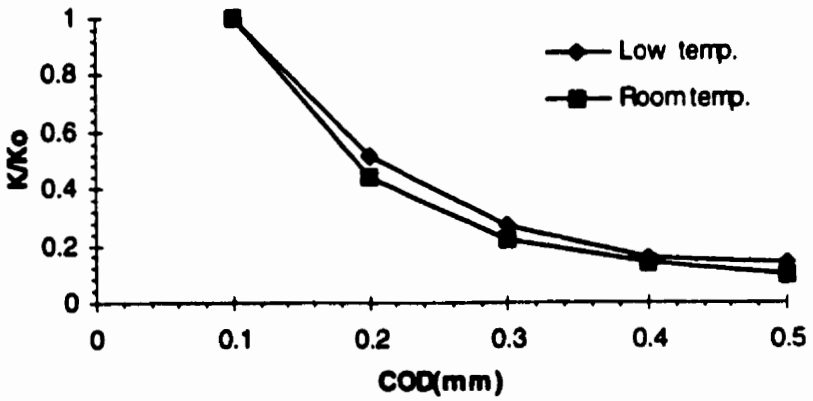

Figure 4.12: Ratio of initial to current stiffness K/K_o as a function of COD

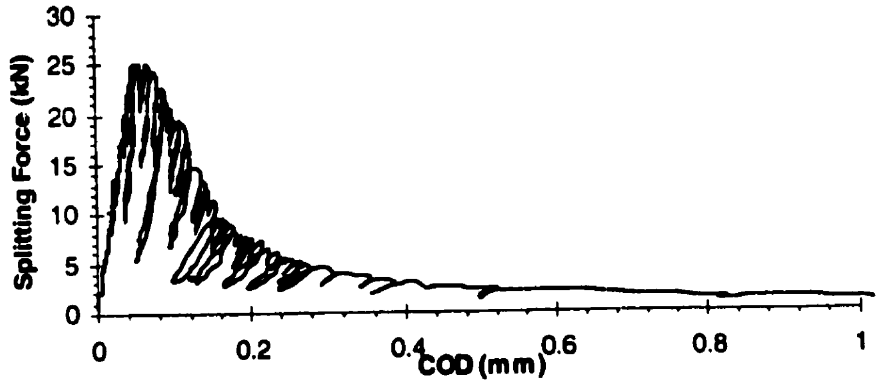

Figure 4.13: Response of epoxy-K at room temperature in dry condition

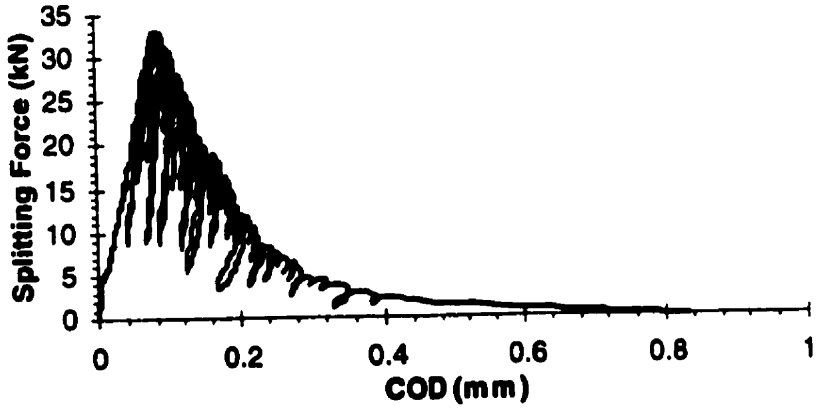

Figure 4.14: Response of epoxy-K at low temperature in dry condition

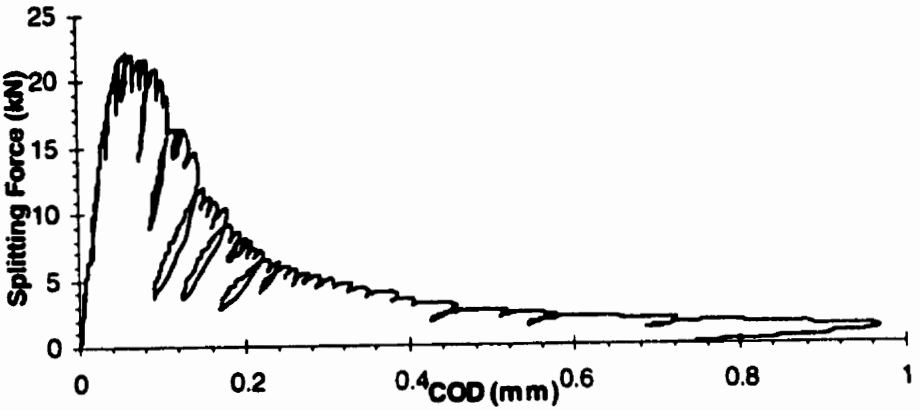

Figure 4.15: Response of epoxy-W at room temperature in dry condition

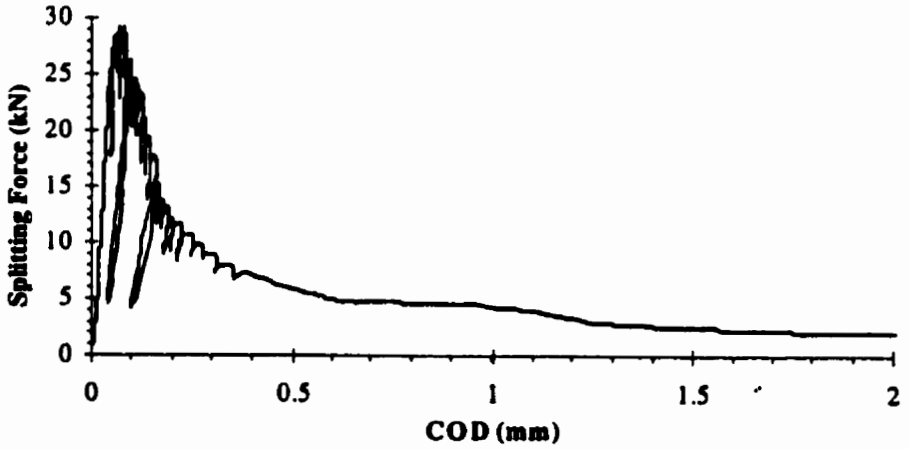

Figure 4.16: Response of epoxy-W at low temperature in dry condition

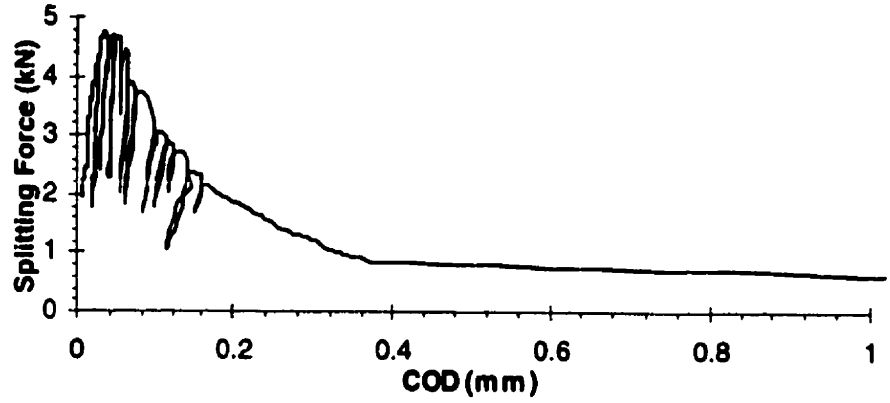

Figure 4.17: Response of ultra-fine cement at room temperature in dry condition

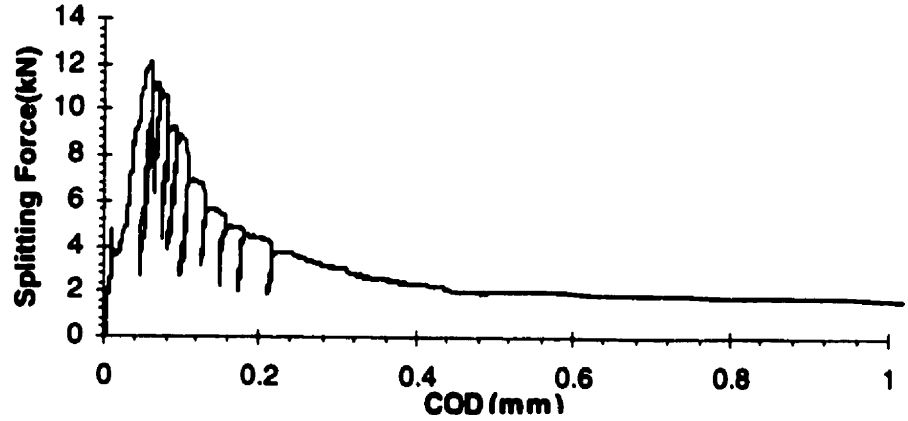

Figure 4.18: Response of ultra-fine cement at low temperature in dry condition

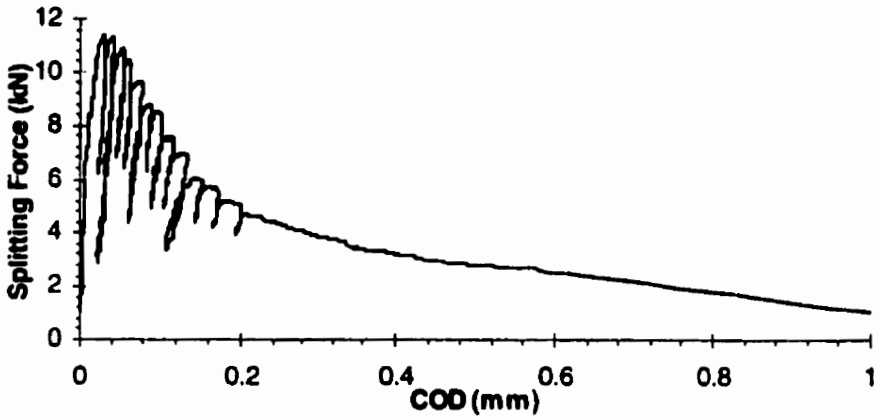

Figure 4.19: Response of epoxy-K at room temperature in wet condition

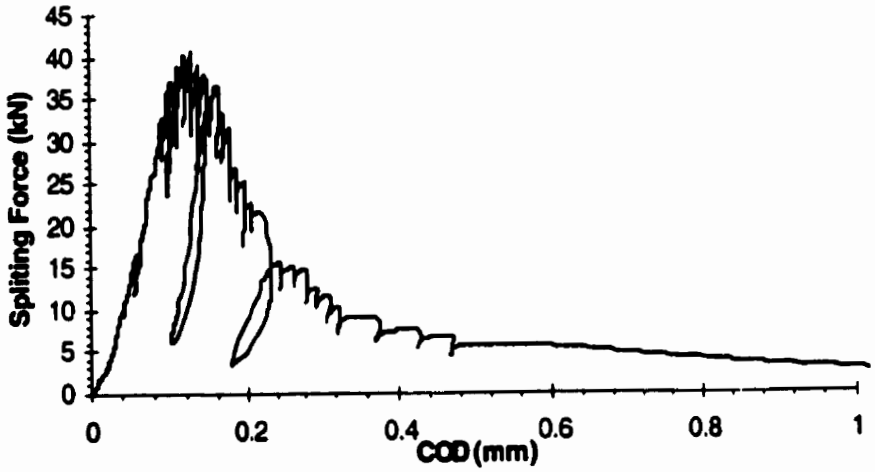

Figure 4.20: Response of epoxy-K at low temperature in wet condition

Page missing from library's copy

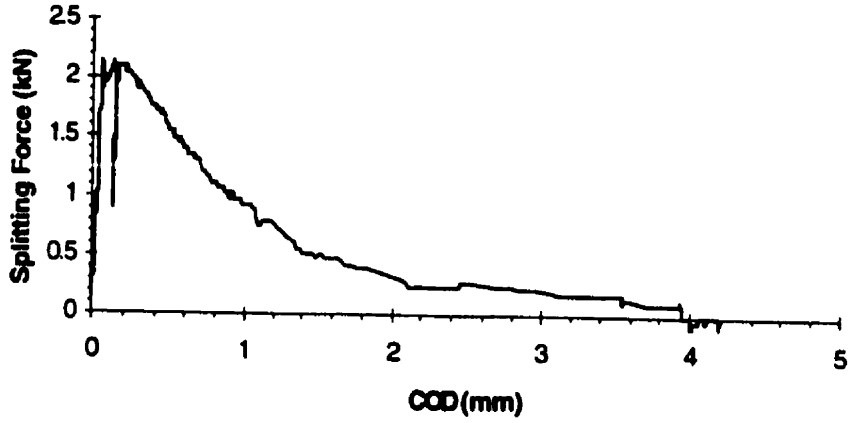

Figure 4.22: Response of epoxy-W at low temperature in wet condition

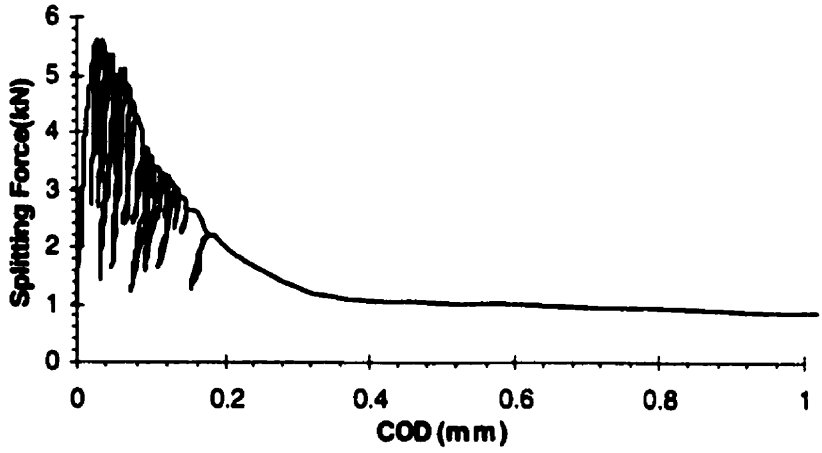

Figure 4.23: Response of ultra-fine cement at room temperature in wet condition

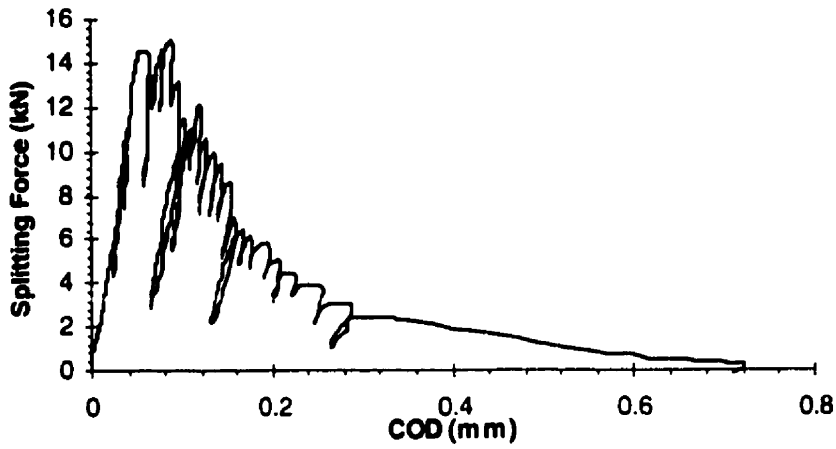

Figure 4.24: Response of ultra-fine cement at low temperature in wet condition

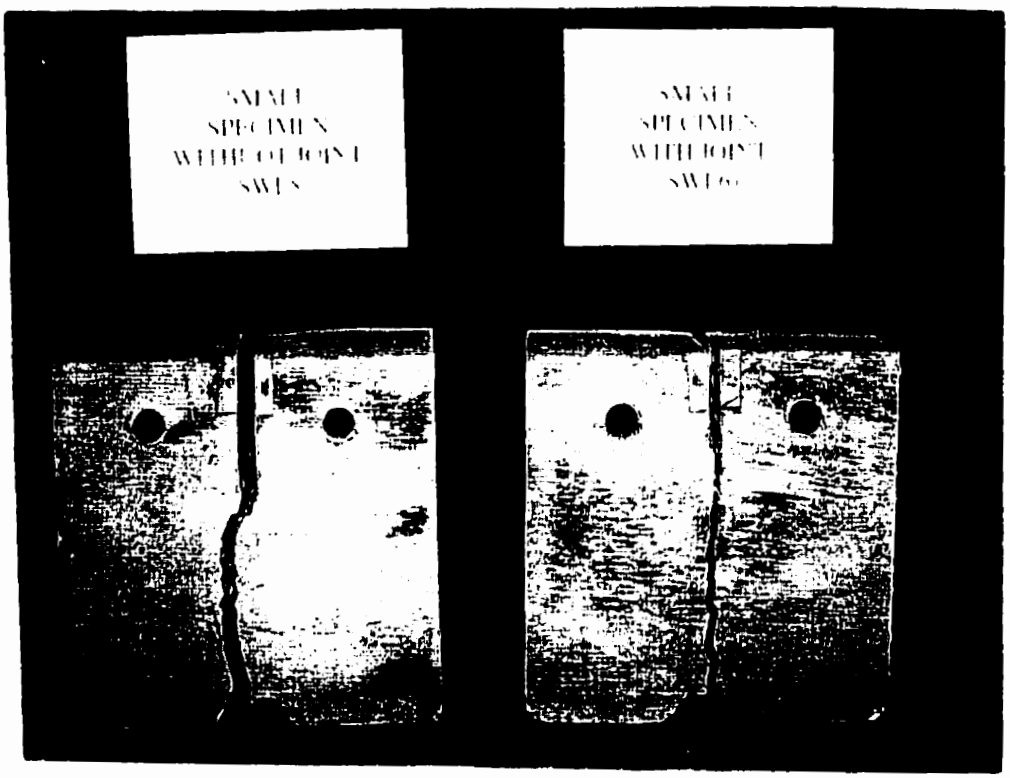

Figure 4.25: Test specimens with and without joint

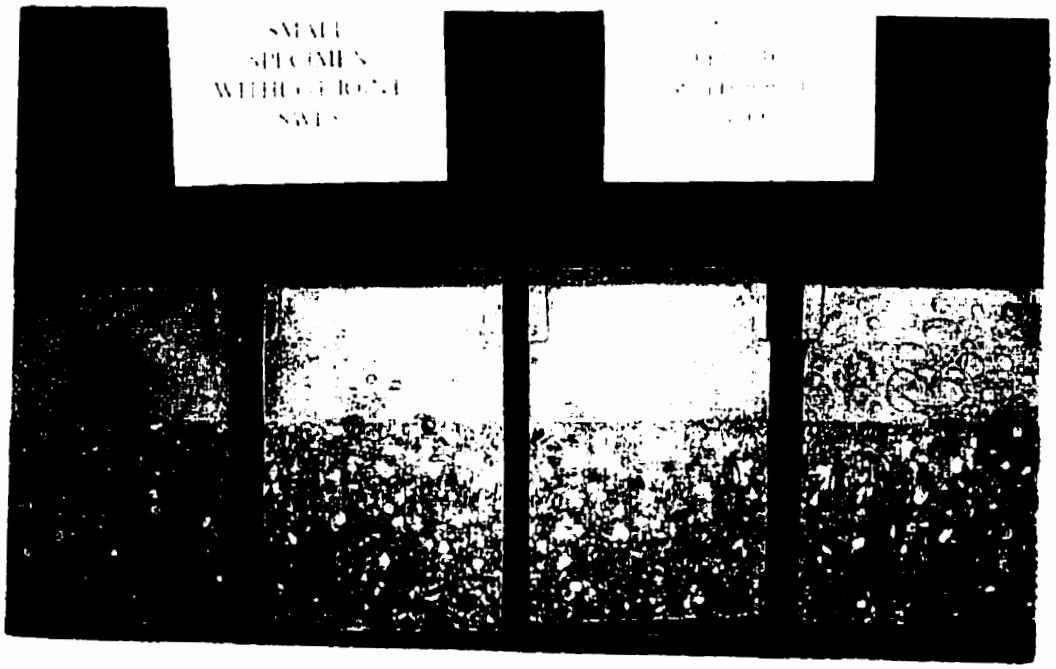

Figure 4.26: Test specimens with and without joint

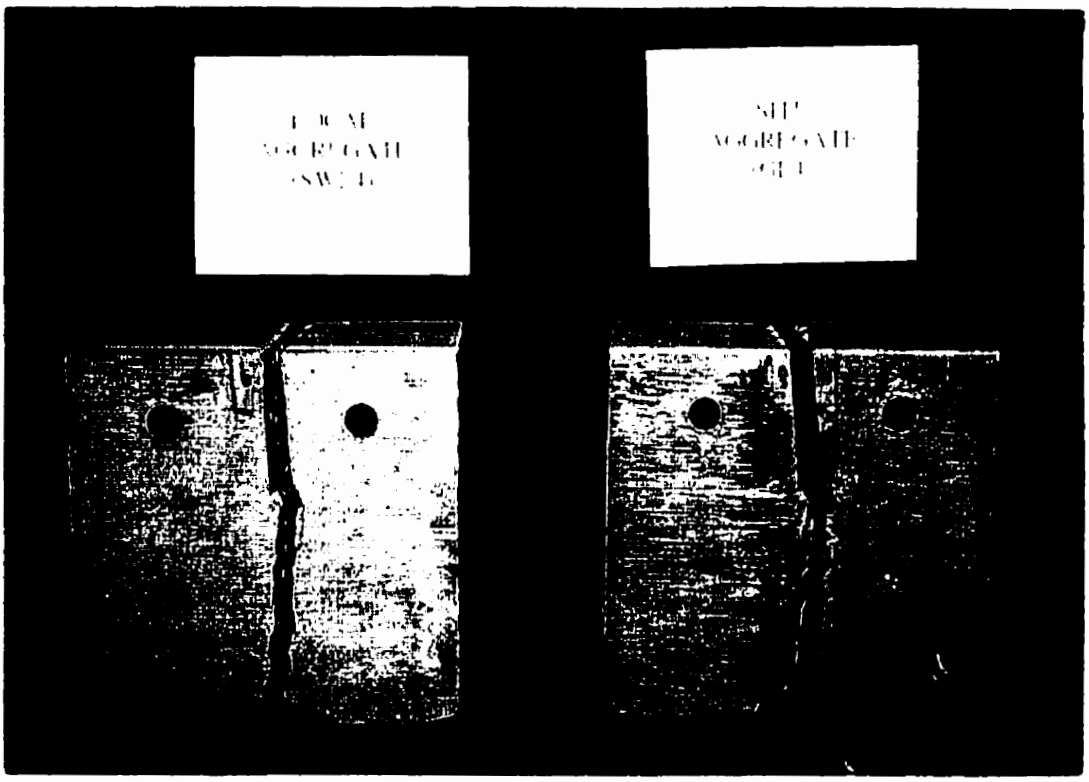

Figure 4.27: Tested specimens using different types of aggregate

Figure 4.28: Tested specimens using different types of aggregate

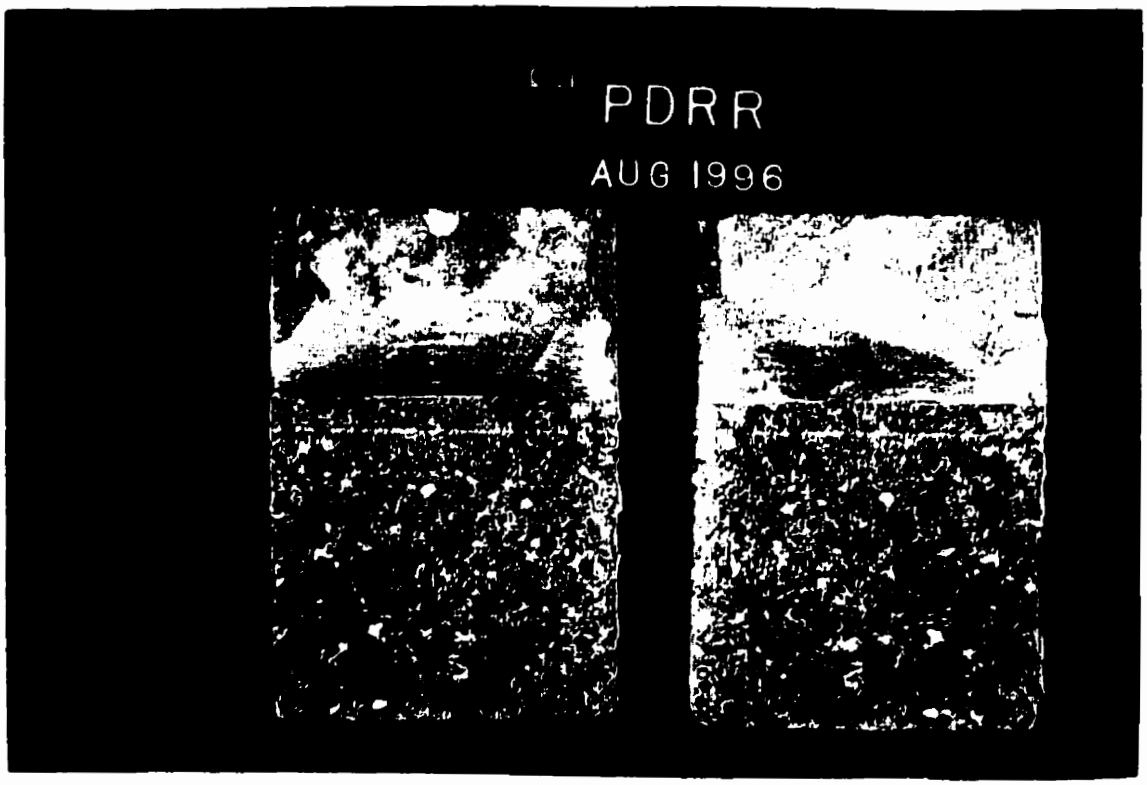

Figure 4.29: Cracked surface through fine cement material

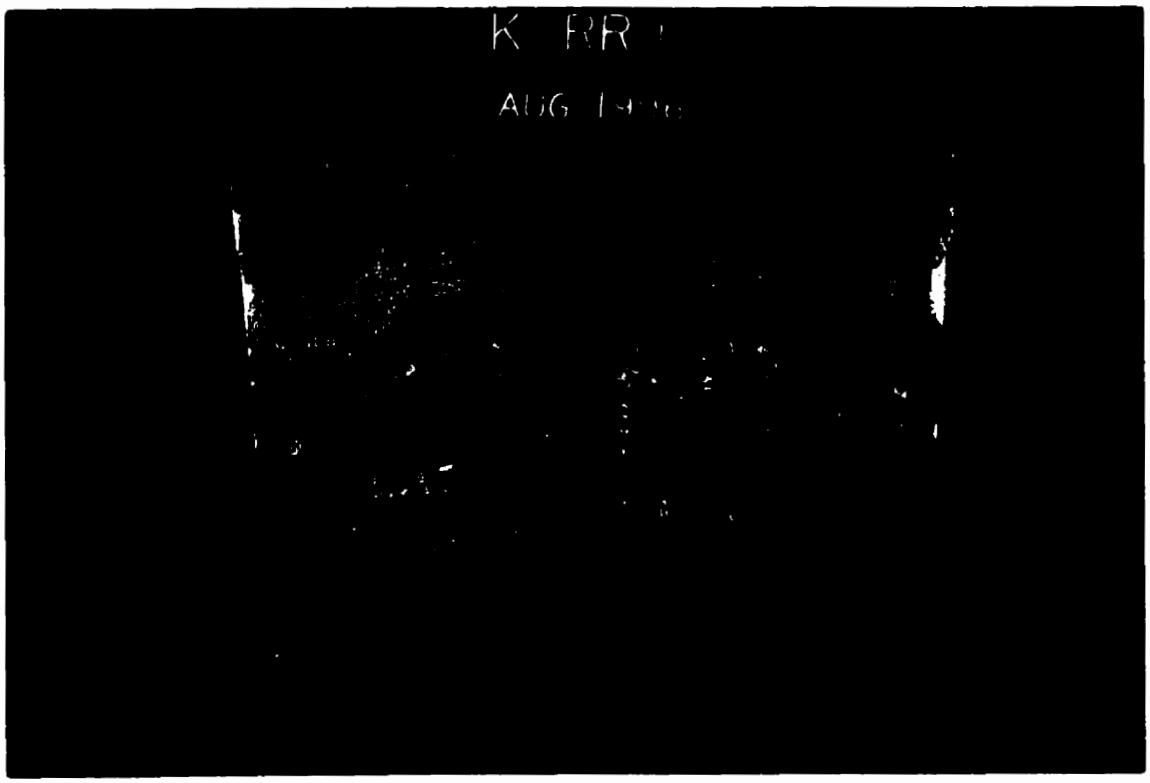

Figure 4.30: Cracked surface through epoxy-K

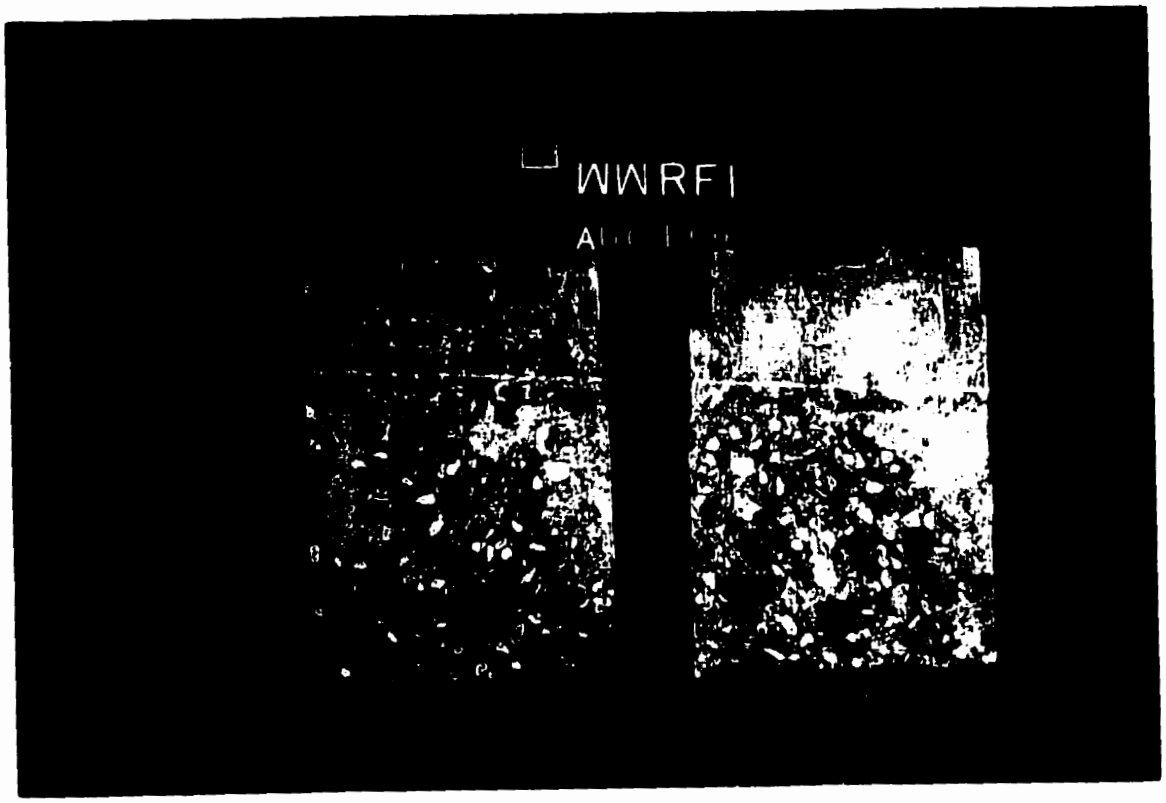

Figure 4.31: Cracked surface through epoxy-W

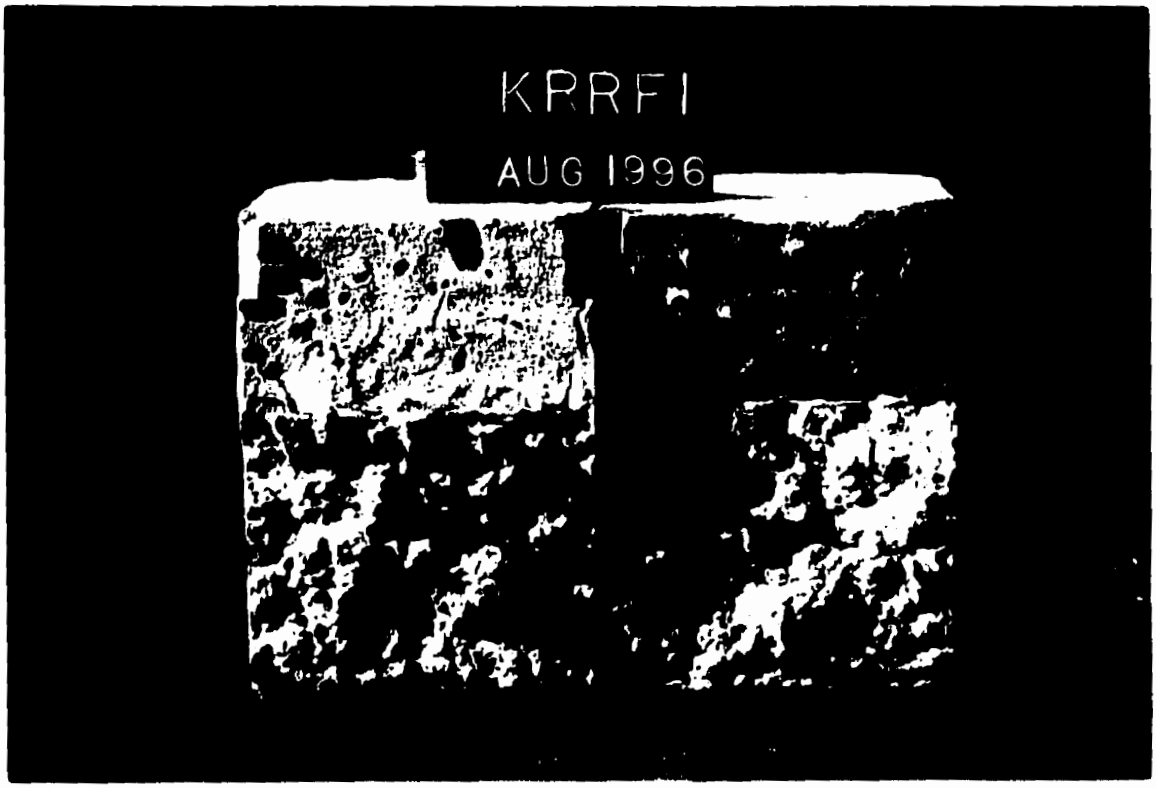

Figure 4.32: Typical low temperature test

Chapter 5

DISCUSSION OF RESULTS

5.1 Phase I

All tests show initial linear elastic response, with an increase in applied tensile force, and microcracks form at the mortar/aggregate interfaces leading to the pre-peak non-linearity. The transition from linear to nonlinear response is primarily governed by the extent of available interfaces. A softening part follows where the damage is localized to a narrow zone. The eventual failure of the material takes place along this localized damage zone which forms the dominant macrocrack. The scattered microcracks elsewhere in the material no longer play a major role in determining the response of the material. The role belongs only to the macrocrack. An immediate advance of the macrocrack is prevented by some mechanisms, the major among these mechanisms is the so called 'bridging mechanism' which breaks the continuity of the dominant macrocrack so that the discontinuous segments can no longer grow unstably. The bridging is provided by the interlocking of hard phase particles, by the strain

hardening capacity of unbroken ligaments between macrocrack and any voids which attract the macrocracks. It is however worth noting that the feed-back control signals play a big role in recording the tension softening behavior. This feed-back control signals are provided by displacement control test and not by the decreasing tensile force

5.1.1 Effect of joints

Figure 5.4 represents the effect of simulated joint on the material response at room temperature, a decrease in fracture energy of 58% and a reduction in splitting force of 30% was observed. Figure 5.5 represents the effect of simulated joint on the material response at -50°C temperature, again a decrease in fracture energy of 54% and a reduction in splitting force of 38%. This behavior is due to an unavoidable flow of moisture and heat across the interface during construction time, because the new concrete initially exhibits processes of hardening, and subsequently holds up external climatic action which do not directly reach the deeper parts of old concrete.

5.1.2 Effect of temperature

Specimen dimensions were selected to enable a comparison with results obtained by other researchers. During the test, the vertical load, vertical displacement, time and the crack opening displacement (COD) were measured. The fracture energy G_F for each size and temperature is obtained by dividing the area under the splitting force versus COD curve by the ligament area (ligament length x thickness). Averages of

the experimental results are summarized in Tables 4.1 and 4.2 with errors of $\mp 8\%$. In general, there is a large increase of fracture energy with decrease in temperature. It appears that structures are safer at low temperature, from a fracture point of view, than structures operating at room temperature when subjected to the same loading. Also, the tensile strength of concrete increases considerably with the reduction in temperature, the main cause of this increase being exerted by the moisture content. Water saturated concrete may obtain a relative strength increases at -50°C of 200% or more when compared to room temperature. This is in agrement with the results obtained by Elices *at. el.* (1987) in his three point bending beam test.

Specimens with joints

Small specimens A total of thirty six tests were preformed. The response of small specimens cast in two blocks at - 50°C and room temperature is represented in Figure 5.6. There is an increase oF fracture energy with decrease in temperature of 55 - 60% with an increase of 150% in splitting force. Figures 5.7 and 5.8 represent the effect of simulated joint on the material response at different temperature, where the gradual temperature effect can be seen.

Large specimens A total of eight tests were preformed. Four specimens for each level of temperature. Figures 5.9 and 5.10. show an increase on fracture energy with decrease in temperature of 100-150 % with an increase of more than 200% in splitting force value.

Specimens without joints

A total of twelve small specimens were tested, six of which were tested at -50°C while the remaining were tested at room temperature. No large specimens were tested under this series.

Small specimens Figure 5.11 represents the response of the specimen cast in a single block at low and room temperature. there is an increase on fracture energy with decrease in temperature of 45 to 55% with an increase of 190% in the splitting force. By comparing the room temperature results with the results obtained by Brähwiler *et. al* (1991), a very good agrement was obtained.

5.1.3 Influence of different aggregate on fracture energy

Figure 5.12 shows schematically the influence of the tortuosity of the crack path on the stress transferring capacity in the descending branch. The tensile strength, f_t, and the fracture energy G_F are based partly on different material characteristic. The tensile strength depends on the undamaged material, while the fracture energy depends mainly on interlocking, which in turn depends on the smoothness of the crack surfaces.

5.1.4 Size effect

For the application of size effect method, it is required to test geometrically similar notched concrete specimens of different sizes. Two different sizes of specimens were used for this purpose with geometrical similarities. The specimens were cast from the

same batch of concrete. The nominal stress for each specimen was calculated using Equation 5.1 and Figure 5.1, which is derived from linear elastic beam approximation applied to the specimens with consideration to the effect of vertical component of applied load , Saouma *et. al* (1991).

$$\sigma_N = \frac{6}{th^2}[F_{sp} * y + F_v * e] + \frac{F_{sp}}{th} \tag{5.1}$$

where

F_{sp}= maximum splitting force

F_v = maximum vertical force

h = ligament length

t = specimen thickness

For the purpose of statistical regression analysis of test data, Equation (2.38) may be transformed to a linear plot, see Figure 5.2.

$$Y = A + C\lambda \tag{5.2}$$

$$Y = \left(\frac{f_t'}{\sigma_N}\right)^2 \tag{5.3}$$

$$A = \frac{1}{B^2} \qquad \text{and} \qquad C = \frac{1}{B^2\lambda_o}$$

where λ is relative structure size$(\frac{d}{d_a})$

From Figure 5.3 and at f_t' = 300 psi (2MPa), the two constants B and λ_o were found to be: B = 0.8555 and λ_o= 42.2.

5.1.5 Brittleness number

If equation (5.2) is followed exactly, the plot of Y versus λ should be a straight line. The characteristic dimension for this geometry can be found from the point of intersection. At the point of intersection, the brittleness number as suggested by Bažant (1987), is given by:

$$\beta = \frac{d}{\lambda_o d_a} \qquad or \qquad d = \lambda_o d_a = d_o \tag{5.4}$$

where β is brittleness number and d_o is the characteristic dimension of the specimen geometry.

$\beta = 1$, indicate the relative size $\frac{d}{d_a}$ at the point where the horizontal asymptote for the strength criterion intersects the inclined straight line asymptote for the energy failure criterion of linear elastic fracture mechanics, i.e., $\beta = 1$ represents the transition between these two elementary failure criterion.

For $\beta < 1$ the behavior is closer to strength of materials (SOM) criterion and for $\beta > 1$ it is closer to LEFM criterion. Bažant (1987) found that for $\beta \leq 0.1$ or $d < 0.157m$, the SOM analysis may be used as approximation and for $\beta \geq 10$ or $d > 15.7m$ (51 $feet$), linear elastic fracture mechanics must be used.

Thus for $19\,mm$ MSA (aggregate size used for this experimental program), for LEFM to be applicable the structure should have a characteristic dimension and two cases are plotted in Figure 5.3. In the case study under consideration (Long Spruce Generation Station) in this thesis, the maximum aggregate size (d_a) was to equal 3

in ($80\,mm$) and $d_o = \lambda_o * 80 = 3.376\,m$. According to the brittle number criterion, for MSA found in this dam:

1- for SOM to be applicable, $d_o < 0.3376\,m$

2- for LEFM to be applicable, $d_o > 33.76\,m$

Therefor for 80 *mm* MSA, LEFM can be applied to a structure with characteristic dimension equal or greater than 33.76 *m*. A structure of this dimensions a large gravity dam.

5.2 Phase II

A total of 60 small specimens were tested, of these 40 specimens were repaired using epoxies repair materials and 20 specimens were repaired with ultra-fine cement, see experimental program summarized in Table 3.3. The specimens were tested at room temperature and at - 50°C in dry and water saturated conditions. The specimens were left for at least seven days inside cure room before test takes place.

5.2.1 Influence of temperature on the fracture behavior of the repair materials

Dry condition

From the results plotted in Figures 5.13-5.24, the polymer (epoxy resin) repaired concrete tested have good performance in the dry condition. The crack propagating in concrete away from the repaired joint indicated that the repair material provided a

good bond, Figure 5.28 is a potographic presentation. In case of K-epoxy, Figure 5.15, there is an increase on fracture energy with decrease in temperature of 25-30% with an increase of 50% in splitting force value. There is an increase on fracture energy with decrease in temperature of 20% with an increase of 35% in splitting force in case of epoxy W, see Figure 5.24. The ultra fine cement shows good performance with an increase of fracture energy with a decrease in temperature of 100% with an increase of 200% in splitting force over the room temperature values, see Figure 5.19, but ultra fine-cement appears to be quite weak in comparison with polymers.

Wet condition

The wet condition specimens were kept immersed under water for 24 hours before taken out and repaired. A total of thirty tests were used in this test series.

In the case of epoxy K repair material shows a poor efficiency at room temperature with a decrease of 15% in the fracture energy in comparison with the joint before repair and a decrease 65% in fracture energy in comparison with dry condition, Figure 5.16. At low temperature, good efficiencies with increase of approximately 15-20% of the energy and between 30-40% increase of strength, although two of the specimens show a low performance.

Epoxy W in the wet condition shows very poor performance especially at low temperatures, see Figure 5.21. At room temperature, there is a decrease of 20% in the fracture energy in comparison with the joint before repair with no change in the value of the splitting force. At low temperature, the decrease of fracture energy and the splitting force in comparison with dry condition is very high and it

can be seen in Figure 5.21. The ultra fine-cement grouting material, Figure 5.20, show consistencies in its results, where there is almost no effect of the wet condition. Like with other materials, an increase in the strength and the fracture energy with decrease in temperature can be seen. Figure 5.25-5.27 show a comparison between the performance of the homogeneous specimens and the repair materials. In general, poor performance of the three materials in wet condition was noted. Also the ultra-fine cement grouting is considered to be weaker than the epoxies.

5.3 Phase III

5.3.1 Effect of re-repair

Twelve small specimens were re-repaired using ultra fine cement and epoxy K. First the specimens were cleaned of the old repair materials, half of the specimens were cleaned using special knife and the other half cleaned using water jet. All specimens were tested at room temperature. Both materials show extra decrease in the peak load of the joint by approximately 20% to 25%, and a decrease in fracture energy by 20% to 25%. For the second case (water jet), both materials show decrease in strength and fracture energy G_F with considerable variation in results. This behaviour is due to the amount of damage (in vicinity of the crack) the cracked joint experienced before the re-repairing took place, and the contamination of the old repair material which created several points of weakness along the fracture surface, Figure 4.29.

5.4 Summary

The following comments can be drown from the above discussion,

- The peak load for the specimens tested at low temperature, appears to be 50-200% higher than for specimens tested at room temperature.

- Fracture energy increase with a decrease in temperature, which suggests that at low temperature structures are safer, from a fracture point of view, than structures at room temperature when subjected to the same loading.

- Concrete at low temperature becomes more brittle and needs extra care during testing to control crack propagation.

- Successive rehabilitation depends heavily on the type of repair material. Also the response of repair materials depend on the condition of the cracked surface.

- As expected, concrete specimens of different size was observed. Although the specimens were of large laboratory scale, the specimen dimensions were still too small for LEFM analysis. So fracture mechanics principles are applicable to concrete provided a finite nonlinear zone at the fracture front is taken into account.

- Dimensional analysis based on Bazant's size effect shows that, for structures that are geometrically similar, the nominal stress at failure varies with the structure size.

- For the smallest structure that can be made with a given aggregate, the strength criterion governs, and for structures that are sufficiently large, the fracture mechanics criterion governs. The plot of the nominal stress at failure versus the size of the structure represents a smooth transition from the strength criterion to linear fracture mechanics criterion.

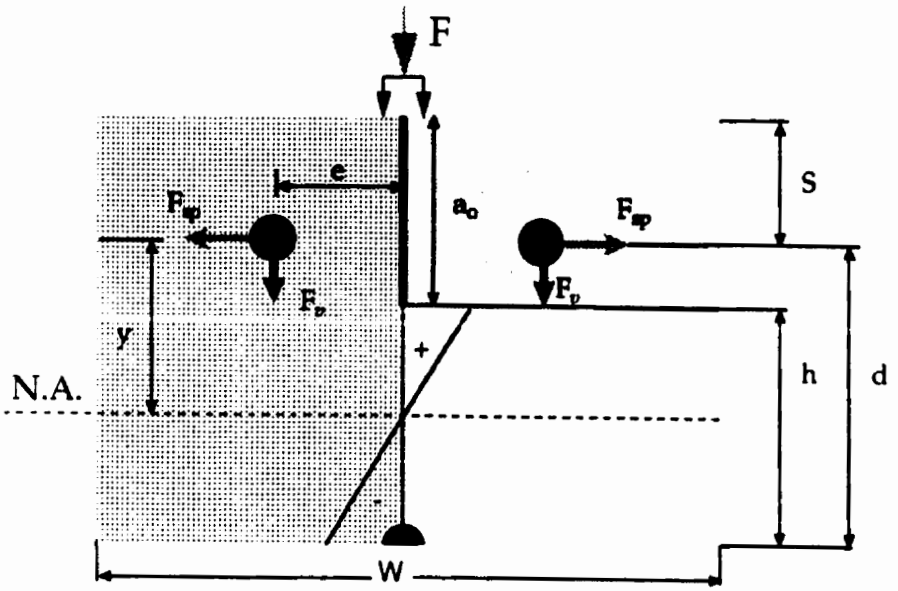

Figure 5.1: Beam theory approximation

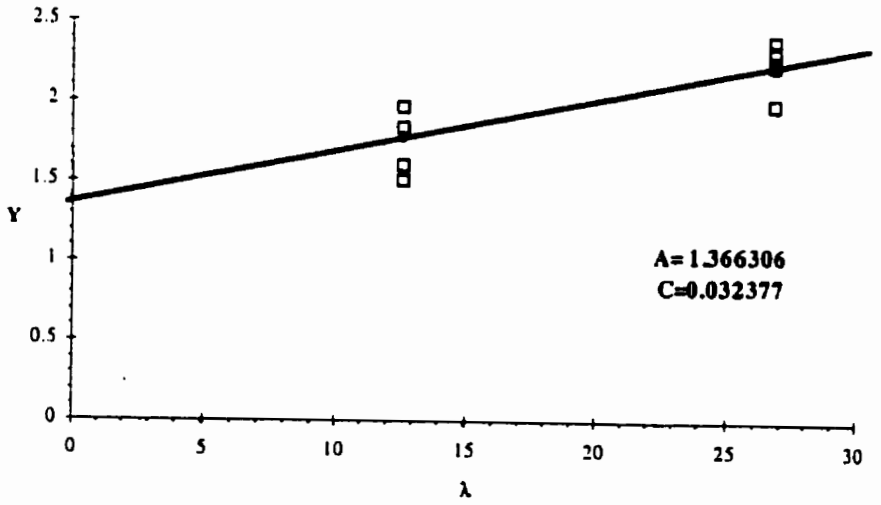

Figure 5.2: Regresstion analysis of fracture test data

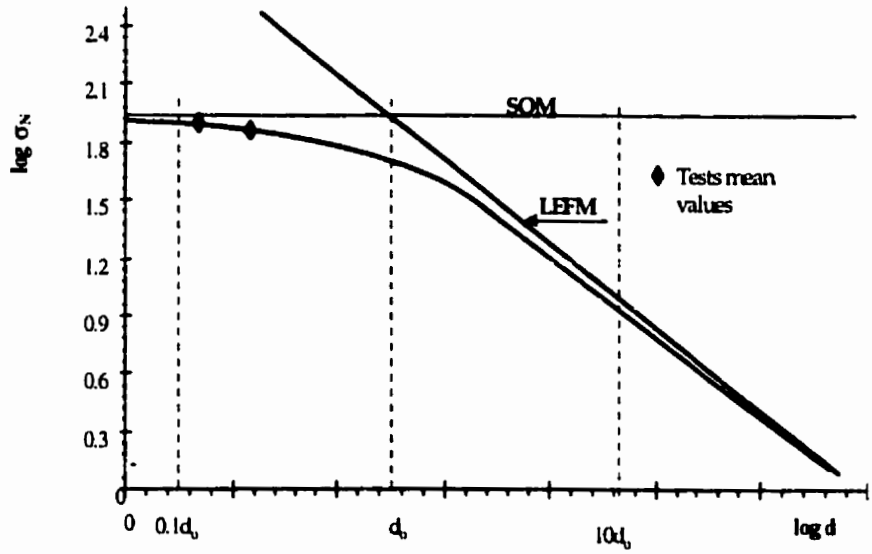

Figure 5.3: Specimens size effect for da = 19 mm

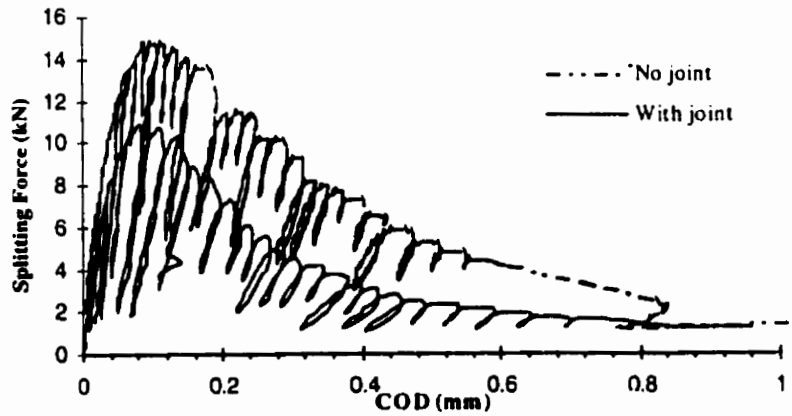

Figure 5.4: Effect of simulated joint on the material response at room temperature

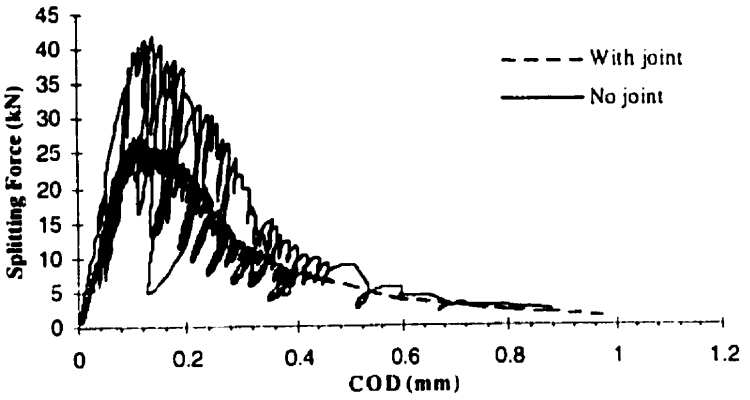

Figure 5.5: Effect of simulated joint on the material response at low temperature

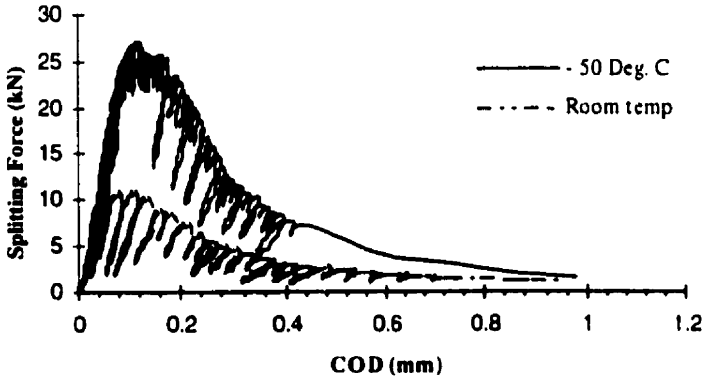

Figure 5.6: Response of small specimen cast in two blocks at low and room temperature

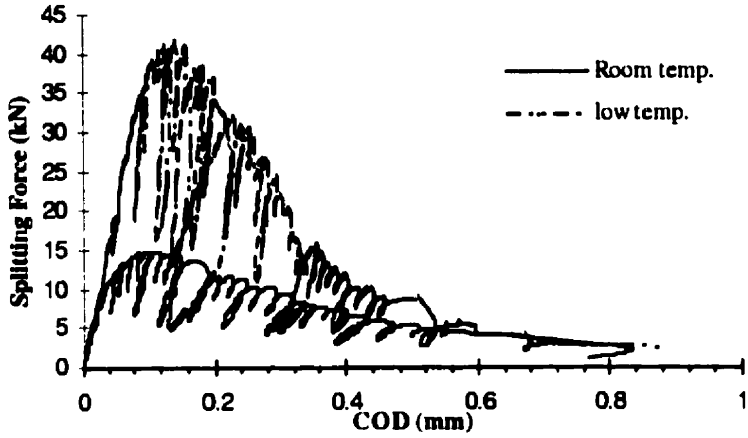

Figure 5.7: Response of specimen cast in single block at low and room tempearture

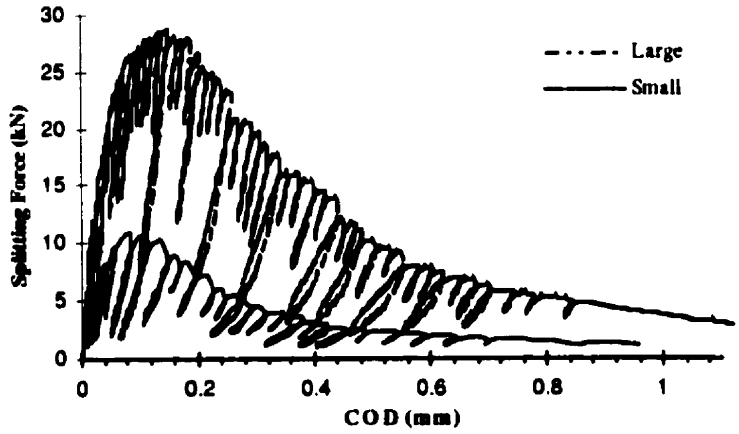

Figure 5.8: Size effect in specimen cast in two blocks at room temperature

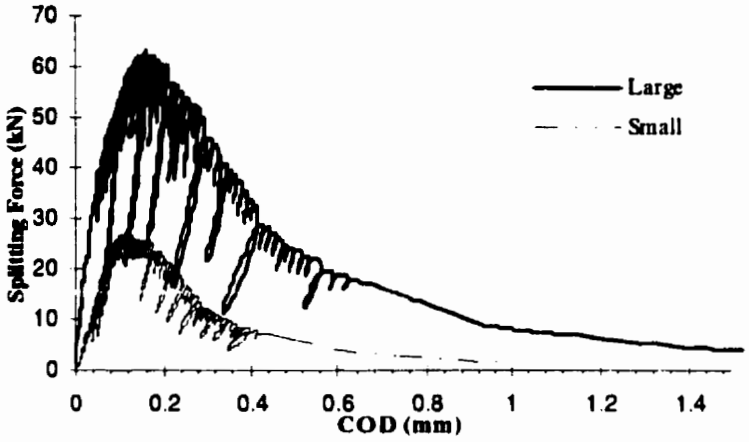

Figure 5.9: Size effect in specimen cast in two blocks at low temperature

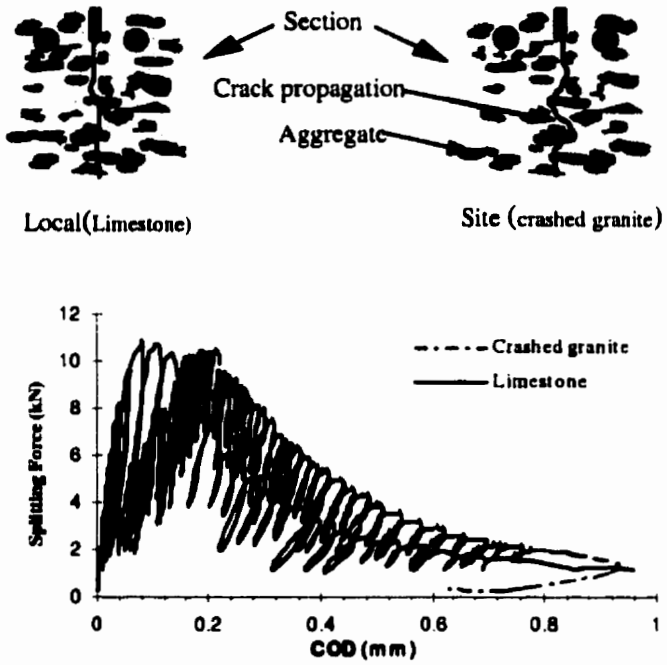

Figure 5.10: Local aggregate versus site aggregate

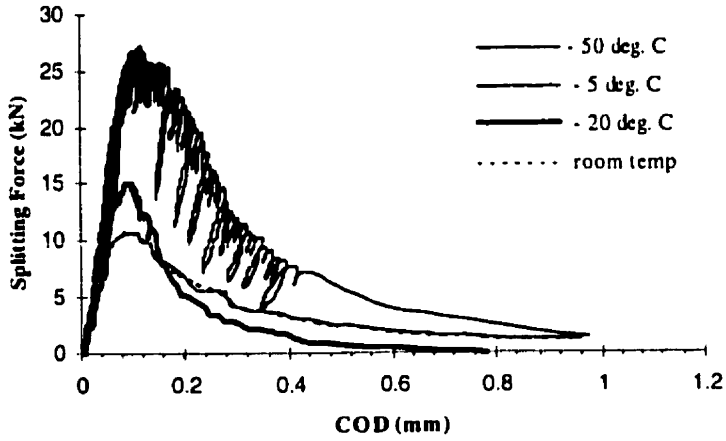

Figure 5.11: Effect of simulated joint on the material response at different temperatures

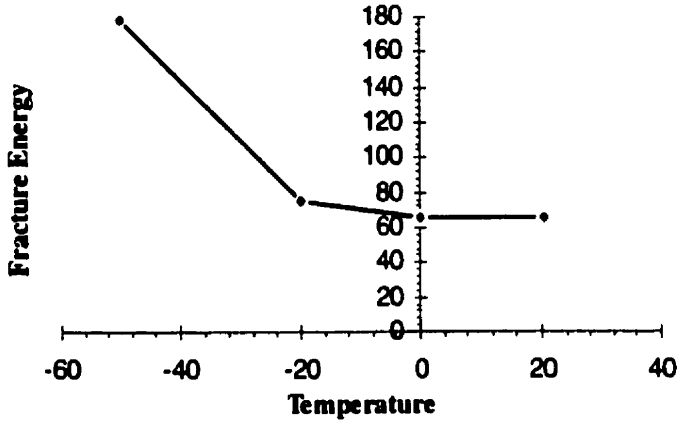

Figure 5.12: Evolution of fracture energy with temperature

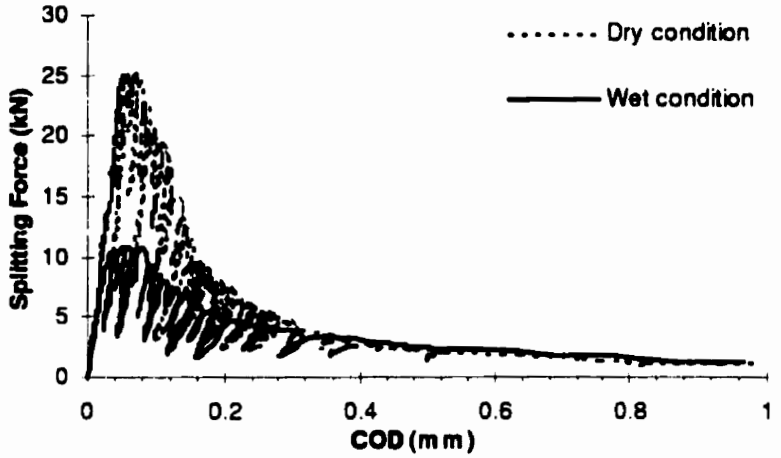

Figure 5.13: Response of epoxy-K at room temperature

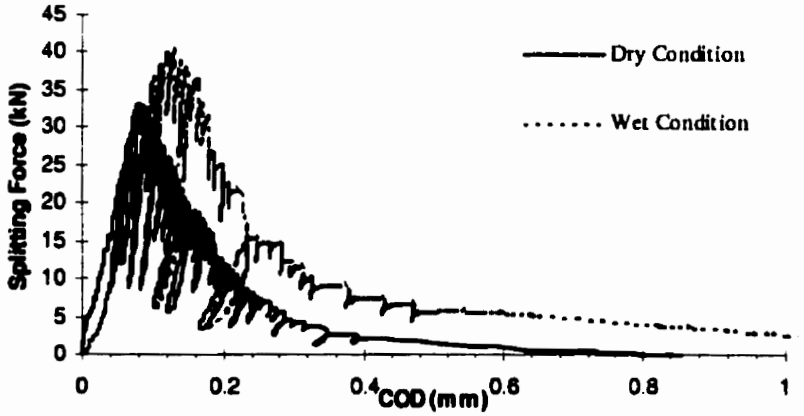

Figure 5.14: Response of epoxy-K at low temperature

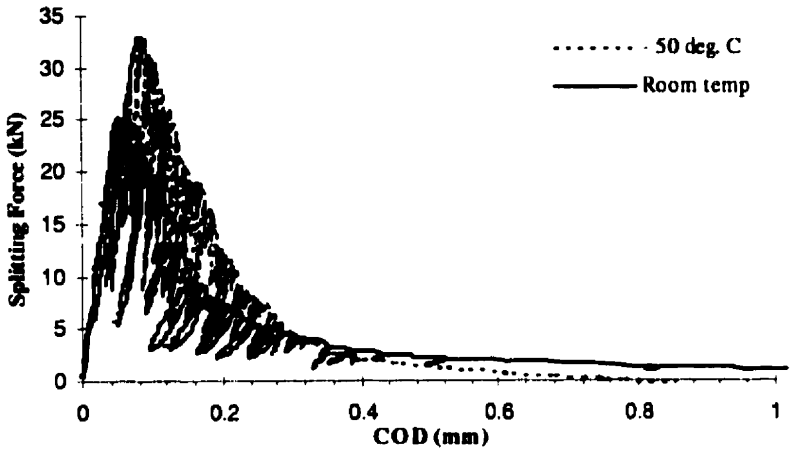

Figure 5.15: Response of epoxy-K at applied to dry surface

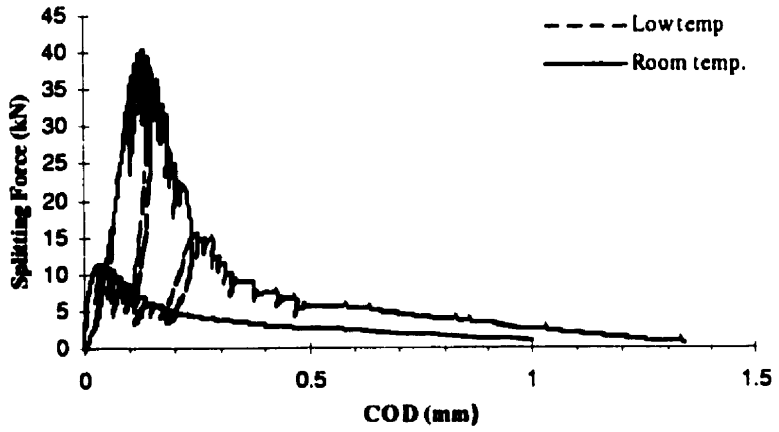

Figure 5.16: Response of epoxy-K applied to wet surface

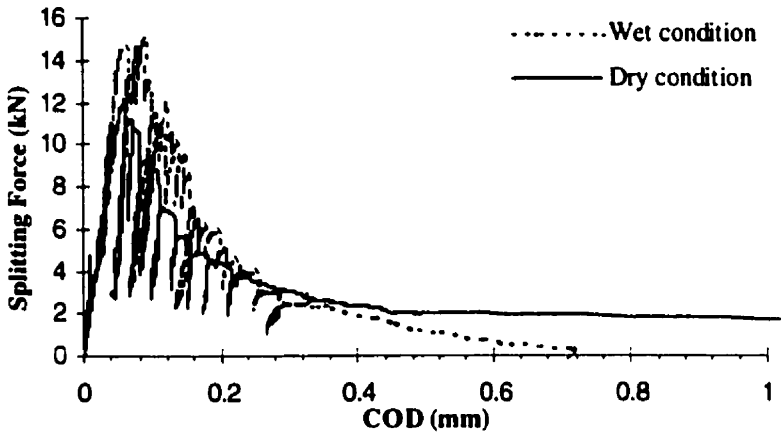

Figure 5.17: Response of ultra-fine cement at low temperature

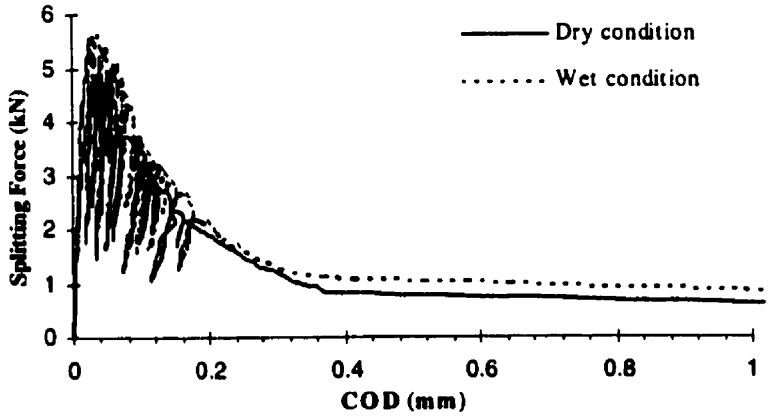

Figure 5.18: Response of ultra-fine cement at room temperature

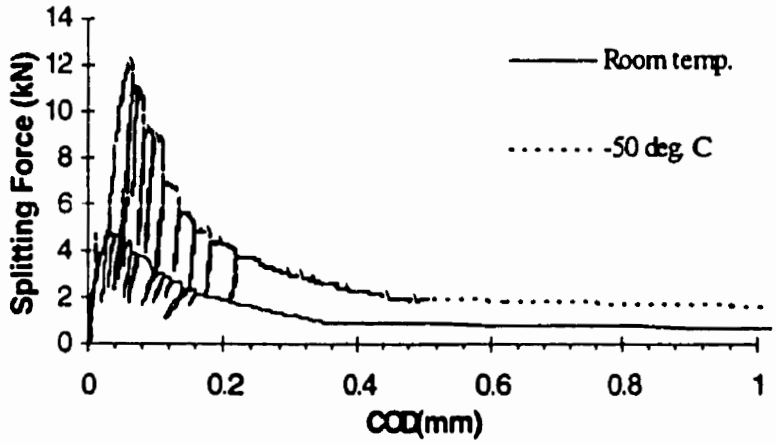

Figure 5.19: Response of ultra-fine cement applied to dry surface

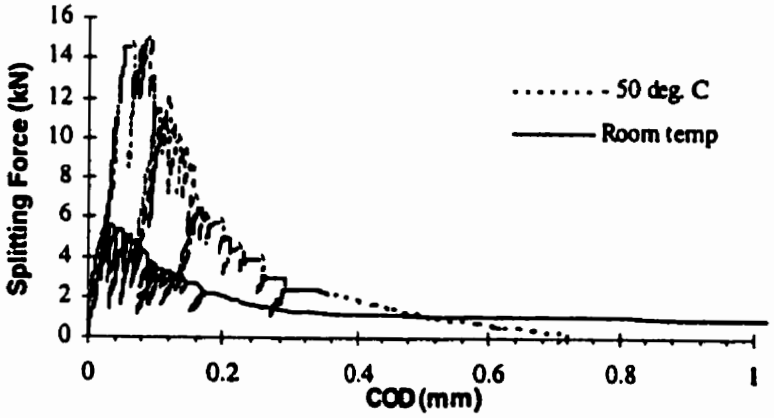

Figure 5.20: Response of ultra-fine cement applied to wet surface

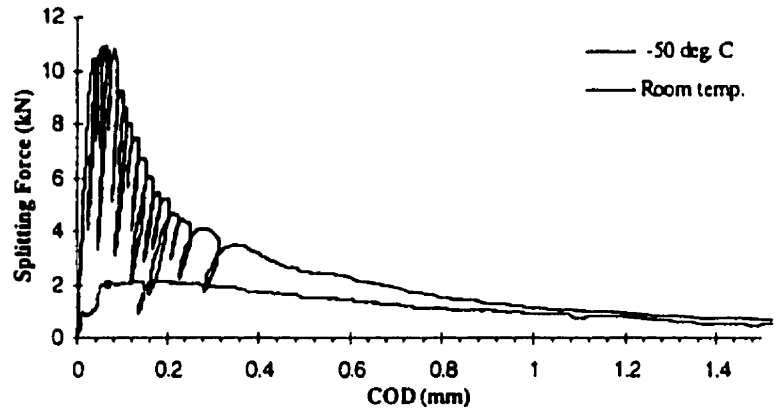

Figure 5.21: Response of epoxy-W applied to wet surface

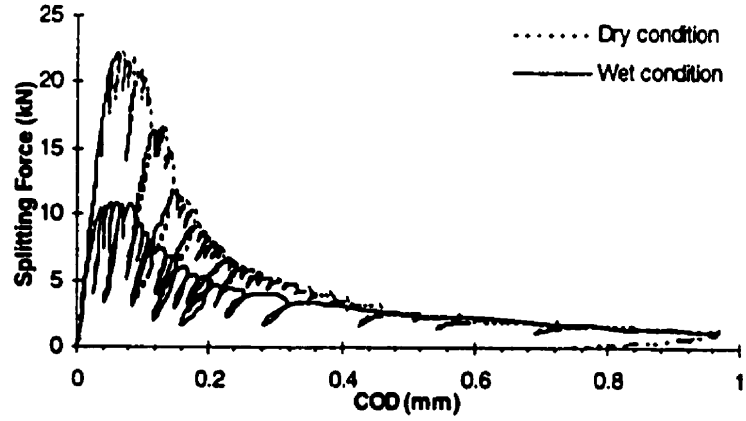

Figure 5.22: Response of epoxy-W at room temperature

Page missing from library's copy

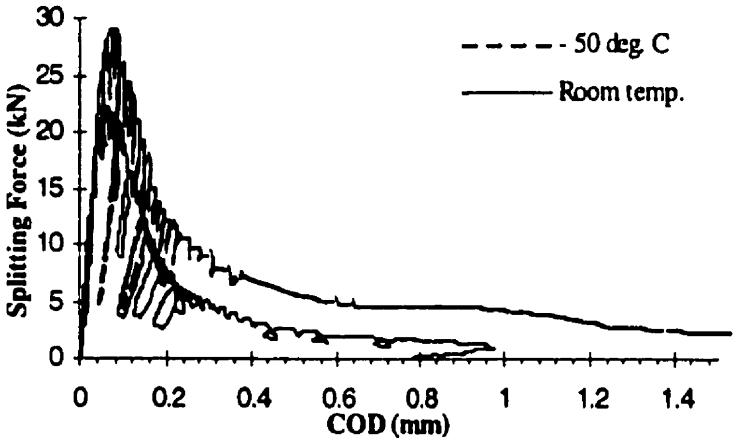

Figure 5.23: Response of epoxy-W at low temperature

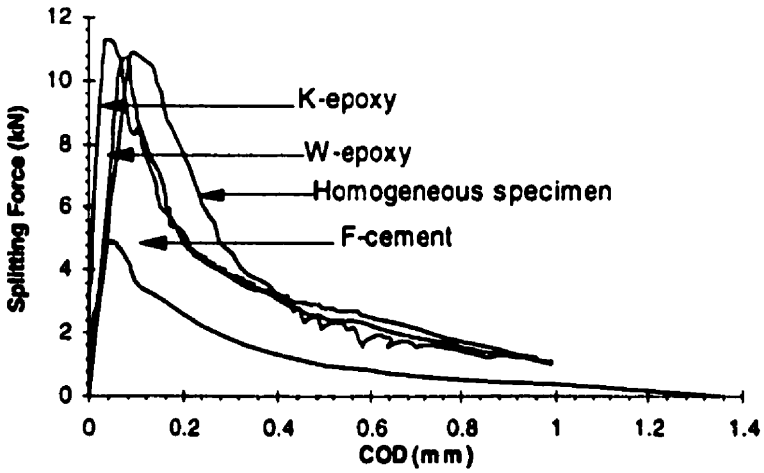

Figure 5.24: Response of repair materials at room temperature for wet condition

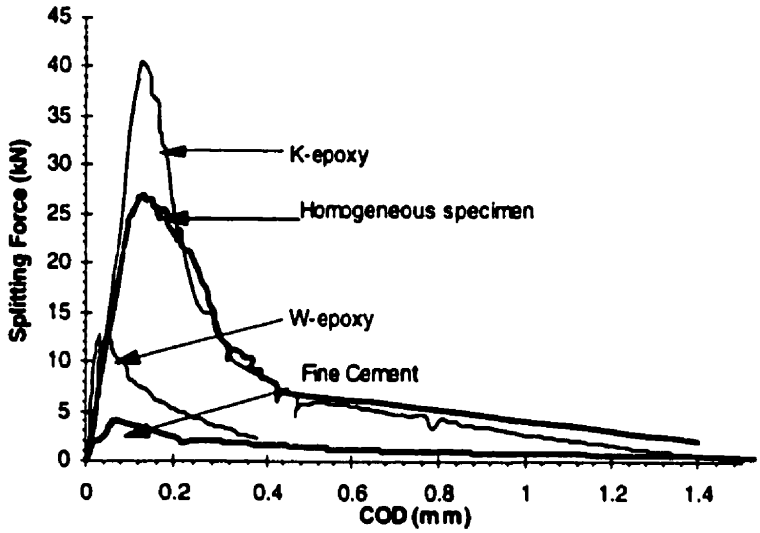

Figure 5.25: Response of repair materials at room temperature for wet condition

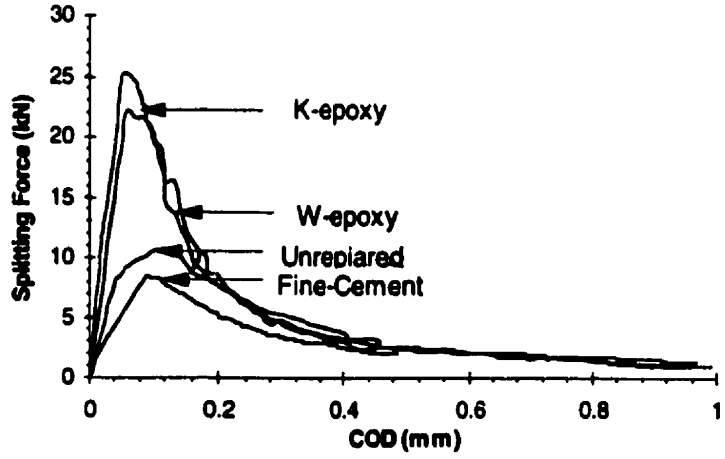

Figure 5.26: Response of repair materials at room temperature for dry condition

Figure 5.27: Weak points created by old repair material

Figure 5.28: Typical strong bond, crack propagate in the nearby concrete

Chapter 6

THEORETICAL CALIBRATION OF TEST RESULTS

6.1 Introduction

In this chapter, the results of the numerical analysis preformed on splitting wedge specimens will be presented, using the finite element program SIMEX. This chapter covers detailed description and procedure involved in the analysis.

6.2 Mathematical Model

A mathematical model was developed with exponential calibrated from the test results and their model can be used in predicting actual practical situations.

6.2.1 Fracture energy

The least squares regression methods with sinewave square were used to determine the "best" equation which fits a set of observations . Nonlinear algorithms are employed to enable us to describe a statistical relationship between graph series, Figure 6.1.

$$\frac{G_F}{G_{Fo}} = \beta_o + \beta_1 \sin(\frac{\pi}{20}T + 5)2 \tag{6.1}$$

where,

G_{Fo} = initial fracture energy at room temperature

β_o, β_1 = constants

T = temperature. The function allows a simple determination of material parameters since it may be written in the form $Y = aX + b$.

6.2.2 Stiffness degradation

TThe least squares regression methods with Gaussian exponential to determine the "best" equation which fits a set of observations. Nonlinear algorithms are employed to enable us to describe a statistical relationship between graph series, Figure 6.2.

$$\frac{K}{K_o} = 3.75\, e^{(-0.5((4COD+1.25)^2)} \tag{6.2}$$

Where,

K = stiffness at any point

K_o = initial stiffness

COD= crack opening displacement. By using measured crack opening displacement and equation 6.2, the amount of degradation in the stiffness of the interface can be predicted.

6.3 Finite Element Program

SIMEX is a finite element program developed at the University of Manitoba by Ayari, Appendix. It is a collection of computer routines linked together through a graphics interface. These routines are specific to certain types of mathematical solutions to engineering problems, including standard structural analysis, heat transfer and others. SIMEX is based on the discrete crack approach. Cracks can be initiated at any desired location during an analysis either by direct input from the user or using interactive computer graphics.Elasticity, plasticity and viscoplastic formulation are linked to libraries that include several classical failure criteria such as Von-Mises, Drucker-Prager, Mohr-Coulomb and Tresca. Additional user-defined material failure criterion can easily be inputed, which allows easy adaptation of SIMEX to analyze cracking and deformation of structures made of any material like metals, plastics, concrete etc. The major features of this program include:

1. two dimensional finite element.

2. use of triangular elements with quadratic shape functions, arbitrary numbering of nodes and elements.

3. element library includes four-noded element, six-noded and eight noded isoparametric serendipity elements.

4. calculation of stress intensity factors using displacement correlation technique or surface integral technique of Babuska and Miller (1984).

5. automatic remeshing can be used to accommodate discrete crack growth.

6. isotropic or anisotropic models .

7. different types of loading can be used including nodal, pressure on element sides, thermal loading and initial nodal displacement.

8. solve nonlinear fracture mechanics problems based on the Hillerberg's model.

9. capability of using interface elements along the crack during growth in order to prevent its closure or to model shear resistance.

Additional information about the use of SIMEX finite element program can be found in the Appendix A.

6.4 Compliance Method

In the thermodynamics approach of linear elastic fracture mechanics, the energy release needed to extend the crack by da is given by:

$$G = \frac{dW_p}{da} \tag{6.3}$$

where W_p is the total potential energy of the crack system and a is the crack length. There are several equivalent expressions for G including the following:

$$G = \frac{1P^2}{2B}\left(\frac{dC}{da}\right) \tag{6.4}$$

where P is the total applied point load, B is the specimen thickness and

C is the compliance or flexibility of the system (inverse of the stiffness) defined by:

$$U = C.P \tag{6.5}$$

where U is the load displacement. According to Griffith criterion (1921), crack growth occurs when

$$G_I = G_{IC} \tag{6.6}$$

and according to Bareblatt's criterion (1962), crack growth occurs when:

$$K_I = K_{IC} \tag{6.7}$$

where G_{IC} and K_{IC} are the critical energy release rate and the critical stress intensity factor respectively. The relationship between G_{IC} and K_{IC} was derived by Irwin (1957):

$$G_{IC} = \frac{K_{IC}^2}{E'} \tag{6.8}$$

where

$$E' = \left\{ \begin{array}{ll} E & \text{for plane stress} \\ \dfrac{E}{(1-\nu)} & \text{for plane strain} \end{array} \right\} \tag{6.9}$$

By using one of the experimental techniques available to obtain G_I , the mode I stress intensity factor, K_I can be determined using Equation 6.8.

Substituting Equations 6.4 and 6.9 into Equation 6.8, we obtain

$$K_I = \left(\frac{E}{2B} P^2 \frac{dC}{da} \right)^{1/2} \qquad \text{for plane stress} \tag{6.10}$$

and

$$K_I = \left(\frac{E}{2B(1-\nu^2)} P^2 \frac{dC}{da} \right)^{1/2} \qquad \text{for plane strain} \tag{6.11}$$

The fracture toughness can be calculated using the above equation. The only unknown is the value of the critical crack length a_c. Rossi *et. al.* (1991) and Bascoul *et. al.* (1987) pointed out that the experimental determination of the critical crack length a_c is difficult and cannot be accurate because the visible crack at the surface does not represent the real crack for a number of reason such as:

- drying shrinkage that induces skin microcracking
- the heterogeneity of the concrete between the volume and the surface
- the change from plane strain behavior in the volume to plane stress behavior at the surface, Figure 6.3.

To solve this problem, the conccept of effective crack length, discussed in chapter two section, is used. With the assumptions that linear elastic fracture mechanics and fracture process zone, true crack in the specimen can be replaced by an effective

crack length, a_{eff} , as shown in Figure 2.7. From the P_{sp} versus COD curve the experimental compliance, C_{exp}, for each cycle was measured by connecting the initial unloading point to the final reloading point of each cycle. The effective Young's modulus, E_{eff}, is determined indirectly from the initial compliance.

$$E_{eff} = \frac{C^i_{nu}}{C^i_{exp}} \tag{6.12}$$

where C^i_{exp} is the initial experimental compliance determined during the first loading in the linear elastic regime before pre-peak nonlinearity which corresponds to the formation of microcracks around the notch tip. C^i_{nu} is the initial normalized numerical compliance for the initial crack length using a unit elastic modulus. From the above equation, the effective Young's modulus is calculated.

6.5 Finite Element Analysis

The experimental results of the tests were numerically predicted using the program SIMEX with the mesh shown in Figure 6.4. For reasons of symmetry, only half of the mesh shown is considered in each case. Also an interface elements was added to the program, Figures 6.5. This element is a linear line element suitable for two-dimensional analysis with six-nodes and zero initial thickness. The iteration process and the interfacial constitutive relations were designed for this interface element . The finite element analysis was first carried out to obtain the relationship between the normalized compliance (numerical compliance) and the effective crack length with the assumptions that linear elastic fracture mechanics is applicable and fracture process

zone true crack in the specimen can be replaced by an effective crack length, a_{eff}. The analysis was repeated several times with the notch as the initial crack length. From each analysis both the stress intensity factor and the numerical compliance were determined. From the above data, a curve relating the numerical compliance to the effective crack length is obtained, Figure 6.6. Using equation 6.12, the finite element calibration obtain several value for normalized C_{nu} equal to

$$C_{nu} = E_{eff}.C \tag{6.13}$$

From the experimental results, and for each successive post-peak unload-reload cycle, the experimental compliances are obtained. Each experimental compliance is normalized with respect to E_{eff} and then, the effective crack length a_{eff} is determined. From the critical peak load for each cycle and the values the effective crack length, the fracture toughness K_{IC} were obtained. The fracture tests were simulated numerically and, then, the calculated F_{sp} versus COD curve was compared to the experimental curve.

Figures 6.7 and 6.8, are chosen to demonstrate the agreement between experimental results and numerical predictions. In the case of room temperatures, the G_F values obtained from the simulated curves are up to 9% larger than G_F values determined from the experimental data. G_F values were 4% as smaller as determined from the experimental curve obtained at -50 °C in comparison to room temperature. This difference could be due to energy dissipated outside the fracture surface.

6.6 Evaluation of Fracture Toughness K_{IC}

Figures 6.9- 6.12 represent the fracture toughness as a function of the effective crack length. The behavior is charactierized by various phases. There is an increase in the value of the fracture toughness with increasing crack length. This increase in K_{IC} may be attributed to increasing size of the microcracked zone at the crack tip, which is the stage of formation of the fracture process zone. The above increase in K_{IC} is followed by a steady state, where there is no increase in K_{IC} with the increase in the crack length. This part of the curve represents the steady crack propagation regime. This phenomena was observed by Saouma *et la* (1992) also by Rossi (1991). The steady part of the curve is followed by a decrease in K_{IC} with an increase in crack length. Both the first and the third part of the curve involve a transitional crack propagation regime.

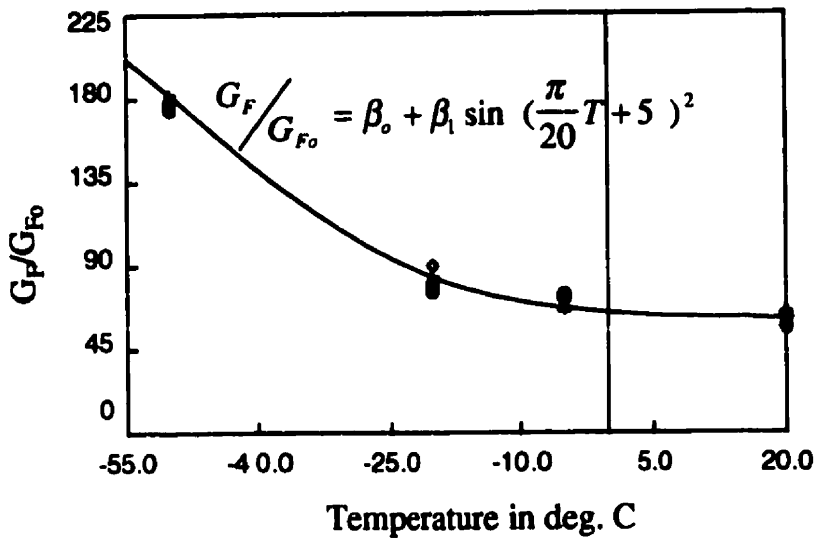

Figure 6.1: Fracture energy ratio versus temperature

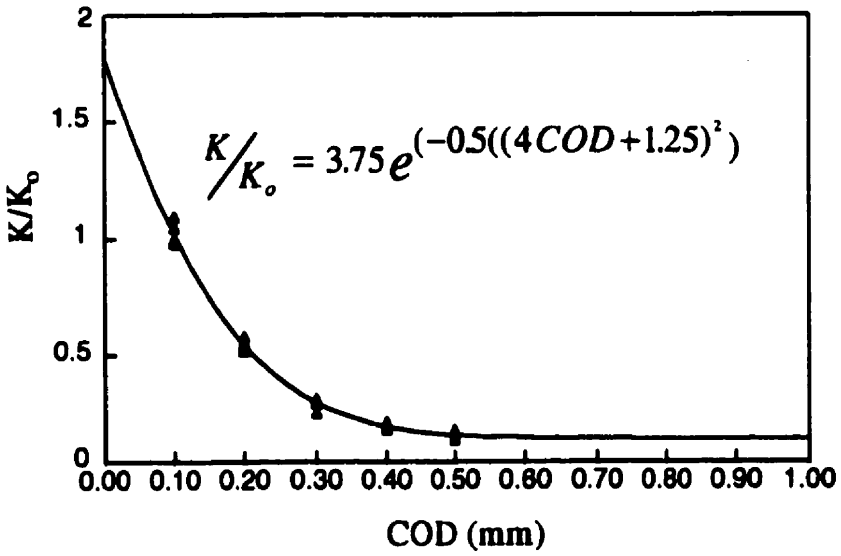

Figure 6.2: Stiffness ratio versus COD

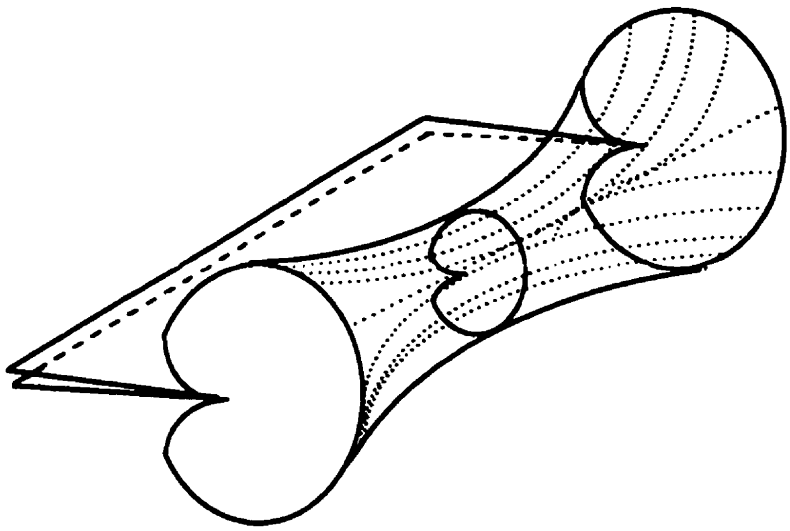

Figure 6.3: Plane stress and plane strain behavior

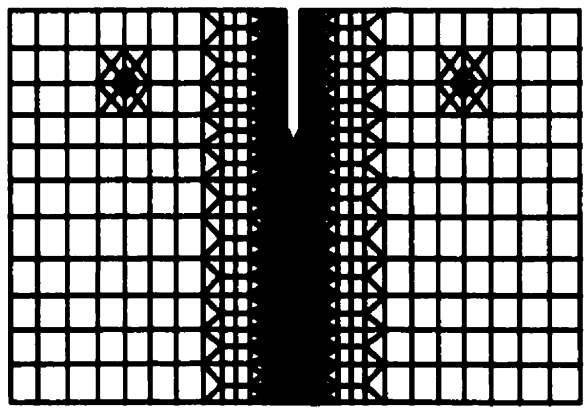

Figure 6.4: Finite element mesh used for the calibration

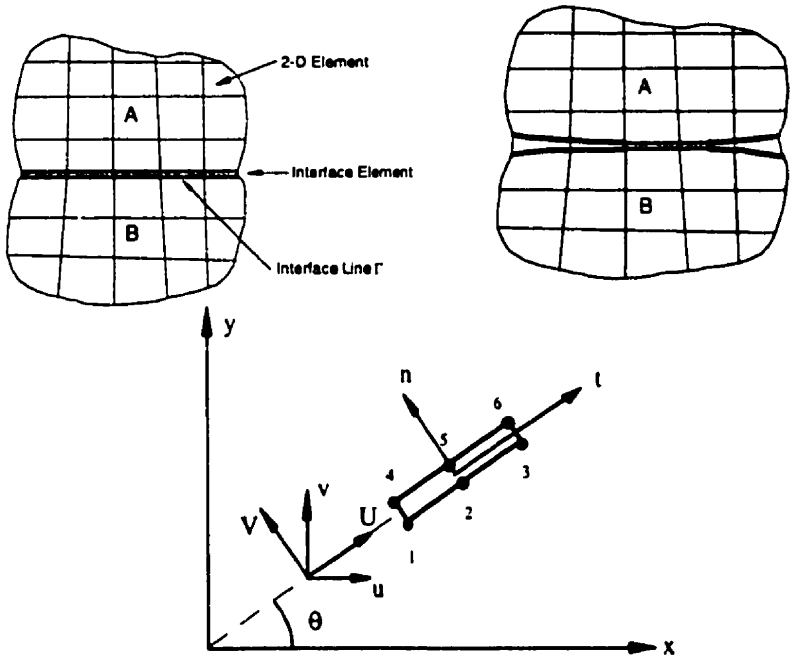

Figure 6.5: (a) Interface in close state (b) Interface with opening (c) Interface element in a body

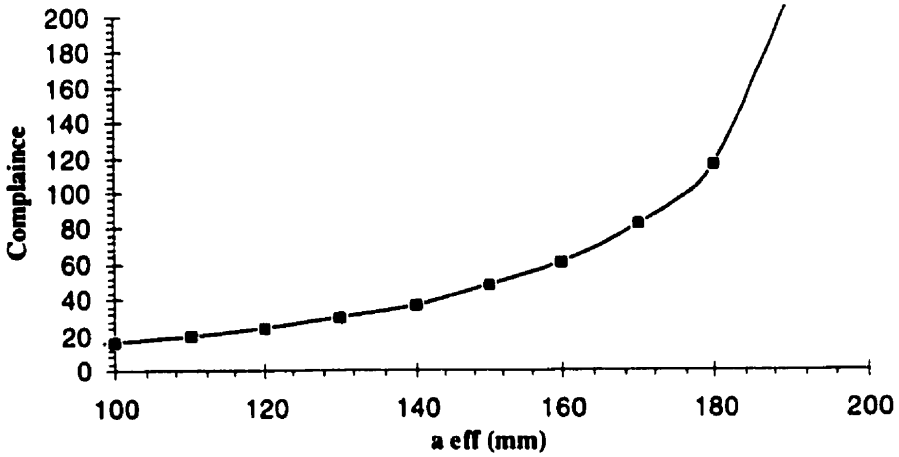

Figure 6.6: Compliance versus effective crack length

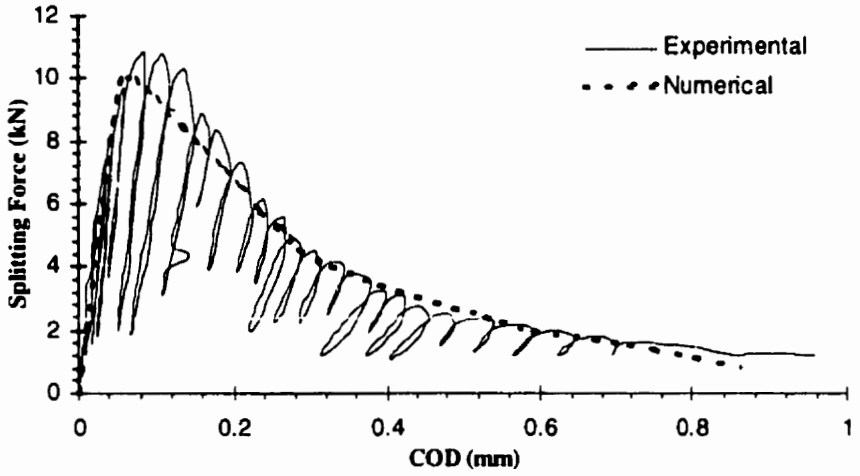

Figure 6.7: Response curve of computed and experimental results at room temperature (with joint)

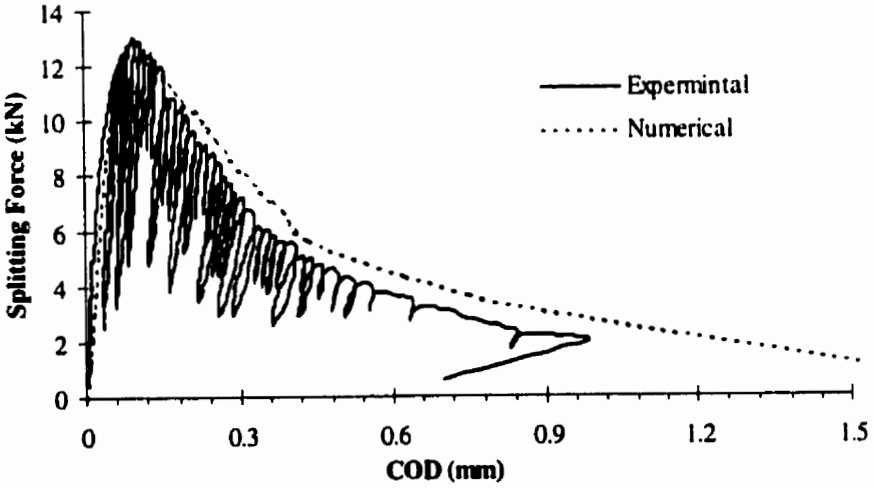

Figure 6.8: Response curve of computed and experimental results at room temperature (without joint)

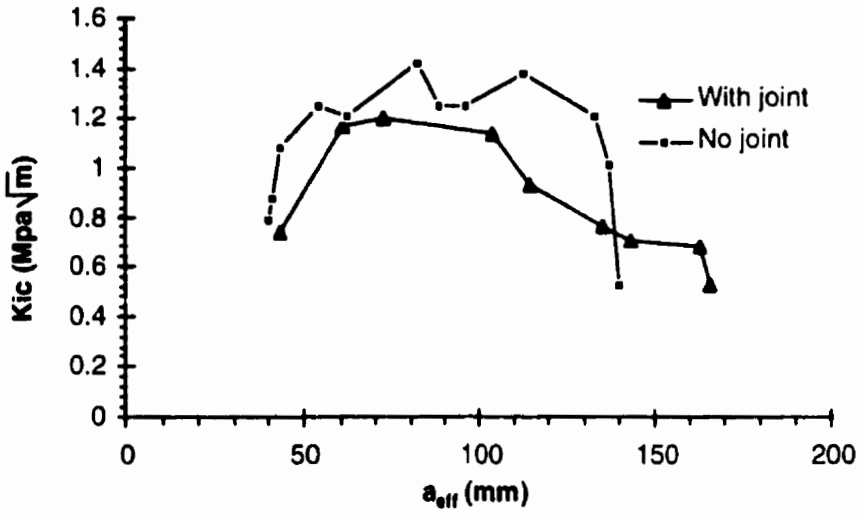

Figure 6.9: Fracture toughness versus effective crack length for small specimen at room temperature

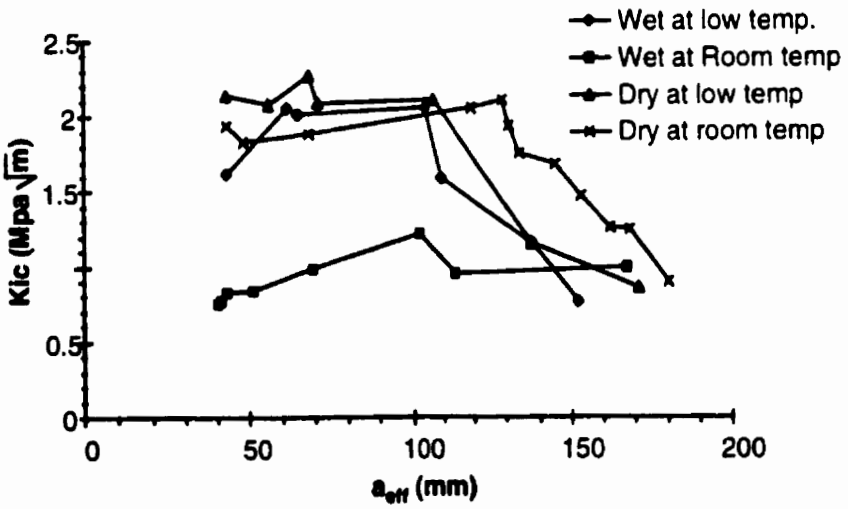

Figure 6.10: Fracture toughness versus effective crack length for K-epoxy

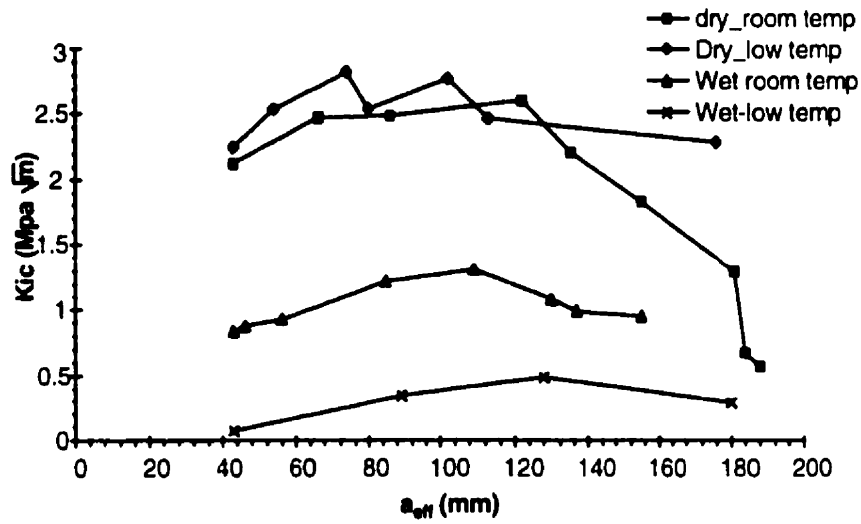

Figure 6.11: Fracture toughness versus effective crack length for W-epoxy

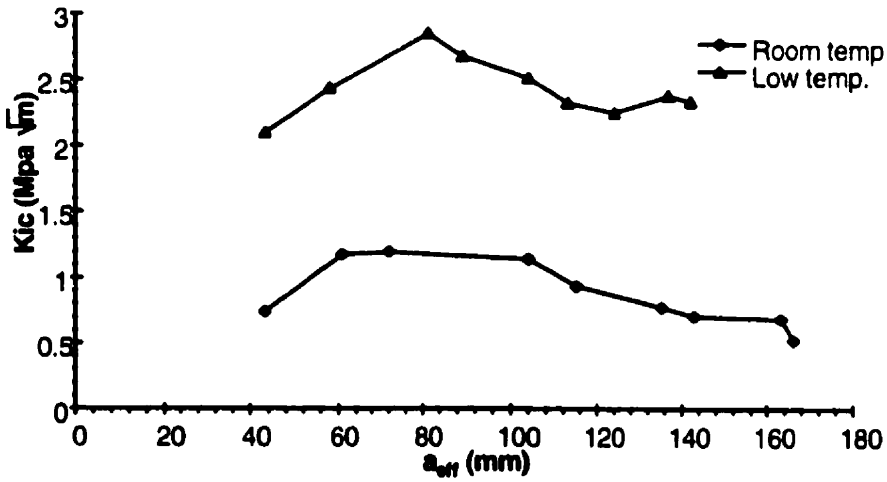

Figure 6.12: Fracture toughness versus effective crack length for specimen with joint

Chapter 7

REPAIR ON CRACKED JOINTS-CASE STUDY

7.1 Introduction

This chapter, discussing the validity of the different repair methods proposed for the specific case study, which leads to give a summery of the work carried out by other researchers working in the same research program in order to give full understanding of the scale o f the problem.

The dam of interest in this study is the Long-Spruce Generation Station on the Nelson river in the northern region of Manitoba. This dam is a low head-high discharge gravity one, 27.28 m high and 1.1 km wide. A cross-section of the dam is shown in Figure 7.1. The construction of the dam started in 1974 and finished in 1979. The site is in a zone of subarctic climate, where the daily maximum temperature in summer can be above 35 ^{o}C, and the daily minimum temperature in winter

can be below - 45 °C. After less than five years in service, leakage began appearing on the downstream face of the south transition structure from the topmost horizontal construction joint, Figures 7.1and 7.2, at a height of 23.62 *m* above the prevailing bedrock surface. The south transition structure is an unreinforced concrete gravity structure. It consists of three blocks, each 50 feet in length. Two vertical PVC waterstops are located between blocks at the upstream side of the contraction joints. The blocks were poured in 9 feet vertical lifts. Horizontal construction joints were prepared by green cutting to expose aggregates and removing all laitance. A thin grout layer was broomed onto the construction joint at the start of a pour to enhance bond at each horizontal joint. It is not likely that poor joint preparation is the cause of the leakage, because it occurs in all three blocks and only at elevation 357.5 *m*. The amount of leakage varies throughout the years. Figure 7.2 shows ice forms in the downstream face of the dam during winter time. In the late 1992, an intensive investigation was initiated by Manitoba Hydro, Canada to determine the cause of the leak and what could be done to ensure the stability of the dam. The investigation was aided by instruments, Figure 7.3, which were installed in the middle block of the south transition structure to automatically record thermal stress movements temperature on an hourly basis. Six Geokon model 4430 vibration wire strain gages, which are designed for long term strain measurements in mass concrete, were installed along the leakage joint. The data indicates that the concrete above the construction joint curls upwards during the cold weather and during the warm spell, the block uncurls but is unable to flatten due to ice build up and this leads to the center jacks up as shown in Figure 7.4.

7.2 Kinematics of Cracked Concrete Dams due to Ambient Condition

Construction joints in dams are considered to be the weakest link of the structure. In sub-arctic regions, where there is a large variation in ambient temperature, the joints become vulnerable to this severe condition, which may partially or totally break the bond of the construction joint. A cracked joint inside the dam causes leakage. Some of those cracks can be very serious and can affect the integrity and the safety of the structure. Motion analysis of the dams with leaking joints is important for both safety assessment and rehabilitation. Recorded data from 1992 until June 1996 were accumulated. The joint opening displacements were recorded at the locations shown in Figure 7.3. The finite element results are compared with the in situ measured data, in Figure 7.6. One important observation made was that the magnitude of the recorded normal displacements are in good agreement with the numerical one at certain time of the year. The numerical results do not coincide well with the recorded data during winter. This is because the effects of ice build-up have not been introduced into the finite element analysis. Figures 7.7 through 7.10, represent the joint opening displacement monitored in the site during the last five years. These data were recorded from the site to help in predicting the best repair time. It can be seen that there is almost no increase in the joint opening displacement during those years. This indicates that the stability of the dam is not an issue and only the leakage is a problem.

7.3 Ice Loads

Ice loads are considered to be one of the major factors causing damage in the structure of the dam. It is an extremely difficult task to get an accurate ice load measurement. Certain load data can be obtained by field measurement. However, ice loads are strongly environment dependent. Ice can exert a load on the structure in two different ways: An ice layer forms inside the crack; and an ice sheet forms on the surface of the forebay. The cracked joint is filled with water. Water freezes during winter time creating the ice layer, Figure 7.11. The phenomena related to the ice layer is quite complicated. To simulate this phenomena, the following factors need to be determined.

1. *Freezing start temperature*: this temperature cannot be set to zero degree. It should be the temperature for the ice to consolidate. This interface temperature might be different from point to point according to the moisture of the location.

2. *Ice layer stopping time*: the ice layer growth does not take place for the whole winter. Freezing ice blocks the water supply for the ice layer to grow. To choose this time as the time when the temperature of the whole joint is below zero degrees.

3. *Ice breaking stress*: the debonding stress for the ice-concrete interface. It might be a function of temperature and can be established experimentally.

4. *Ice melting temperature*: this temperature is related to the start of freezing temperature. The ice layer reduction should also be considered. There might be another factor to be concerned about. That is the ice draft force acting on the upstream side.

The second effect of ice is the load from forebay ice sheet on the upstream side of the dam. The ice sheet forms in winter due to the river freezing. It is believed that this sheet induces a large force on the structure of the dam. Zhang (1998) analyzed the mechanism of the ice load and developed a simple model to determine the thickness (as a function of time) of the ice sheet. Figure 7.12 represents the ice sheet where it is considered to be a large elastic plate. Both horizontal and vertical loads imposed by the ice sheet on the face of the dam, are found to be quite important in determining the model of the dam.

7.4 Repair Strategies

7.4.1 Background

There is a wide choice of solutions for repairing or reinforcing of concrete dams. Grouting with epoxy, chemical compounds or with special cements, is one of the possibilities, where the choice of grout depends on the injectability of the material selected. In the case study under consideration in this research. As mentioned previously in chapter six, all these types of materials showed tremendous changes in the bond properties of the material due to severe thermal condition.

The second rehabilitation method is the use of anchorages (post-tensioning cables). This method was first used in Cheurfas Dam in Algeria by Andre Coyne (1934), (cited in ICOLD, 1995). The use of stressed cables has primarily been associated with the modification of existing dams to take account of modern design standards. Dams which have suffered concrete deterioration or cracking leading to excessive leakage can be repaired economically using stress cables.

The third type of repair methods is the use of geomembrane. With this water proofing method, a flexible geomembrane is fixed to the upstream face. There are cases of non-drain geomembranes glued directly to the concrete, but drained membranes, which are mechanically fixed to concrete, are preferable.

The three different repair methods are discussed in the following sections.

7.4.2 Grouting Technique

Chemical grouting material was used to repair the crack in the Long Spruce dam. The repair method selected consisted of injecting the crack with grouting through holes drilled to intersect the crack. The selection of the material was based on its ability to adhere to the sides of the crack. Below the reservoir water surface, holes were drilled from the gallery to intersect the crack near the upstream face. As the station start operating again, the grouting appeared to have stopped the leakage. However, the leakage was reappeared on the downstream face. The theoretical analysis showed that very high thermal stresses exist and cause the upper block of the dam to curl and uncurl from season to season, the curling may not be hold by any type of grouting

material. This observation is supported by examining different types of grouting material tested in the experimental program undertaken in this thesis. The results of the tests showed that grouting materials fail at lower loads than expected. The failure of these material are attributed to several factors;

- the surface condition of cracked surface.
- change of material properties of repair material at low temperature.
- incomplete filling of the crack between injection points
- incomplete control of water flowing through the crack during grouting.

Because of the many drawbacks of this repair solution, it is recommended not to use this solution unless its combined with other solutions such as use of anchorage which will lead to very high cost.

7.4.3 Anchorage

The choice of the anchorage system depends on the static and dynamic loads required to ensure the stability of the dam. The choice should be based upon the information provided from the site and laboratory tests. Calculations will be required to obtain factors such as anchor load, spacing and transfer lengths. Anchorage tension members can either be high tensile steel wires or of aramid or carbon fiber-reinforced polymers (FRP) rods. The FRP anchorages have advantages over steel anchorages including, durability, high tensile strength and low relaxation, i.e., less load loss, also FRP anchorage need no corrosion protection. The main disadvantage of FRP anchors are

higher material cost, lower lateral compressive strength, lower shear strength and fewer proven application cases.

In general anchorage performance can not be predicted solely on the basis of empirical design rules because it is greatly influenced by the quality of the workmanship during construction. Hence regular checks on the residual load should be made during the service life of the dam to ensure the safe and satisfactory performance of each anchorage system.

7.4.3.1 Stress analysis of anchorage

It has been found from analytical analysis of the thermal and ice loads that high tensile stresses exist near the upstream side. The tensile stress in the downstream side can be as high as 7 MPa and in the upstream side as high as 4 MPa. Typical normal stress distributions are shown in Figures 7.13- 7.14 for winter and summer respectively.

Also, the residual stresses caused by concrete hydration following the construction of the dam is another important factor. Analysis of the residual stresses for the dam were carried out by Radoranoric (1998). The distribution of the residual stress along the construction joint can be seen in Figure 7.15, which has similar pattern as the thermal and ice loads and should be added to the ice and thermal load to produce the total tensile stress on the interface. In worst case, residual stresses can reach a level of 2 MPa. The combination of residual stress with thermal and ice induced stresses, can reach a value of 6 MPa in the vicinity of upstream side and to 9 MPa in the downstream side. Both of these stress levels are far beyond the bond capacity of any

of the grouting materials examined in this thesis.

The analytical study is turned to examine the use of anchors. The analytical analysis was carried out based on dywidag anchorage system (1990) which is threadbar post-tensioning system with double corrosion protection, Figure 7.16. Bars selected are 36 mm ($1\frac{3}{8}in$) diameter with an ultimate tensile strength of 1000 kN (150 ksi). The design prestressing force was 650 kN (142 ksi). The use of anchorage in both sides of the dam, requires the use of very strong anchors. Installation of such anchors in both sides would lead to new cracks in the upper block of the dam, thus failing to solve the leakage problem.

To avoid this problem, anchors can be install only in the upstream side where the downstream side can move freely. Two different cases of anchoring schemes were considered in the analysis. Case I with two anchorage (36 mm diameter) located at 0.47 m and 1.15 m from upstream face and the second case II (36 mm diameter dywidag bars) located at 0.47 m and 1.4 m from the upstream face as shown in Figure 8.17.

In case I, and during summer time, location 2 experiences higher deformation with a load exceeding its prestress force level. At location 2, the opening displacement for case II is larger than that of case I. Figure 7.18, shows a typical joint opening displacement during winter time. It can be seen that with fixing the upstream side, the joint opening displacement in the downstream side is enlarged significantly from 1.7 mm without the installation of anchors to 3.8 mm with anchors installed.

The analytical study by Zhang (1998) showed that during summer, the downstream side can not move freely and the action of the anchor forces is against the

thermal bending deformations. It is not expected that the anchor forces can overcome the bending deformations. Use of anchorage in one side (upstream) solves the problem in the winter time but the problem increase in the summer time when the anchorage can not take the load. To reduce or overcome this problem, a use of installation material on the surface of the top block of the dam is recommended as a thermal control method

7.4.3.2 Thermal control

From the ashrae table, kreith and keider (1978), at none time July 21 at altitude 74 north the incident solar energy on the horizontal road 703 w/m^2 (assuming a clear day) a black top will absorbs 93%, i.e. 654 w/m^2, while concrete will absorb 60% one 422 w/m^2. This is a reduction of (1-422)/624 or 35%. Thus it may concluded that, in order to reduce the thermal load by 35% at summer time, one should never use black top road on the top of the dam. Better one should add white surface to reflect the solar energy. If noon time surface temperature was 40°C and the underline concrete top 20°C, having a concrete surface would reduce the surface temperature to 33°C. If the underline temperature on the dam is 10°C the surface temperature would be 30°C. In conclusion future dams build in the north should never have asphalt roads or any other black material on top. The batch itself should have a reflecting color to minimize the effect of solar heat.

7.4.4 Geomembrane

7.4.4.1 Background

The use of geomembrane in the repair of concrete dams has increased in the past few years, particularly in Europe where geomembranes have been used successfully to resurface the upstream face of a number of old concrete dams.

Applications of geomembrane, have been reported by Koerner (1986). Some of the geotechnical applications of geomembrane are in earth dams, concrete dams, spillway capacity, also on rehabilitation of concrete, masonry, rockfill, gravity dams, reservoirs and canals.

Under extreme cold temperature, most of the available commercial membranes are affected as they become brittle and stiff. If their glass transition temperature is higher than -40^oC, then breaking of membrane occurs. Applying the present technology enables manufacturers to alter membrane composition by incorporating in the mixture, elastomers and binder agents to lower their glass transition temperature and keep the elastic properties of the membrane under colder temperatures One should be aware that stability of the materials can be affected. In choosing membrane for severe thermal climate, there are several properties that should be considered, such as brittleness under cold temperature, stress strain properties, resistance to bursting and sealed joint. A literature survey has shown that very few data on properties of membrane are available for low temperature. These include tests carried out in Hydro Quebec by Rollin *at el* (1985), Also different attempts were carried out in dams in the northern part of Italy, Sweden and France.

In a well documented case, a geomembrane of 2.5 mm thickness, manufactured with a PVC mix, heated-bonded during production to a 500 g/m^3 of polyester felt geotextile was used in the repair of the Publino dam, which is located in the mountains area of the north of Italy. The geomembrane used for the Publino dam was tested first by the Italian National Power Authority (ENEL). The selected geomembrane, showed good resistance to temperature, where the is no sign of cracking when tested at -35°C. During manufacturing, a great care was taken over the choice of the plasticizers added to the mix, so as to obtain a geomembrane with good performance in view of the difficult climatic conditions.

In another cases, the Lago Noro dam also in Italy, an anti-ice device was installed in order to prevent the formations of large ice blocks that could produce lacerations, also the anti-ice system would create a water movement in the surface of the upstream face by means of a continuous erogation of compressed air.

7.4.4.2 Properties of geomambrane in cold regions

7.4.4.2.1 Brittleness and stiffness the literature shows that geomembrane materials become less flexible and more brittle as temperature is lowered. Under cold temperature, these properties control the membrane behavior. In the presence of elastomers, the membrane keeps it's flexibility under a wide ranges of temperatures.

7.4.4.2.2 Stress-strain As the load is increased the membrane elongates until reaching a breaking point. Rollin *at el* (1985), carried out tests of 21 different types of membrane materials at low temperatures. Figure 7.19, represents the stress-strain

relationship. The temperature has a great influence on the elastic behavior of a membrane such that its elastic modulus increases with the lowering of temperature so the yield point and breaking point appear at lower strain level.

7.4.4.2.3 Resistance to puncture and bursting

Giroud (1982) found that the puncturing and the bursting risk are a function of the elastic properties of membrane. At cold temperature resistance to bursting and puncturing increases as long as the glass transition temperature are not exceeded.

7.4.4.2.4 Installation

Figures 7.20 and 7.21 show the method of installation in case of empty reservoir as well as under water installations. The installation procedure used in Europe are described by the International Committee of Large Dams, ICOLD (1995) can be listed as follows:

The water tightness layer of geomembrane of 2-4 *mm* thick with a geotextile attached to the back of it. The geotextile is provided both as support for the geomembrane against the surface of the dam and for drainge. The geotextile strips are anchored to the face of the dam by vertical stainless steel double profiles. The inner profile has a U-shaped section with two small wings and the outer profile has small wings that bends inward, Figures 7.22-7.23. The two profiles are fixed to the concrete by a threaded rod. These profile also provide drainge downstream of the geomembrane. The water is conveyed to the drainge pipes at the bottom of the dam. No profiles are located close to the vertical joints, so any movement in vertical joints

can be accommodated.

The parameter of the membrane is sealed by a stainless steel strip, fixed to the concrete face, Figure 7.20. At the change of the slope or any other changes of direction the membrane is also anchored by stainless steel strip, fixed to the face of the concrete. Special connection and other devices are needed for difficult locations on the surface of the dam.

A wire system should be install behind the geomembrane over the whole covered area to monitor any discontinuity or sliding of the waterproof membrane.

7.4.5 The Long Spruce- Case Study

Based on the analytical study, mentioned previously, also based on the experimental results described in chapter six. It can be concluded that:

grouting material can not be use for this case, because of the changes occurs in the properties of grouting material due to the influence temperature and surface condition.

Anchors can not be used in both up and downstream sides. In view of the considerable stresses that develop due to the use of anchorage in both sides of the dam, which could initiate a new cracks in the top block of the dam.

Numerical tests have been carried out to simulate the dam motion with the joint fixed by anchors only in the upstream side, where the downstream side can still move freely as indicated in Figure 7.18. Based on these results of the numerical analysis. The use of anchors can reduce the deformation but it can not stop the leaking. Its

believed that the use of anchors could stop the leaking, if they are used in combination with one of the following:

1. The use of thermal control material to reduce the thermal load which will leads to further reduction in the thermal deformation.

2. Grouting material. where the anchors take the load and the grouting material fill the cracks.

The disadvantage of the above two solutions is that they will lead to a very high cost. Based on the data collected from the site over the last seven years which indicates that, during the last four years, Figure 7.7 through 7.10, the top block of the dam shows no increase in deformation which is a sign of stability. In this case where stability is not affected, it is recommended that the crack should be left free to deform and a suitable material like geomembrane acting as a waterstop could be used. But should be able to allow relative displacements to account for the seasonal deformations.

For the case of Long Spruce, the selected membrane must exhibit a low modulus of elasticity under wide range of temperatures (from 20 to -40 °C) to allow sufficient strain before reaching the yield point or breaking point. One must be aware not to choose too weak membrane that will not offer enough resistance to applied loads. Under stresses the membrane must be inaccessible and must participate in the slope stability by resisting the applied load.

Because of the location of the Long Spruce Generation Station, the behavior of geomembrane under cold temperature conditions can not be mispredicted and

laboratory test must be preformed on samples at room as well as low temperature.

The selected membranes should not be affected by the temperature fluctuations such as to break under expected loads especially at edges, joint and folds. Under cold conditions, one should avoid the use of a membrane that becomes brittle enough that any load transmitted from the ice action on the rip might damage the membrane. Similarly the types of glue used to seal the overlapping joints and to increase adherence between the textiles and the membrane should not be affected by cold temperatures. Any product with a glass transition temperature lower than -40°C is acceptable.

The membrane to be laid down on the upstream face of a dam should be anchored at the top section of the dam. Care should be taken to select a membrane with a high flexibility and to avoid sharp bends that will represent sites for stresses to build up when the membrane will be submitted to loads under cold temperatures. The risk of breaking the membrane at anchor location under these conditions can be very high.

The overlapping width of rolls should be determined to predict the slipping risk. Tests must then be performed at higher temperatures at which the risk of slipping is greater because, as believed, most joints will behave better at colder temperatures unless the seal material becomes brittle. Fusion techniques as well as sealing materials should be thoroughly checked under cold temperatures.

An efficient draining system is essential in order to eliminate the accumulation of water condensation and from filtration.

Also anti-ice systems can be used with the installation of a membrane to prevent the formation of large ice. The anti-ice system create a water movement in the upstream face by means of a continuous pumping of compressed air.

7.4.6 Summary

- In case of using grouting material, account must be taken of the characteristics of the grout mix (viscosity, pot-life, bleeding, wash-out resistance, temperature effect) and of the crack (active or passive, dry or wet, water pressure and running water).

- If the stability in the case study dam is considered not affected, the cracks should be left free to deform and filled with a suitable material acting as a water-stop but able to allow relative displacement or by using geomembrane. Geomembrane can be used not only to eliminate leakage, but also to protect the concrete from aggressive water and to prevent decay.

- Attention must be paid to the correct time to undertake the repairing procedure which can depend on the concrete and air temperature

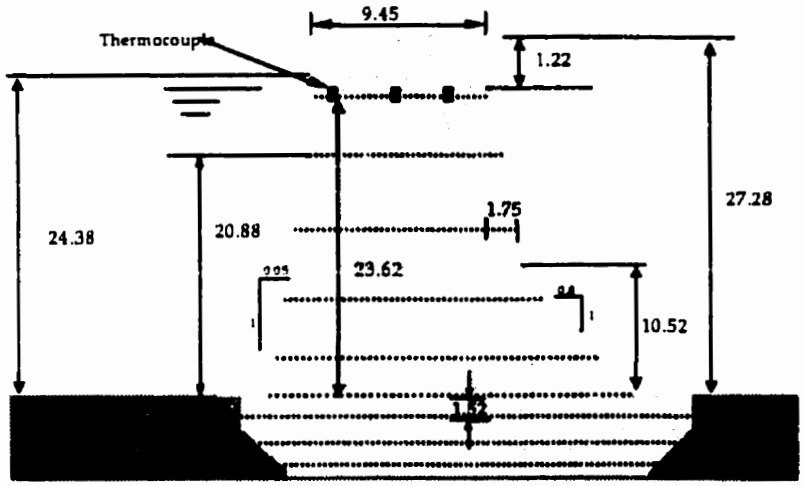

Figure 7.1: Dimensions of the south transition structure (dimensions in mm)

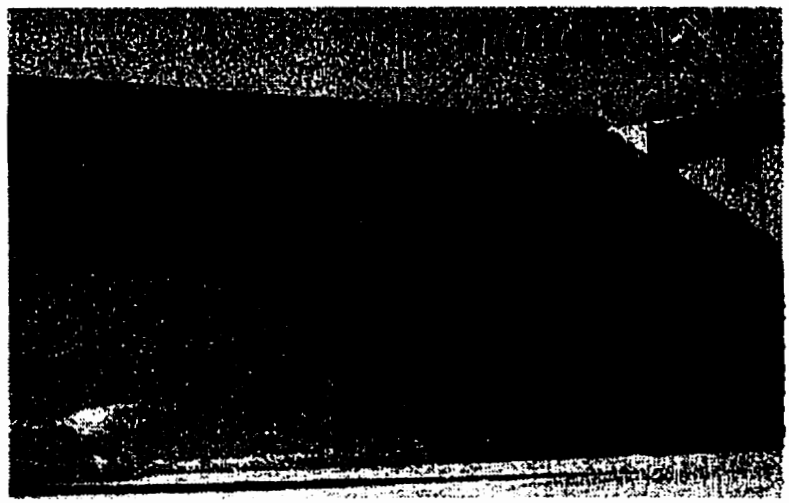

Figure 7.2: Leakage in the south transition on the horizontal construction joint (winter, 1994)

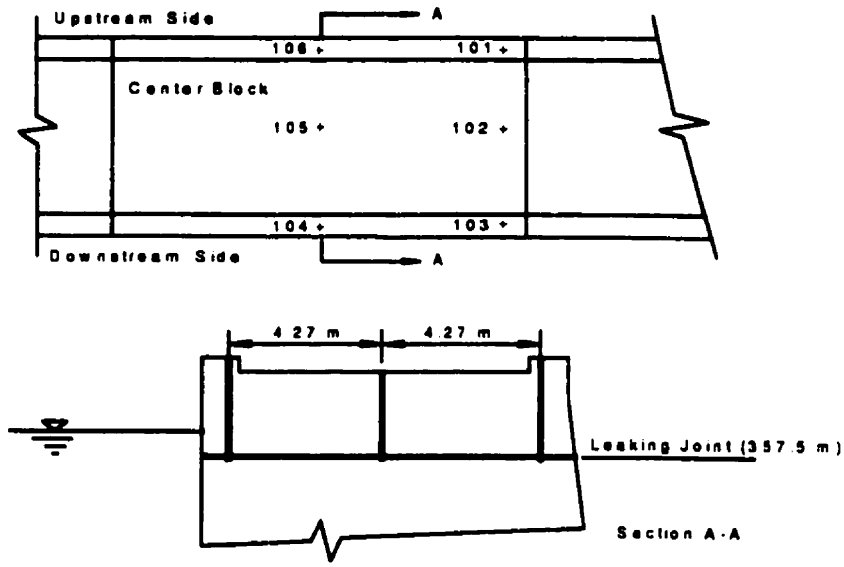

Figure 7.3: Location of instrumentation (Manitoba Hydro 1994)

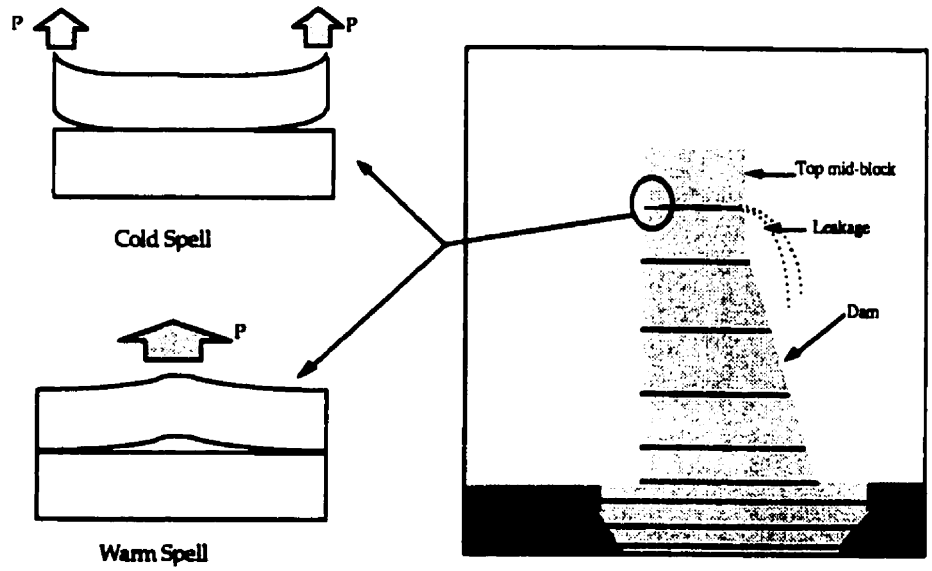

Figure 7.4: Deformation pattern of the dam with debonding joint

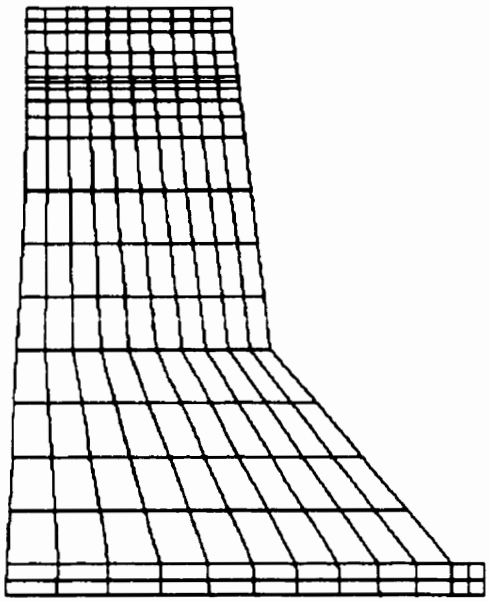

Figure 7.5: Finite element mesh for the south transition

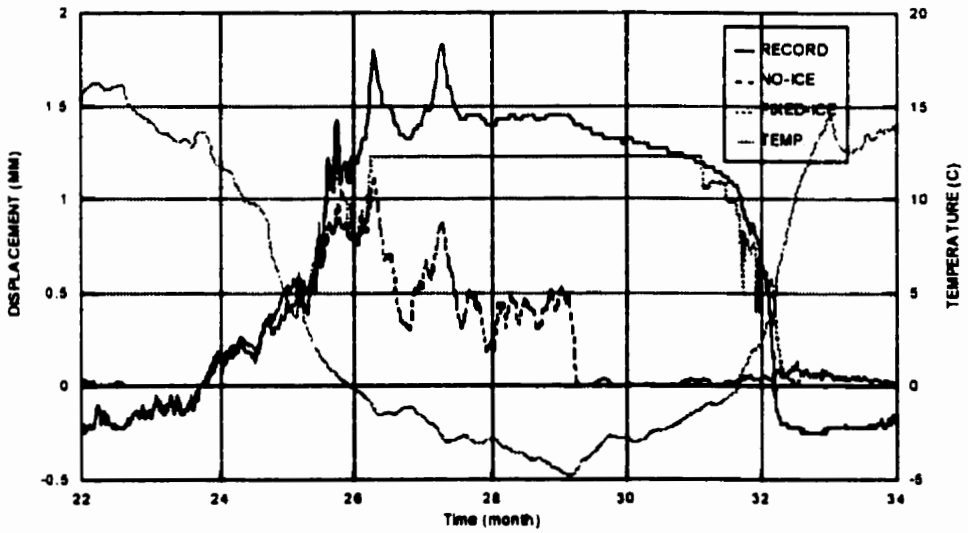

Figure 7.6: Model comparison for upstream side, Zhang (1998)

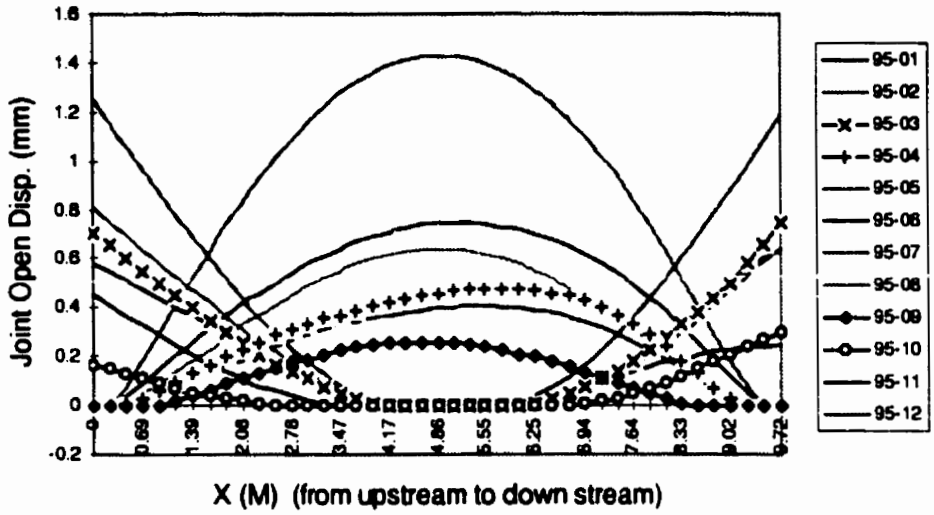

Figure 7.7: Joint opening displacement in (1994)

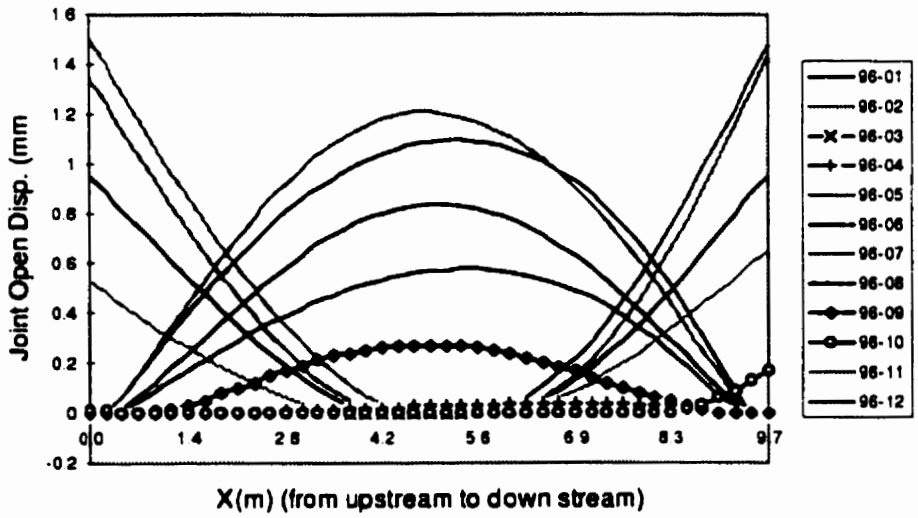

Figure 7.8: Joint opening displacement in(1995)

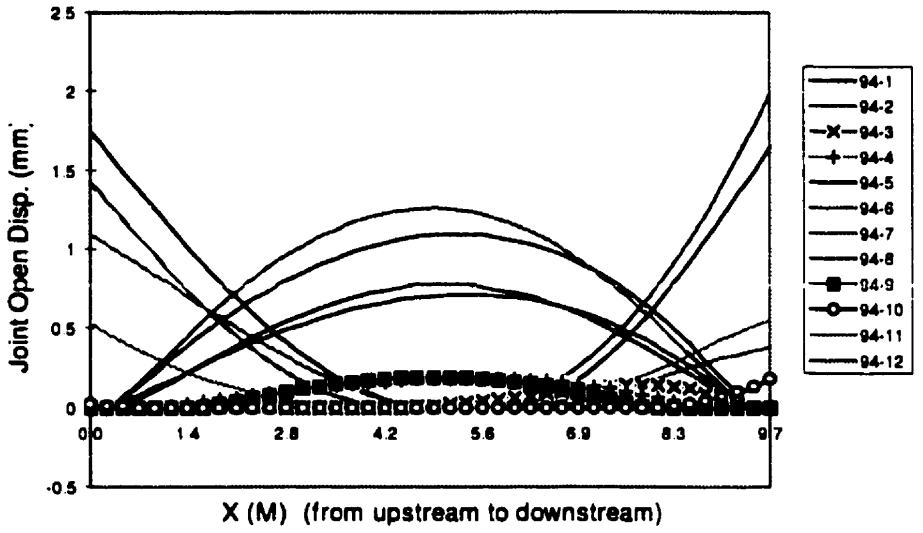

Figure 7.9: Joint opening displacement in(1996)

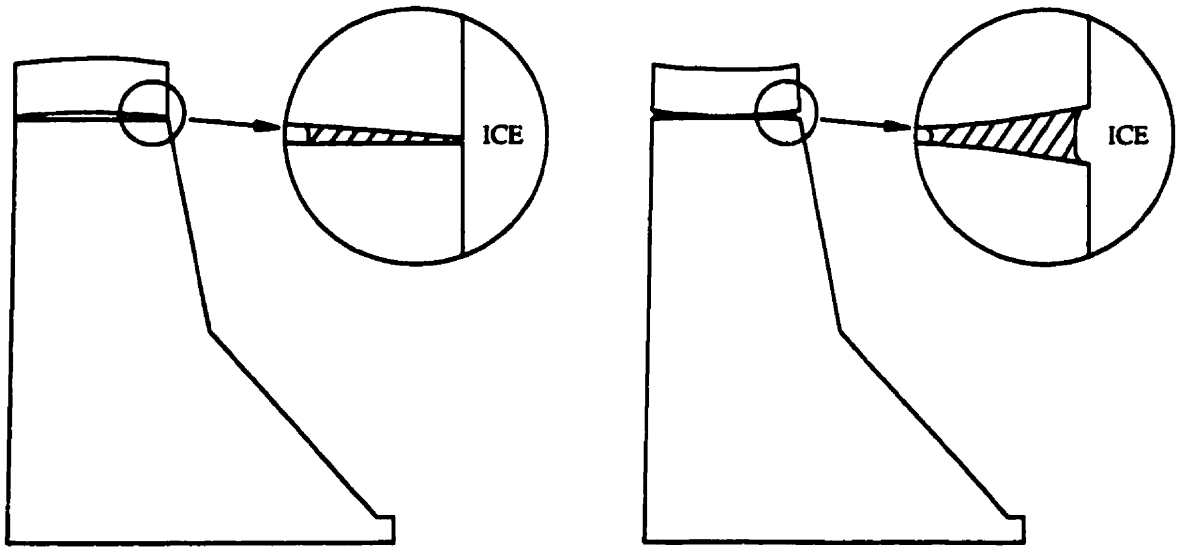

Figure 7.10: Ice layer forms inside the crack

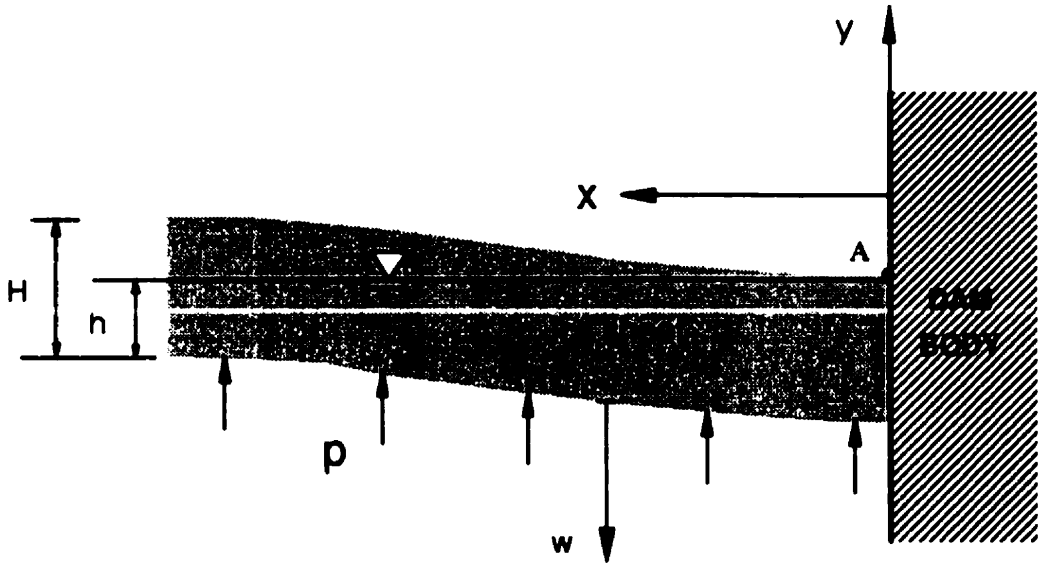

Figure 7.11: Sketch of the forbay ice sheet

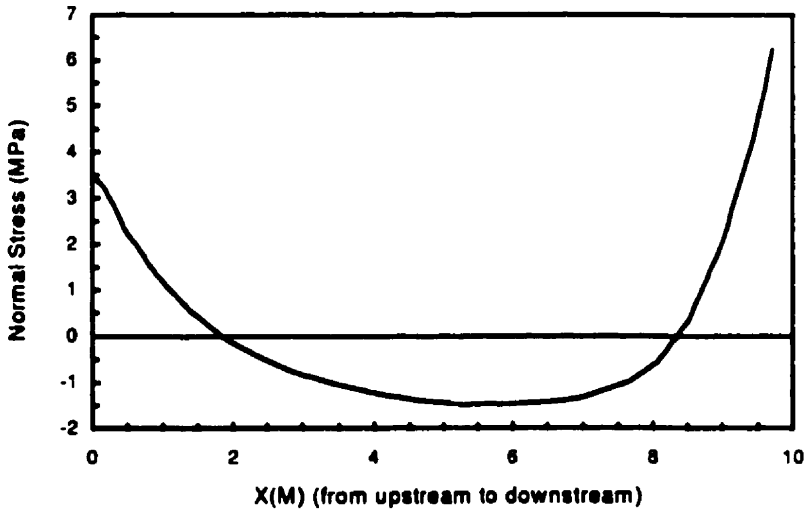

Figure 7.12: Normal stress distribution along joint interface during winter

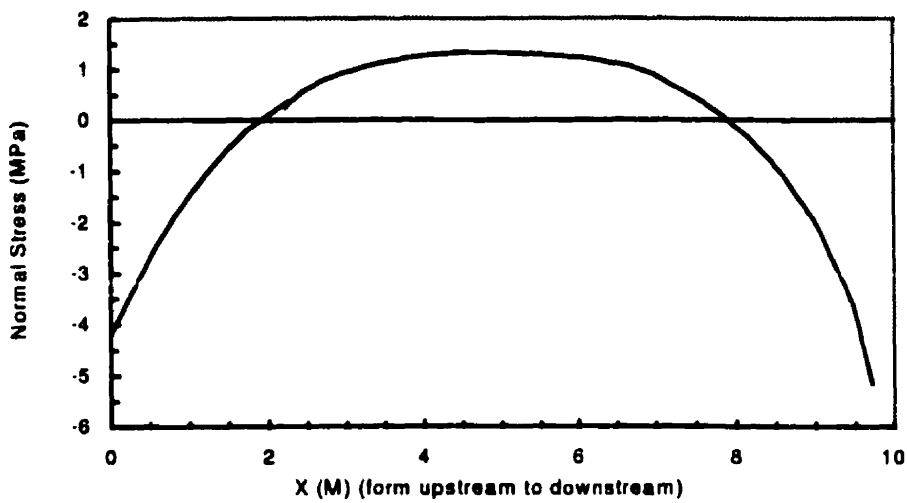

Figure 7.13: Normal stress distribution along joint interface during summer

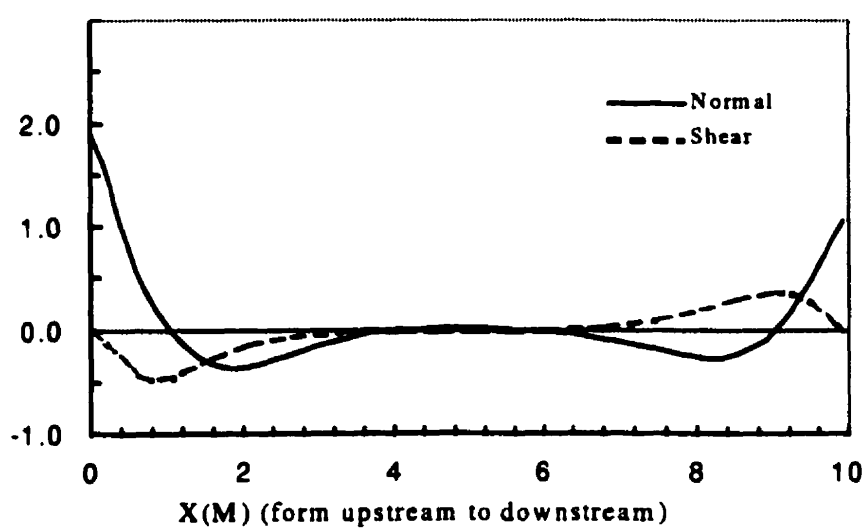

Figure 7.14: Residual stresses along the joint interface

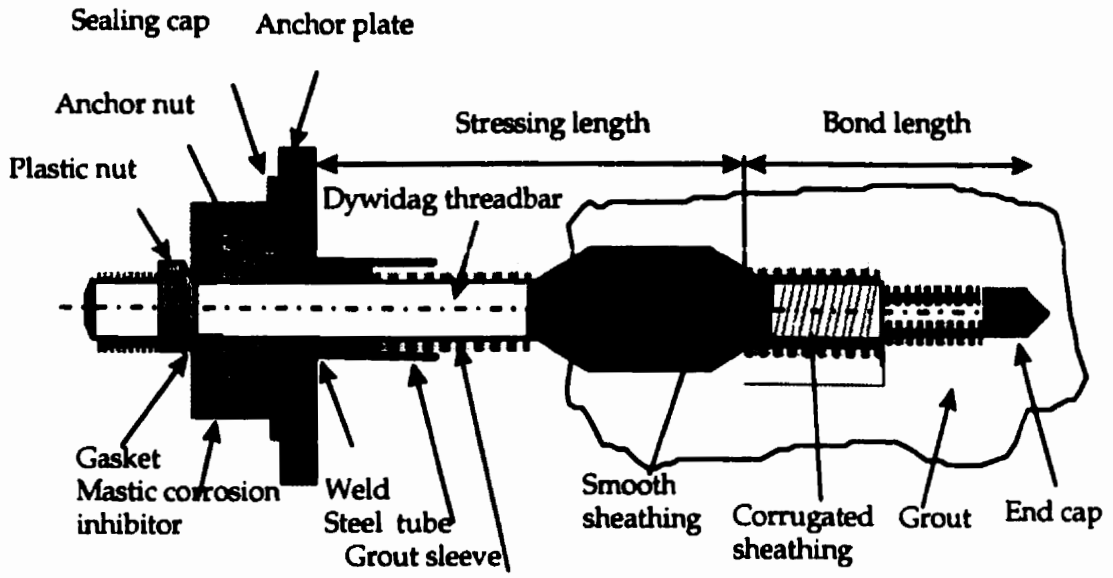

Figure 7.15: Dywidag threadbar anchor with double corrosion protection

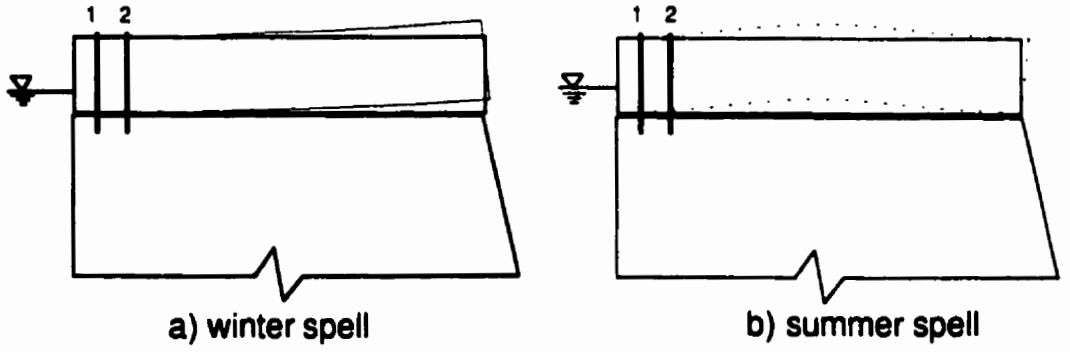

Figure 7.16: Anchors installation position

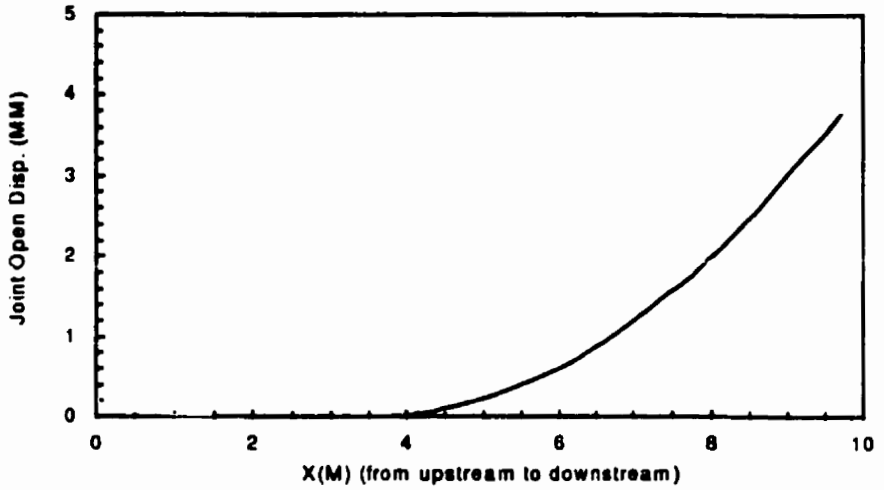

Figure 7.17: Open displacement along the joint interface

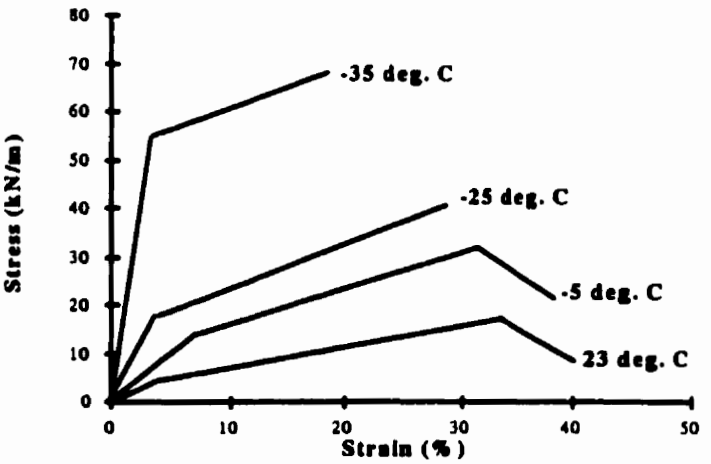

Figure 7.18: Temperature influence on tensile strength

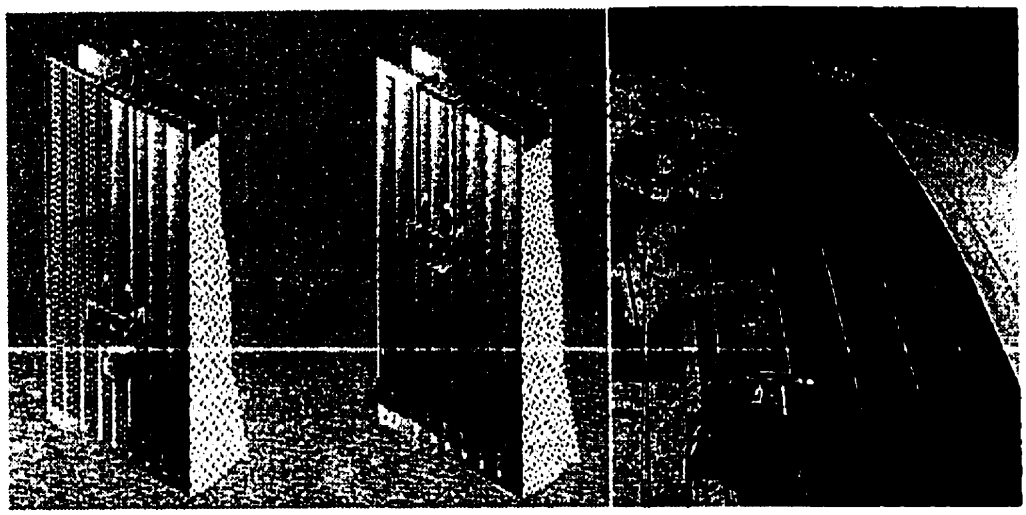

Figure 7.19: Installations of geomembrane

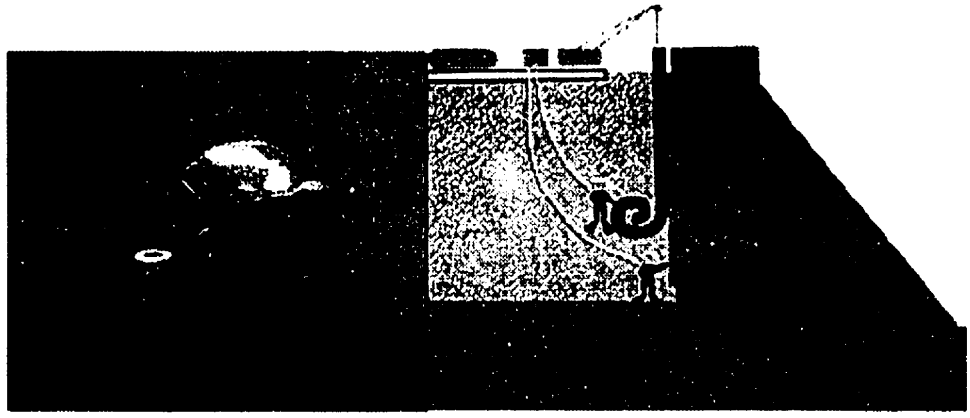

Figure 7.20: Under water installations

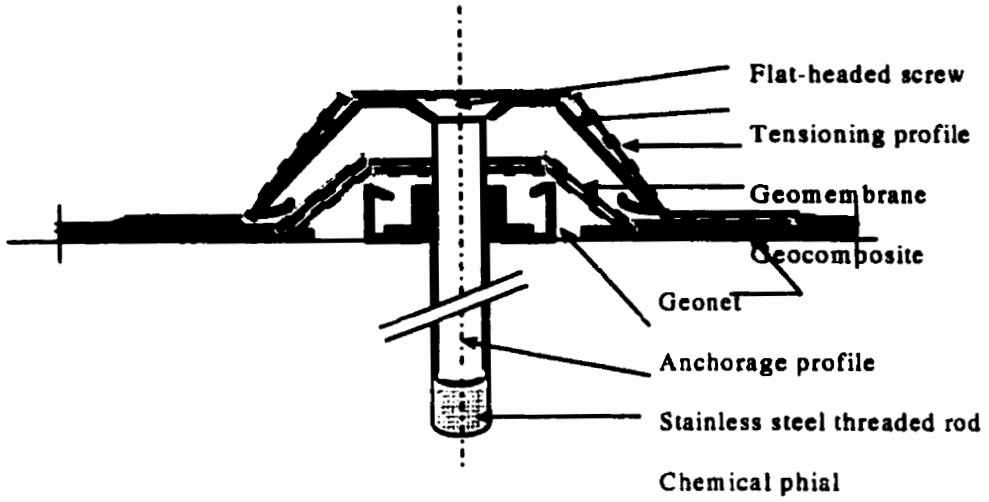

Figure 7.21: Detail of vertical anchorage and drainage profiles (ICOLD 1997)

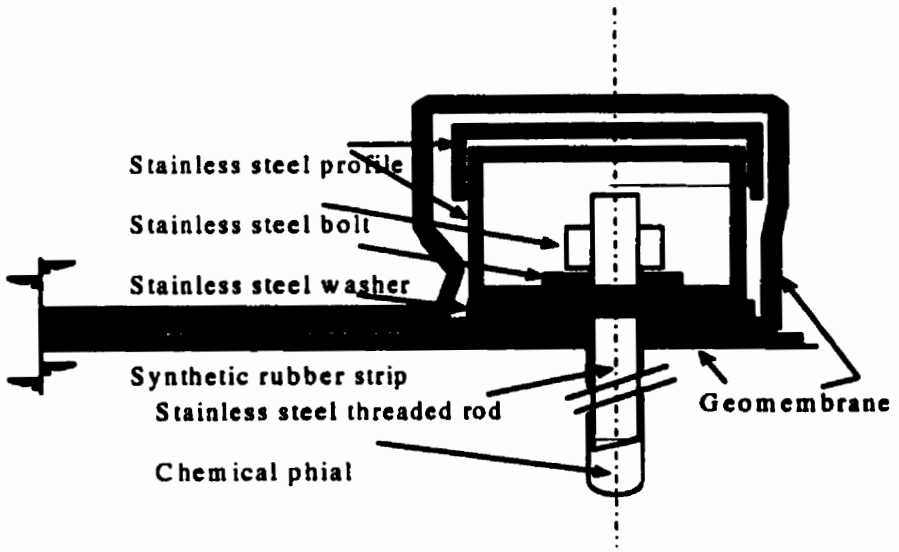

Figure 7.22: Detail of sealing profiles (ICOLD 1997)

Chapter 8

CONCLUSIONS AND RECOMMENDATIONS

8.1 Introduction

This research addressed the repair of concrete dams under sever thermal conditions. The main objectives were to:

1. identify and characterize cracking in concrete dams, when subjected to severe thermal conditions.

2. establish the fracture properties of joints between adjacent concrete lifts under extreme low temperature

3. study the effectiveness of repair materials commonly used to seal and prevent leakage from joints,

4. study the overall failure mechanism of concrete joints in dams operating in cold regions and develope proper repair strategies for a specific case study.

The program consisted of experimental and an analytical study. The experimental program was divided into three phases and includes the testing of one hundred and thirty specimens.

In phase I, the specimens were tested under different temperatures and with different sizes of specimens. For phase II, specimens tested in phase one were repaired and tested again and the same procedure was used for phase III. The variables in the experiments were temperature, repair materials, aggregate type, size of specimens and the moisture condition of cracked surface.

The experimental results were numerically reproduced and the compliance method was used. The finite element calibration analysis with the finite element program SIMEX. The fracture tests were simulated numerically and, then, the calculated load (F_{sp}) versus crack opening displacement (COD) curve compared to the experimental curve. The analysis was repeated until good agreement between calculated and experimental curve is obtained. The softening post-peak regime of the (F_{sp} *vs* COD) diagram leading to this agreement was considered to be the tensile softening response of the tested concrete.

Based on this research program repair strategy of an actual case study of cracked concrete dam operating in the north region of Canada were proposed.

8.2 Conclusions

The following summarizes the finding of this investigation

1. The peak load for the specimens tested at low temperature, appear to be 50-200% higher than specimens tested at room temperature. Concrete at low temperature becomes more brittle and needs extra care during testing to control crack propagation.

2. Fracture energy increase with a decrease in temperature (up to 250% higher), which suggest that at low temperature structures are safer, from the fracture point of view, than structures at room temperature when subjected to the same loading.

3. The limestone concrete behaves more brittle according to the definition in the fracture mechanics approach than the gravel concrete. Also more energy was required to fracture the gravel aggregate concrete than to debond the limestone one.

4. Size effects in concrete specimens of different size was observed. Although the specimens were of large laboratory scale, the specimen dimensions were still too small for LEFM analysis.

5. Dimensional analysis based on Bažant's size effect shows that, for structures with geometrically similar, the nominal stress at failure varies with the structure size.

6. For the smallest structure that can be made with a given aggregate, the strength criterion governs, and for structure that are sufficiently large, the fracture mechanics criterion governs.

7. The fracture properties of specimens cast in two stages exhibited lower energy than the specimens cast in one stage (40-50% less) and this is due to weakness in interface joints.

8. The compressive strength of concrete increases with a reduction in temperature. This increase is due to the moisture in the concrete being frozen.

9. In terms of overall performance of the repair materials, the material can be ranked from best to poorest as follows: Epoxy-K, fine cement, epoxy-W when perform at room temperature and compared with the performance of specimens with interface joint.

10. Temperature effects on the fracture properties of the materials are significant. In general, the decrease in temperature causes increase in the fracture energy, G_F. This is not the case in the repaired specimens, where the effect depends on the type of the materials.

11. Successive rehabilitation depends heavily on the type of repair material. Also the response of repair materials depend on the condition of the cracked surface.

12. A second repair is even weaker than the first one, because of the amount of damage, the cracked joint experiences before the re-repair, and also the contamination of the old repair material which creates several points of weakness

in the fracture plane.

13. Wetting of concrete specimens, induces a reduction in the capacity of the specimens and this is believed to be due to residual stresses, also due to the effect of wetting condition on the properties of the repair material.

14. This study gives the basic information on repair materials commonly used in concrete dams. It gives a practical method for repair of cracks in terms of surface preparation, surface moisture condition and application of repair material in wet and dry condition. This information are not available from manufactures, however, it is very essential for repair the process. Right application of repair materials will results in significant reductions of cost and time used in the repair process.

15. new techniques for measuring fracture parameters will be of great practical importance. Further results from studies of the composite concrete- repair materials under low temperature will provide procedures to address the ever re-occurring failure due to cracking.

8.3 Recommendations for Future Research

Several issues remain open for further work. Some of the important ones are:

1. Further tests are needed on specimens with different kinds of interface and exposure to other types of loading. It may be expected that the influence of the

scale of the specimens examined is of importance, particularly as it concerns stresses induces induced by differential shrinkage and thermal deformations.

2. Further research on the phenomenon of a residual stress for laboratory tests as well as for real structures is recommended.

3. Further study of the measurements of horizontal and vertical ice loading affecting large concrete structures.

4. Testing larger specimens to study the size effect on strength and fracture properties.

5. Achieving thermal control of concrete dams in the north. The question to answer here is: Is there an economically feasible way to keep the temperature of critical section of dams in an acceptable range?.

REFERENCES

1. ACI Committe 446, (1995)."Fracture Mechanics: Applications to Concrete Structures and Implications with Regard to the Code," American Concrete Institute, Detroit, MI, USA.

2. Alfaiate, J., *et.al.*, (1992). "A finite element model for the study of crack propagation in concrete, Localized Damage II, Vol I: Fatique and Fracture Mechanics, Computational Mechanics Publication, Southampton, Boston, USA, pp. 261-280.

3. Area, M., and Ingraffea, A. R., (1982). Mixed mode crack propagation in mortar and concrete, Report No. 81-13, Dept. of Structural Engineering, School of Civil and Environmental Engineering, Conell, University.

4. Armstrong, T., and Ayari, M . L., (1994). "Computation of the transient thermal load in incrementally constructed concrete dams," Proceeding of the Int. Workshop on Dam Fracture and Damage, Chambery, France .

5. Arya, S. K, Hegemier. A., (1982). "Finite Element Method for Interface Problems," ASCE, Journal of the Structure Division, Vol. 108.

6. Atkinson, C., (1977). "On Stress Singularities and in linear elastic fracture mechanics," Int. J. Fracture, Vol. 13, No. 6.

7. Ayari, L. M. and Saouma, V. E., (1991). "Static and dynamic contact/impact problems using fictitious forces," Int. J. Numer. Meth. Eng., Vol. 32, No. 3.

8. Ayari, L. M., (1988). "Static and dynamic fracture mechanics of concrete gravity dams," Ph.D thesis, University of Colorado.

9. Babuska, I., and Miller, A., (1984). " The post-processing approach to finite element method," Int. J. Num. Meth. Engrg., Vol. 20.

10. Barenblatt, G. I., (1962). " The mathematical theory of equilibrium of cracks in brittle fracture," Advances in Appl. Mech., Vol. 7. pp. 55-129.

11. Bascoul, A., *et. al.*,(1987). "Concerning the measurement of fracture renergy of a microconcrete according to the crack growth in a three point bending test on notched beams," Proceedings of the int. Conf. on Fracture of Concrete and Rock, Houston, pp. 613-643.

12. Bažant, Z. P., and Cedolin, L., (1979). "Blunt Crack Band Propagation in Finite Element Analysis," J. Engrg. Mech., ASCE, Vol. 102, No. 2, pp. 331-344.

13. Bažant, Z. P., and Kazemi, M. T.,(1990). " Determination of fracture energy, process-zone length and brittleness number from size effect, with application to rock and concrete,"Int. J. Fracture, Vol. 44, pp. 111-131.

14. Bažant, Z. P., (1984). "Size Effect in blunt fracture: concrete, rock, matel," Journal of Eng. Mech., ASCE, Vol 110, No. 4, pp. 518-535.

15. Bažant, Z. P., (1992). "Fracture Mechanics and Size Effect of Concrete Tension," Journal of Structural Eng, Vol. 118, No. 11.

16. Bažant, Z. P., *et.al.*, (1994). "Fracture Size Effect: Review of Evidence forConcrete Structures," Journal of Structural Eng., Vol. 120, No. 8.

17. Bažant, Z. P., and Pfeiffer, P. A.,(1987). "Determination of Fracture Energy from Size Effect and Brittleness Mumber," ACI Materials Journal. Vol. 84, No. 6.

18. Bažant, Z. P., (1993). "Scaling Laws in Mechanics of Failure," Journal of Eng. Mechanics. Vol. 119, No. 9.

19. Beer, G., (1985). "An Isoparametric Joint/Interface Element For Finite Element Analysis," Int. J. Numerical Methods in Eng. Vol. 21, pp. 858-600.

20. Bhattacharjee, S., and Leger, P., (1993). "Finite element modeling of the tensile strain softening behavior of plan concrete structures," Eng. Computations, Vol. 10, pp. 205-221.

21. Brincker, R., and Dahl, H., (1989). "Fictious crack model of concrete fracture," Magazine of concrete research, Vol. 41, No. 147.

22. Broek, D., (1986). elementary engineering fracture mechanics, (4rd revised ed.), Martinus, Netherlands.

23. Brühwiler, E., Broz, J. J., and Saouma, V. E., (1991). " Fracture model evaluation of dam concrete," Journal Mater. Civil Engng, Vol 3, No 4, pp. 235-251.

24. Brühwiler, E., and Wittmann, F. H., (1990). " The wedge splitting test—a method of performing stable fracture mechanics tests," Fracture and Damage of Concrete and Rock, (Proc.1st Int Conf FDCR-1, Viena 1988), ed. Rossmanith, H. P., Pergamon Press, Oxford, pp.117-126.

25. Carrere, A., (1990). "Ten Years of Experience in Calculation of Cracked Concrete Dams and Other Non-Linear Structures," Cement and Concrete Research, Vol. 20, pp. 559-578.

26. Carpinteri, A., (1986). Mechanical damage and crack growth in concrete. Marinus Nijhoff Publishers.

27. Cervenka, J., (1994). "Discrete Crack Modeling In Concrete Structures" Ph.D. Thesis, University of Colorado.

28. Chan, S. K., and Tuba, I. S., (1971). "A finite element method for contact problems of solid bodies," Int. J. Mech. Sci., Vol. 13, pp. 627-639.

29. Chappell, J. F., and Ingraffea. A. R., (1981). A Fracutre Mechanics Investigation of the cracking of Fontana Dam, Report No: 81-7, Dept. of Structural Engineering, School of Civil and Environmental Engineering, Conell, University, New York, USA.

30. Comninou, M., (1990). "An Overview Of Interface Cracks," Eng. Frac. Mechanics, Vol. 37, No 3.

31. Comninou, M., (1977). "The Interface Crack," Journal of Applied Mechanics, Tran. of the ASME, Vol. 44. No 4.

32. Dahlblom, O., and Ottosen, N.S., (1990). " Smeared crack analysis using generalized fictitious crack model," J. Eng. Mech., Vol. 116, No. 1.

33. De Borst, R., (1986). "Constitutive models for continua and numerical techniques for analysis of granulat materials, Ph.D. thesis, Delft University of Technology, Delft, The Netherland.

34. Dewey, R., Reich, W., and Saouma, V. E., (1994). "Uplift Modeling for Fracture Mechanics Analysis of Concrete Dams," Journal of Structural Eng., Vol. 120, No. 10.

35. Diamond, S., and Bentur, A., (1985). "On the Cracking of Concrete and Fiber-reinforced Cement" Application of Fracture Mechanics to Cementitious Composites, Shah. S.P. (ed.), Martinus Nijhoff Publishers, Dordrecht, pp. 87-140.

36. Drugan, W .J., (1991). "Near-Tip Fields for Quasi-Static Crack Growth Along a Ductile-Brittle Interface," Journal of Applied Mechanics, Tran. of the ASME, Vol. 58.

37. Dunders, J., (1969). "Edge-bonded dissimilar orthogonal elastic wedges under normal and shear loading," Journal of Applied Mechanics Vol. 36, pp. 650-652.

38. Dunger, R., Saouma, V., and Wittmann, F., (1994). "Conference report: The application of fracture mechanics in dam engineering," Dam Engineering, Vol. II, Issue I.

39. Elfgren, L., ed., (1989). "Fracture Mechanics of Concrete Structure- From theory to applications, state of art report," RILEM TC 90-FMA, Chapman

and Hall, London, England.

40. Elices, M., Planas, J. and Maturana, P., (1987). "Fracture of concrete at cryogenic temperatures," SEM/RILEM Int. conference on fracture of concrete and rock, Houston,Texas.

41. England, A. H., (1965). "A Crack Between Dissimilar Media," Journal of Applied Mechanics, Tran. of the ASME, Vol. 32.

42. Erdogan, F., (1965). "Stress Distribution in Bonded Dissimilar Material with Cracks," Journal of Applied Mechanics, Tran. of the ASME, Vol. 32.

43. Erdogan, F., and Delale, F., (1988). "Interface Crack in a Non-homogeneous Elastic Medium," Int. J. Eng. Sc. Vol. 26, No 6 .

44. Erdogan, F., and Delale, F., (1988). "On the Mechanical Modeling of the Interfacial Region in Bonded Half-planes," Journal of Applied Mechanics, Tran. of the ASME, Vol. 55.

45. Erdogan, F., (1963). "Stress Distribution in a Non-homogeneous Elastic Plane with Cracks," Journal of Applied Mechanics, Tran. of the ASME, Vol. 85, Series E.

46. Francavilla, A., and Zienkiewicz, O. C., (1975). "A note on numerical computation of elastic contact problems," Int. J. Numer. Methods Eng., Vol. 9, pp. 913-924.

47. Fujii, K., and Nakagawa, K., (1993). "The Stress Concentration Ratio of The Interface Crack Between Dissimilar Anisotropic Composite Materials," Eng. frac. Mechanics Vol. 44 No 1.

48. Ghaboussi, J., Wilson, E. L., and Isenberg, J., (1973). "Finite element for rock joints and interfaces," J. Soil. Mech. and Found. Div., A.S.C.E., Vol. 99, pp. 833 - 848.

49. Giroud, J. P., (1982). " Design of Geotextiles Associated with Geomembtrane." Proc. 2nd Int. Conf. on Geotextiles, Vol. IV, Las Vegas, pp. 37-42.

50. Gladwell, G. M. L., (1973). "Contact Problems in the Classical Theory of Elasticity," Sijthof and Nordhoff, The Netherlands.

51. Goodman, R. E., Taylor, R. C., and Brekke, T. C., (1986). " A Model for the Mechanics of Jointed Rocks," J. Soil Mech. Div., Vol. 94.

52. Griffith, A. A., (1921). " The phenomena of Rupture and Flow in Solids," Phil. Trans. Roy. Soc. London, A221, pp. 163-197.

53. Guo, Z. K. , *et.al.*, (1993). "Future studies on fracture process zone for mode I concrete fracture," Eng. Frac. Mech., Vol. 46 No. 6.

54. Hamoush, S. A, and Ahmad, S. H, (1989). "Mode I and II Stress Intensity Factors for Interface Cracks in Bi-Material Media," Eng. Fract. Mechanics Vol. 33 No 3.

55. Henshell, R., and Shaw, K., (1975). "Crack Tip Finite Elements are Unnecessary," International Journal for Numerical Methods in Engineering, Vol. 9, pp. 495-507.

56. Herrmann, L., (1978). "Finite Element Analysis of Contact Problems," ASCE, Journal of Eng. Mechanics. Vol. 104.

57. Hillerborg, A., *et.al.*, (1976). "Analysis of Crack Formation and Crack Growth in concrete by means of Fracture Mechanics anf Finite Elements," Cement and Concr. Res., Vol. 6, pp. 773-782.

58. Hillerborg, A., (1991). "Application of the fictitious crack model to different types of materials," Int. J. Frac. Vol. 51, pp. 95-102.

59. Houlsby, A. C., (1977). "Engineering of Grout Curtains to Standards," Journal of Geotechnical Engineering Division, ASCE, Vol. 103, No 2.

60. Houlsby, A. C., (1990). Construction and design of Cement Grouting, John Wiley & sons, New York.

61. ICOLD report, (1995). " Control and treatment of cracks in concrete dams,' billetin of ICOLD committee on concrete for dams. Paris, France.

62. Ishikawa, M., (1991). "Thermal Stress Analysis of a Concrete Dam," Computes and Structures, Vol.40, No. 2, pp. 347-352.

63. Ingraffea, A. R., and Saouma, V., (1981). "Fracure Analysis of Discrete Cracking," colloquium on Advanced Mechanics of Reinforced Concrete, IABSE, Delft,

Netherlands.

64. Irhouma, A. M., Ayari, L. M., Robinson L. C., and Glanville J. I., (1998). "Rehabilitation Of Cracked Concrete Dams In Cold Regions- Case Study," accepted by Journal of Concrete Eng. International.

65. Irhouma, A. M., Ayari, L. M., and Robinson L. C., (1997). "Fracture Characterization of Repair-Material in Sub-arctic Region" submitted to ASCE, Journal of Cold Regions Engineering.

66. Irhouma, A. M., Ayari, L. M., and Glanville, J. I., (1997). "Rehabilitation of Cracked Concrete Dams in Sub-arctic Region" 7th International Conference of Structural Faults and Repair, Edinburgh, Scotland, 8th -10th July.

67. Irhouma, A. M., Ayari, L. M., and Glanville, J. I. (1997). "Repair of Cracked/Leaked Concrete-Dams in Cold Region" The 25th CSCE Conference, Sherbrooke.

68. Irhouma, A. M., Ayari, M. L., and Robinson L. C., (1998). "Effect Of Low Temperature On Fracture Characteristics Of Concrete Joints And Repair Materials" Accepted for publication in the Third International Conference on Fracture Mechanics of Concrete and Concrete Struc-tures, Gifu, Japan, 12th-16th Octobr.

69. Irwin, G. R., (1957). "Analysis of Stress and Strain Near the Ends of a Crack Traversing a Plate," Journal of Applied Mechanics, Vol. 24, pp. 361-364.

70. Izumi, M., Mihashi, H., and Nomura, N., (1986). " Acoustic Emission Technique to evaluate Fracture Mechanics Parameters of Concrete" (ed.) Wittmann,

F. H., Fracture Toughness and Fracture Energy of Concrete, Elsevier Science Publishers, Amsterdam, pp. 259-268.

71. Jenq, Y. S., and Shah, S. P., (1985). "Two Parameter Fracture for Concrete," Journal of Eng. Mechanics, Vol. 111, No. 10.

72. Kaplan, M. F., (1961). "Crack Propagation and Fracture of Concrete," ACI Journal, Vol. 58, No. 5, pp. 591-610.

73. Klisinski, M. *et.al.*, (1991). "Finite element with inner softening band," J. Eng. Mech., Vol. 117, No. 3.

74. Lee, K., (1991). "Fracture Analysis of Mortar-Aggregate Interfaces in Concrete," Journal of Eng. Mechanics.Vol. 118, No. 10.

75. Koerner, R., (1986). " Designing with Geosynthetics," Perntice- Hall, Englewood, Cliffs, New Jersey, USA.

76. Lee. K., (1991). " Fracture Analysis of Mortar-Aggregate Interfacesin Concrete," Journal of Engrg. Mechanics, Vol. 118, No. 10.

77. Leger, P., Cote, M., and Tinawi, R., (1994). Evaluation of thermal protection systems for concrete dams subjected to severe winter conditions, Report No. EPM/GCS-1994-03, Ecole Polytechnique.

78. Leger, P., Venturelli, J., and Bhattacharjee, S. S., (1993). "Seasonal temperature and stress distribution in concrete gravity dams," Canadian J. of Civil Eng., Vol. 20, No. 6, pp. 999-1029.

79. Li, Y. N., and Liang, Y.L., (1994). "Peak load determination in linear fictitious crack model," J. Eng. Mech., Vol. 120, No. 2.0

80. Linsbauer, H. N., (1985). "Fracture Mechanics Models for Characterizing Crack Behavior in Concrete Gravity Dams,"Quinzienne Congress des grands barrages, Lausanne, pp. Q57, R16.

81. Lokuliyana, D., and Tanabe, T., (1990). "Thermal Crack Propagation in Massive Concrete Structures Using Fracture Mechanics," Transactions of the Japan Concrete Institute, Vol. 12.

82. Loland, K. E., (1980). "Continuous Damage Model for Load- Response Estimation of Concrete," Cement and Concrete Research, Vol. 10, pp. 395-402.

83. Lubarda, V.A., *et.al.*, (1994). "Damage model for brittle elastic solids with unequal tensile and compressive strengths," Eng. Frac. Mech., Vol. 49, No. 5.

84. Machida, K., and Uehara, K., (1987). "Nonlinear Thermal Stress Analysis of a Massive Concrete Structure," Computes and Structures Vol. 26, No. 2, pp. 287-296.

85. Mai, Y. (1979) "Strength and Fracture Properties of asbestos Cement Morter Composites," Journal of Material Sci., Vol. 14, pp. 2091-2102.

86. Maji, A., *et. al*, (1991). "Fracture Mechanics of Concrete, Rock and Interface," International Symposium on Fatigue and Fracture in Steel and Concrete Structure.

87. Maji, A. K., and Shah, S. P., (1988). "Process Zone and Acoustic Emission Measurement in Concrete, " J. of Experimental Mechanics, Vol.28, pp. 27-33.

88. Majorana, C., Zavarise, G., Boroetto, M., and Giuseppetti, M., (1990). "Non-linear Analysis of Thermal Stresses in Mass Concrete Castings," Cement and Concrete Research, Vol. 20, pp. 559-578.

89. Mang, H., Bicanic, N., and Borst, R., (ed.) (1994). Proceedings Int. Conference in Computational Modeling of Concrete Structures, EURO-C, Innsbruck, Austria.

90. Manitoba Hydro, (1993). Evalution of low viscosity epoxies for discharge ring grouting, Report No. 93-G16, Winnipeg Manitoba, Canada.

91. Mazar, J., and Pijaudier-Cabot, G., (1989). "Continuum damage theory-application to concrete," J. Eng. Mech., Vol. 115, No. 2.

92. Mazars, J., (1980). "Mechanical Damage and Fracture of Concrete Structures," 5^{th} Int. Conference on Fracture Mechanics, Cannes, France.

93. Mazars, J., (1986). "A Description of Micro- and Macroscale Damage of Concrete Structure," Engineering Fracture Mechanics, Vol. 25, Nos. 5/6, pp.729-737.

94. Mazars, J., and Pijaudier-cabot, G., (1994). "damage localization analyzed as a crack propagation?, " Proceedings of the US-Europe Workshop on Fracture and Damage in Quasibrittile Structures, Prague, Czech Republic.

95. McDonal, J. E., (1993). " Geomembrane for repair of concrete hydraulic structures," The Bulletin, Vol. 10, No. 4.

96. Mihashi, H., *et.al.*, (1991). "Fracture Energy of Concrete with Different Specimen Size and Strength by Wedge Splitting Test," International Symposium on Fatigue and Fracture in Steel and Concrete Structure, India.

97. Mihashi, H., and Nomura, N., (1994). " Fracture Mechanics Parameters of Cementitous Composite Materials and Fractured Surface Properties," Proceedings of the US-Europe Workshop on Fracture and Damage in Quasibrittile Structures, Prague, Czech Republic.

98. Mindess, S., and Young, J. F.,(1981). Concrete, Prentice-Hall, inc., Englewood Cliffs, NJ, USA.

99. Mindess, S., (1983). "The Cracking and Fracrure of Concrete: an Annotated Bibliography 1928-1981," Fracture Mechanics of Concrete, Ed. by Wittmann, F. H., Elsevier 1983.

100. Muskhelishvili, N., (1963). Some Basic Problems of the Mathematical Theory of Elasticity, Nordhoff, The Netherlands

101. Oh, B., (1991). "Fracture Energy of Concrete and Equivalent Crack Length," International Symposium on Fatigue and Fracture in Steel and Concrete Structure. India.

102. Ohlsson, U., *et.al.*, (1990), "Fracture Energy and Fatigue Strength of Unreinforced Concrete at Normal and Low Temperature," Eng. Fract. Mech. Vol. 35,

No 1/2/3, pp. 195-203.

103. Otsuka, K., (1991). "Detection of Fracture Process Zone in Concrete by Means of X-ray with Contrast Medium," International Symposium on Fatigue and Fracture in Steel and Concrete Structure, India.

104. Ozbolt, J., and Bažant, Z. P., (1991). "Cyclic Microplane Model for Concrete, Fracture processes in Concrete," Rock and ceramics Edited by Van Mier, J. G., Rots, J. G., and Bakker,. A.,RILEM.

105. Plum, D. R., (1990). "The Behavior of Polymer Materials in Concrete Repair, and Factors Influencing Selection," Institution of Structural Engineer, Vol. 55, No. 9.

106. Radoranoric, S., (1998). "Rehabilitation of Hydroelectric Power Stations in Northern Regions," MS.c Thesis, University of Manitoba, Winnipeg, Manitoba, Canada.

107. Rahman, M. U., Rowlands, R. E., Cook, R. D., and Wilkinson, T. L., (1984). "An iterative procedure for finite-element stress analysis of frictional contact problems," Computer and structures, Vol.18, No. 6, pp. 947-954.

108. Rashid, Y. R., (1968). "Ultimate Strength Analysis of Prestressed Concrete Pressure Vessels," Nuclear Engrg. and Design, Vol.7, No. 4, pp. 334-355.

109. Reinhardt, H. W., (1984). "Fracture mechanics of an elastic softening material like concrete," HERON, Delft, Netherlands, Vol. 29, No. 2.

110. Rice, J. R, and Sih.G. C., (1965). "Plane Problems of Cracks in Dissimilar Media," Journal of Applied Mechanics, Tran. of the ASME, Vol. 32.

111. Rice, J. R., (1988). "Elatic Fracture Mechanics Concepts for Interfacial Cracks," Journal of Applied Mechanics, Tran. of the ASME, Vol. 55.

112. Rollin, A. L., *et.al*, (1985). "Selection Criteria for the Use of Geomembranes in Dams and Dykes in Northern Climate," Int. Conference on Geomembranes, Denver, USA.

113. Rossi, P., Brühwiler, E., Chhuy, S., Jenq, Y., S., and Shah, S. P., (1991). " Fracture properties of concrete dams as determined by means of wedge splitting tests and tapered double cantilever beam test Fracture Mechanics Test Methods for Concrete," (Report of RELIM FMT-89), eds. Shah, S. P., and Carpinteri, A., Chapman & Hall, pp. 87-128.

114. Rots, J. G., (1991). "Smeared and discrete representation of localized fracture," Int. J. Frac., Vol. 51, pp. 45-59.

115. Saetta, A., Scotta, R., and Vitaliani, R., (1995). "Stress Analysis of concrete Structures Subjected to Variable Thermal Loads," Journal of structure Eng., Vol. 121, No. 3.

116. Saouma, V., Borz, J. J., and Boggs, H. L., (1991). "In Situ Field Testing for Fracture Properties of Dam Concrete," Journal of Materials in Civil Engineering, Vol. 3, No. 3, pp. 219-234.

117. Saouma, V., Ayari, M. L., and Boggs, H. L., (1987). " Fracture mechanics of concrete gravity dams," (ed.) Shah, S. P., and Swarts, S. E., Fracture of Concrete and rock, Proc. SEM-RILEM Int. Conf., Houston, USA, pp. 311-333.

118. Saouma, V., Borz, J. J., Brühwiler, E., and Boggs, H. L., (1991). "Effect of Aggregate and Specimen Size on Fracture Properties of Dam Concrete, "Journal of Materials in Civil Engineering, Vol. 3, No. 3, pp. 204-218.

119. Saouma, V., Brühwiler, E., and Boggs, H. L., (1991). "A review of fracture mechanics applied to concrete dams," Dam Engng. Vol. 1, pp. 41-57.

120. Saouma, V., and Ingraffea, A. R., and Catalano, D. M., (1982). "Fracure toughness of concrete: K_{IC}," ASCE, J. Engng Mech, Vol. 108, pp. 1152-1156.

121. Schlangen, E., (1993). "Experimental and Numerical Analysis of Fracture Processes in Concrete," HERON, Delft, Netherlands, Vol. 38, No. 2.

122. Schreyer, H. L., (1988). "Smooth limit surface for metals, concrete and geotechnical materials," J. Eng. Mech., Vol. 115, No. 9.

123. Shah, S. P. (Ed.), (1985). "Application of Fracture Mechanics to Cementitious," NATO ASI series, No 94.

124. Shah, S. P., (1988)."Fracture toughness of cement-Based Materials," Material and Structure, Rsearch and testing (RILEM, Paris), Vol. 21, No 122, pp. 145-150.

125. Sharma, S., Aravas, N., (1993). "On The Development of Variable-Separable Asymptotic Elastoplastic Solutions For Interfacial Cracks," Int. J. Solids Structures Vol. 30. No 5.

126. Shih, C. F., Asaro, R. J., (1991). " Elastic-Plastic Analysis of Cracks on Bimaterial Interfaces: Part I - Large-Scale Yielding," Journal of Applied Mechanics, Tran. of the ASME, Vol. 58.

127. Shih, C. F., and Asaro, R. J., (1988). "Elastic-Plastic Analysis of Cracks on Bimaterial Interfaces: Part I-Small Scale Yielding," Journal of Applied Mechanics, Tran. of the ASME, Vol. 55. pp. 2314-2320.

128. Shih, C. F., and Asaro, R. J, (1988). "Elastic-Plastic Analysis of Cracks on Bimaterial Interfaces: Part II," Journal of Applied Mechanics, Tran. of the ASME, Vol. 55 pp.2321-2335.

129. Sih, G. C., and Ditommaso, A (Ed.), (1985). " Fracture Mechanics of Concrete: Structure application and Numerical calculation," Marinus Nijhoff Publishers.

130. Slowik, V., and Wittmann F., (1991). "Influence of Strain Gradient on Fracture Energy," International Symposium on Fatique and Fracture in Steel and Concrete Structure, India.

131. Stankowski, T., Runesson, K., and Sture, S., (1993). "Fracture and Slip of interfaces in cementitious composites I: characteristics," J. of Eng. Mech. Vol. 119 No. 2.

132. Suaris, W. *et.al.*,(1990). "Damage model for cyclic loading of concrete," J. Engi. Mech., Vol. 116, No. 5.

133. Sun.C.T., and Jih, C. J., (1987). "On strain Energy Release Rate for Interfacial Cracks in Bi-Material Media," Eng. Fract. Mechanics Vol. 28, No 1.

134. Sundara Raja, K.,(1991). "Evaluation of a Few Models for the Fracture of Plain Concrete Beams," International Symposium on Fatigue and Fracture in Steel and Concrete Structure, India.

135. Swartz, E., (1991). "Concrete Fracture-Plain and Reinforced Concrete Beams," International Symposium on Fatigue and Fracture in Steel and Concrete Structure, India.

136. Takatsuji, K. *et.al.*, (1990)."Study of Mechanism of Thermal Stress Generation in Massive Concrete Structures," Transaction of the Japan Concrete Institute, Vol. 12.

137. The Concrete Societies of the Netherlands and the UK, (1983) "Cryogenic concrete," Proceeding of the 2nd Int. conference, Amsterdam, Netherlands.

138. Tinawi, R., and Leger, P., (1994). " A biblography on structural analysis, behavior and safety of concrete dams," Dept. of Civil Engrg., Eole Polytechnique, Montereal, Quebec, Canada.

139. Toi, Y., and Che, J. S., (1994). "Computational damage mechanics model for brittle microcracking solids," Eng. Frac. Mech., Vol. 48, No. 4.

140. Ulfkjar, J. P., *et.al.*,(1995). "Analytical model for fictitious crack propagation in concrete beams," J. of Eng. Mech., Vol. 121, No. 1, Oxford University Press.

141. Van Der Veen, C.,(1990). "Theoretical determination of the crack width in reinforced concrete at very low temperatures," HERON, Delft, Netherlands, Vol. 35, No.2

142. Venturelli, J., and Leger, P., (1992). Seasonal temperature and stress distributions in concrete gravity dams, Report No. EPM/GCS-1992-08, Ecole Polytechnique, Montereal, Quebec, Canada.

143. Vipulanandan, D., and Dharmarajan, N., (1989). "Effect of Temperature on the Fracture Properties of Epoxy Polymer Concrete," ACI Material Journal Vol. 86, No 4, pp. 383-393.

144. Vipulanandan, D., and Dharmarajan, N., (1987). "Fracture Parameters of Epoxy Poylmer Concrete," SEM/RILEM Int. conference on fracture of concrete and rock, Houston ,Texas.

145. Voyiadjis, G. Z., and Abu-Lebdeh, T. M., (1993). " Damage model for concrete using bounding surface concept," J. Eng. Mech., Vol. 119, No. 9.

146. Wang. T. C, (1990). " Elastic-Plastic Asymptotic Fields For Cracks on Bimaterial interfaces," Int. J. Fracture, Vol. 37, No 3.

147. Williams, M. L., (1959). "The Stresses Around a Fault or Crack in Dissimilar Media," Bulletin of the Seismological Society of America, Vol., 49.

148. Wilson, E. A., and Parsons, B., (1970). "Finite element analysis of elastic contact problems using differential displacements," Computer and Structure, Vol. 2, pp. 387-395.

149. Wittmann, F.(Editor), (1983). Fracture Mechanics of Concrete, Elsevier, Amsterdam.

150. Yamaguchi, E., and Chen, W., (1990). "Cracking Model for Finite Element Analysis of Concrete Materials," Journal of Eng. Mechanics. Vol. 116, No. 6.

151. Yamaguchi, E., and Chen, W. F., (1990). " Cracking model for finite element analysis of concrete materials," J. Eng. Mech., Vol. 116, No. 6.

152. Yeh, J. R., (1992). "The effect of interface on the transverse properties of composites," Int. J. Solids Structures, Vol. 29. No 20, pp. 2493 - 2502.

153. Zhang, P., (1998). " Thermal Cracking of Concrete Mass in Power Generation Stations," Ph.D. Thesis University of Manitoba, Winnpeg, Manitoba, Canada.

154. Ziegeldorf, S., (1983). " Fracture Mechanics parameters of hardened cement paste, aggregates and interface," Fracture Mechanics of Concrete (Report of RILEM FMC-50), ed. Wittmann, F. H., Elsevier, Amsterdam.

Appendix A

SIMEX User's Manual

By:
M. L. AYARI
Faculty of engineering
the university of Manitoba
Winnipeg, Manitoba, Canada R3T 2N2

1.1 The Data File "simex.inp"

The program SIMEX reads the data input from the file "simex.inp". The data input is entered in an unformatted sequential layout with a maximum of 80 characters per record.

1.1.1 Card Number 1: The problem header

this card is composed of one or more entry lines, where the user can write comments describing the nature of the problem, or any other information. More importantly, this card must contain five key parameters which control the problem submitted for analysis. The control parameters are:

The maximum number of elements (for example 80)
The maximum number of nodes (for example 300)
The maximum number of different materials (for example 3)
The order of gauss integration (for example 2 by 2)
Problem type: 2D axisymmetric, or 2D plane stress, or 2D plane strain

Once the problem Simex reads a control parameter (highlighted in this text), the value attributed to this parameter is read from the first subsequent word containing numeric characters which follows in the text of the problem header. Note that the example data given above can by itself be input as it is for a tow dimensional plane strain analysis of a solid discretized into a number of

elements not exceeding 80, and a total number of nodes less than 3000. The maximum number of different materials is 3 and the order of gauss integration is 2 by 2.

1.1.2 Card Number 2: The Connectivity Matrix $elements

The program SIMEX detects card number 2 by the keyword:

$elements

Once the connectivity environment is detected the code will expect a subsection title of the form:

Q4, or

Q6, or

Q8

for four noded elements, triangular six noded elements, or eight noded isoparametric serendipity elements, respectively. The connectivity matrix is then entered, for each element, as follows:

element_number material_number $node_1$ $node_2$ ..... $node_k$

Where k can be either the number four, six or eight.

Example

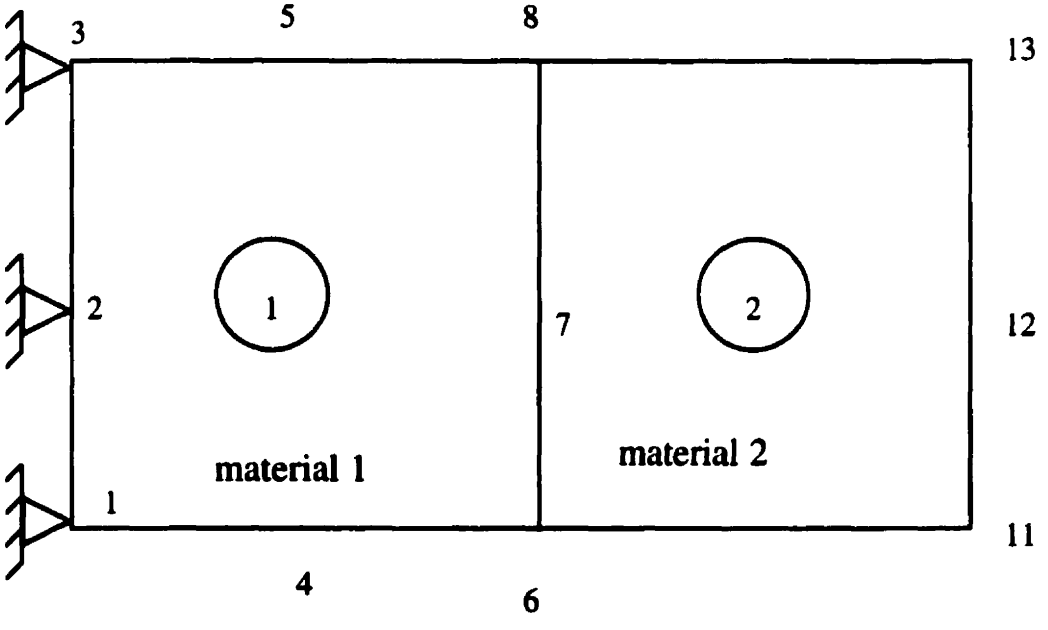

Figure 1.1: The Connectivity Matrix.

Input Data Card Number2

$elements

Q8

1	1		1	4	6	7	8	5	3	2
2	2		6	9	11	12	13	10	8	7

1.1.3 Card Number 3: The Nodal Coordinates $nodes

This card is detected by the keyword:

$nodes

Once the nodal coordinates environment is detected, each line must contain:

node_number x_coordinate y_coordinate

The midside nodes need not to be input, unless a specific position required.

Example

Input Data Card Number 3

$nodes

1	0	0
2	0	5
3	0	10
4	5	0
5	5	10

6	10	0
7	10	5
8	10	10
9	15	0
10	15	10
11	20	0
12	20	5
13	20	10

1.1.4 Card Number 4: The automatic Mesh Generation $generate

This card is optional, and detected by the keyword

$generate

it performs an automatic generation of elements by partitioning the elements (considered now as superelements) entered in card number2. Each superelement must have three entry lines of the form:

elem_i j k l

where *elem_i* is the superelement number *i* to be subdivided into *Qj* type of elements with *k* subdivisions in the e direction and l subdivision in the n direction,

p_1 ..... p_k

the weights of the subdivisions *1*.....*k* in the e direction, and

v_1.....v_l

the weights of the subdivisions *1*.....*l* in the n direction

Example

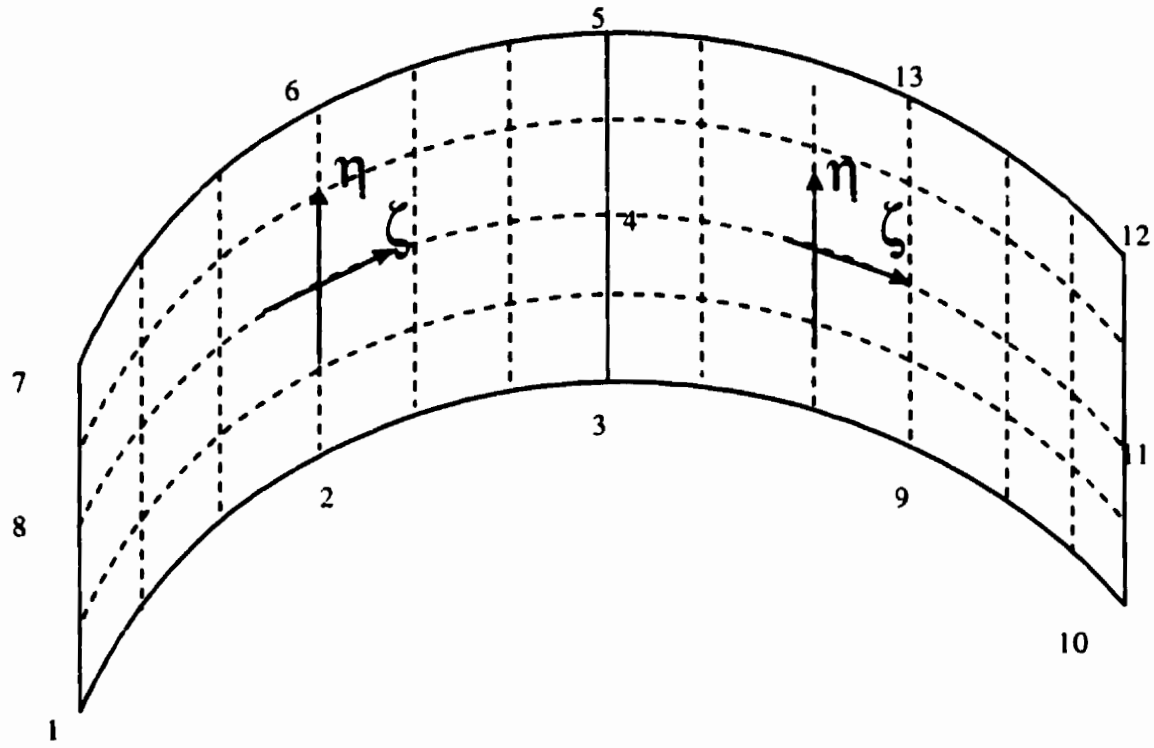

Figure 1.2: Automatic Mesh Generation.

Input Data Card Number 4

$generate

1 8 5 6

1 1 1 1 1

1 1 1 1 1 1

2 8 5 6

1 1 1 1 1

1 1 1 1 1 1

1.1.5 Card Number 5: The boundary Conditions $boundary

This Card is detected by the keyword:

$boundary

Each node is considered to be free, unless restrained in this section. Each restrained node must have an entry of the form:

node_i i_x i_y dis_x dis_y

where node_i is the node number *i*, i_x and i_y point to the fixity conditions in the x and y directions respectively (1 is fixed and 0 is free).

dis_x and dis_y are prescribed displacements in the *x* and *y* directions respectively.

Example

Input Data Card Number 5

$boundary

1	1	1	0	0
2	1	1	0	0
3	1	1	0	0

1.1.6 Card Number 6: The material Properties $material

This card is detected by the keyword:

$material

Once the material environment is detected, **SIMEX** expects to read a material model, and a failure surface. In this case the material type is:

*elastic with surface

Surface can be either **Von-Mises**, or **Mohr-Coulomb**, or **Druker-Parager**, or **Tresca**, or **Self**. **Self** is a user supplied failure surface. A documentation of the available failure surfaces can be found in the Theory Document. The next entry must be the material number identifier mati followed by the properties

$prop_1$ $prop_2$.....$prop_{10}$

where:

- *mat i* is the material number
- $prop_1$ is Young's modulus,
- $prop_2$ is Poisson's ratio,
- $prop_3$ is the material thickness in the case of plane stress and unity for plane strain. This entry must be zero otherwise.
- $prop_4$ is the mass density of the material
- $prop_5$ is the coefficient of thermal expansion
- $prop_6$ is the uniaxial tensile strength
- $prop_8$ is the cohesion of the material

- $prop_9$ is the angle of friction of the material (in deg.),
- $prop_{10}$ is the fracture toughness of the material.

The above information is entered as many time as required by the number of different material properties, and material models in the previously described sequence.

Example
Input Data Card number 6
$material
*elastic with von Mises
1
10000. .3 1. 1. 10. 2 0. 0.01 1.0 1.0
*end

1.1.7 Card Number 7: The loading $loading

This loading data card is detected by the keyword

$loading
followed by the number of load steps over which the total load is to be applied:
n_loadcases
The subsequent instruction must be either:
***nodal load**, or
***edge load**, or
***gravity**, or
***initial displacement**

The user can input one or more of the above instructions. The end of the loading section is detected by the instruction:

***end**

The *nodal load

Each loaded node must have an entry of the form:

i_node x_component y_component

where i_node is the loaded node number, x_component and y_component are the x and y components of the applied nodal force respectively.

The *edge load Environment

Each element subjected to an applied traction must have two entry lines of the form:

$elem_i$ $node_1$ $node_2$ ..... $node_k$

$sign_1$ tau_1 $sign_2$ tau_{12}..... $sign_k$ tau_k

where $elem_i$ is the element number$_i$ and, $node_1$ $node_2$ ... $node_k$ are nodes forming the side of the element $elem_i$ to be loaded. This set of nodes are entered in an anti-clockwise sequence. $sign_1$ ... $sign_k$ *and* tau_1 ... tau_k are the magnitudes of normal (positive if inward) and tangential distributed loading at the corresponding nodes $node_1$ ...$node_k$ of the element side, as shown in figure 1.4.

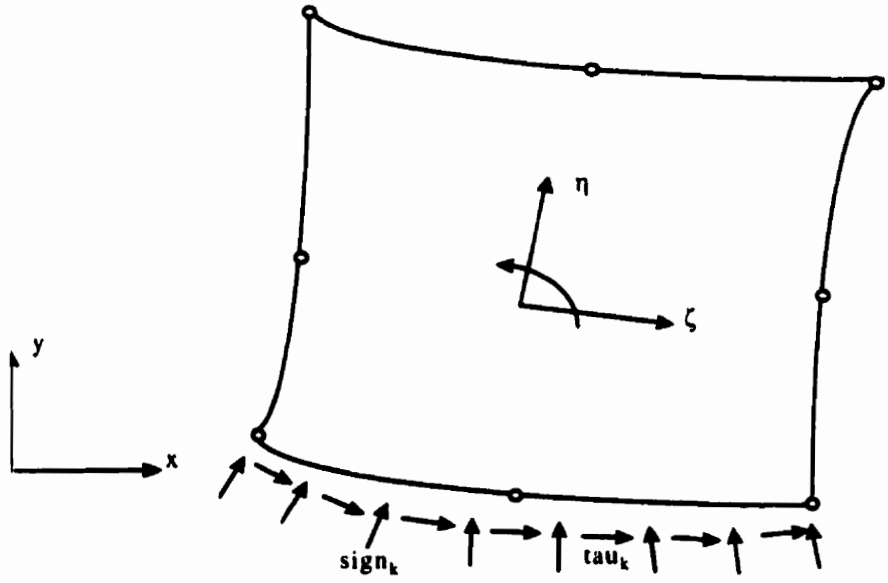

Figure 1.4: Normal and tangential distributed loading

The *gravity Environment

tow parameters are required for specifying a gravity load:

angle Ng

where angle is the angle measured counterclockwise from the positive y direction, as shown in figure 1.5 and *Ng* is a multiple of the gravity acceleration g. For example to simulate twice earth's gravity field, use *Ng = 2*.

The *initial displacement Environment

No entry is required in this section, the specified displacements are entered already in the **$boundary** section.

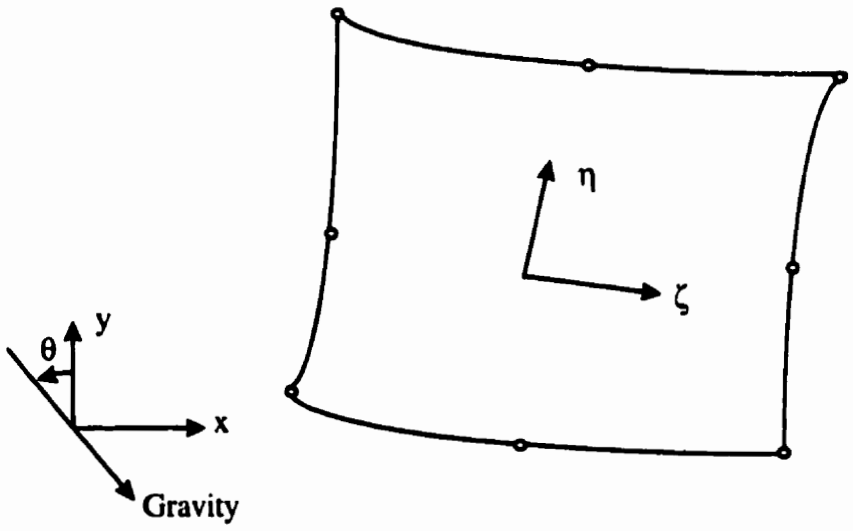

Figure 1.5: Gravity axis for 2 dimensions.

The *end Control

This entry is designed to end the loading card section.

Example

Input Data Card Number 7

$loading

1

*edgeload

1 1 4 6

10 0 10 0 10 0

*end

1.1.8 Card Number 10: The end of input $end

This card detected by the keyword

$end

and is required to end the input in "simex.inp".

1.2 Example of a "simplex.inp" Input File

1.3 The Hardware Data File "device.inp"

The hardware configuration file, named "device.inp" contains six lines of information. The first tow lines pertain to the graphics hardware environment in use, the third line contains information about the locator device, the fourth line contains the type of font to use, and finally, the last two lines are required for the printing hardware and attributes. This file is made accessible to the user to configure, or, update as required.

1.3.1 Card no.1: Graphics Device Driver

A wide range of graphics cards is supported under the **HALO PROFESSIONAL** graphics environment. The graphics driver has a standard DOS file name of the form:

ahdxxxx.dsp

where xxxx is usually a four letter word unique to the device drive in question. Following is listing of the available drivers:

ahdatil.dsp	ahdatip.dsp	ahdherc.dsp	ahdhlvl.dsp
ahdibm.dsp	ahdibme.dsp	ahdibmg.dsp	ahdibmi.dsp
ahdbmp.dsp	ahdibmv.dsp	ahdpar1.dsp	ahdparp.dsp
ahdtec1.dsp	ahdtecp.dsp	ahdtl4l.dsp	ahdtril.dsp
ahdtrip.dsp	ahdv7v1.dsp	ahdv7vp.dsp	ahdvlin.dsp
ahdvpln.dsp	ahdvri.dsp		

A complete description of these drivers is available in the HALO PROFESSIONAL Device Reference Manual.

1.3.2 Card Number 2: Mode of Operation

The mode of operation of the device drivers described by an integer flag which value depends on the resolution in use by the graphics card. Again the value of mode can be found in same Appendix.

1.3.3 Card Number 3: Locator Device Driver

The user has the choice of using the locator's manufacturer driver by simply loading the mouse prior to running the program, or use a Halo supplied driver. Following is a list of the available locator drivers:

ahdbpoi.loc ahgtci.loc ahdmou.loc ahdmsmi.loc
ahdsdti.loc

1.3.4 Card Number 4: Port

An integer entry which identifies the serial communications port for the locator.

1.3.5 Card Number 5: Font File Name Fontfile

The display of stoke text on the screen of the monitor can be specified by the user. The stoke file "ahd106.fnt" member of the high density stoke family has given adequate display on most EGA and VGA cards, and is suggested to be used as a first trial. This file has to be resident in the current directory where the program is being executed. Following is the list of the halo supplied fonts:

ahd001.fnt	ahd002.fnt	ahd010.fnt	ahd011.fnt
ahd012.fnt	ahd013.fnt	ahd102.fnt	ahd103.fnt
ahd104.fnt	ahd105.fnt	ahd106.fnt	ahd107.fnt
ahd108.fnt	ahd109.fnt	ahd111.fnt	ahd115.fnt
ahd201.fnt	ahd202.fnt	ahd203.fnt	ahd204.fnt
ahd205.fnt	ahd206.fnt	ahd207.fnt	ahd208.fnt
ahd250.fnt	ahd310.fnt	ahd311.fnt	ahd312.fnt
ahd320.fnt	ahd321.fnt	ahd322.fnt	ahd330.fnt

ahd331.fnt ahd332.fnt ahd405.fnt ahd406.fnt

1.3.6 Card number 6: Printer Driver printerdriver

The user has to specify a printer driver, printerdriver, which will be loaded into memory before any printing can occur. A list of printer drivers can be found in the Appendix. A wide range of printers are supported by HALO Professional. The printer driver has a standard DOS file name of the form:

ahdxxxx.prt

where xxxx is usually a four letter word unique to each specific printer. Following is a listing of the available printer drivers:

ahdbw24.prt	ahdbw8.prt	ahdcna2.prt	ahdco24.prt
ahdco8.prt	ahdcpst.prt	ahddjet.prt	ahdepgq.prt
ahdljtp.prt	ahdokip.prt	ahdpa44.prt	ahdpjet.prt
ahdpjx1.prt	ahdpsct.prt	ahdsh73.prt	ahdshrp.prt
ahdtk93.prt	ahdtk97.prt	ahdxjet.prt	

1.3.7 Card Number7: Printer Attributes

The printer attributes are set through 22 integer numbers:
prn(1) prn(2).....prn(22)

Following is a description of the printer attribute table

1- Width of output in dots
-1 = Normal

>0 = Specify the printer width

2- Height of output in dots

-1 = Normal

>0 = Specify the printer width

3- Image orientation

0 = Normal (default)

1 = Landscape (sideways)

4- Black/white reversal

0 = Perform Black/white reversal

1 = Do not perform Black/white reversal

5- Dither flag

0 = Perform dithering (default)

1 = Do not perform dithering

6- Form feed flag

0 = Perform form feed after image (default)

1 = Do not perform form feed

7- Printer output

0 = Printing through BIOS (efault)

1 = Printing through DOS

8- Dots per inch

Printer specific

9- Number of copies

Printer specific

10- Centering

0 = Perform centering (default)

1 = Do not perform centering

11- X offset in dots

0 = No offset (default)

n = Specify n dots in x-offset

12- Y offset in dots

0 = No offset (default)

n = Specify n dots in y-offset

13- Printer ID

Printer specific

14- COM port

0 = COM1 (default)

1 = COM2

15- Process ID for EMS

Printer specific

16- Bold printing

0 = Normal printing

1 = Double printing

17- Parallel port

0 = LPT1 (default)

1 = LPT2

2 = LPT3

18- Image size

0 = Original size (default)

Other to replicate or interpolate

image to maximum size

19- Color conversion

Others gamma correction

20- Halftone Angle

21- Hue Adjustment

22- Saturation Adjustment

1.4 Example of a "device.inp" File Input

Following is an example of how to enter the necessary data in the "device.inp" file

```
ahdatip.dsp
0
ahdmou.loc
0
ahd106.fnt
ahdljtp.prn
2400  1658  1  0  0  1  0  3  0  0  0  0  0  -1  -1  -1  0  0  0  0  0  0
```

In this example we have used

1. The device driver for commercially available ATI VGA WONDER card, named "ahdatip.dsp".
2. A resolution of 800x600 corresponding to mode =0.
3. A Microsoft compatible mouse driver "ahdmou.loc"
4. The locator communications port in this case has a zero value
5. The display stroke file name is "ahd106.fnt"
6. The printer to be used in this case is a Hewlett Packard LaserJet series II.

1.5 The device initializer "initdev" Subroutine

The data described in the previous section is read from the routine initializedevice. This subroutine is written to accommodate a variable hardware configuration by performing the following tasks:

1. read the graphics and drive
2.
3.
4.

5.

6.

```
c  this subroutine initializes the graphics environment
c  of the PC by loading device dependent parameters
c  from the user supplied file 'device.inp'
c
c-------------------------------------------------------------------


c
c**   device dependent routines
c -----------------------------------
c** Graphic Card
      read(7,*,err=99) device
      call setdev(device)
      call inqerr(233,ierr)
      if (ierr.ne.0) then
        write (output,*) 'error in setdev =', ierr
        stop
      end if
c** Initialize graphics mode
      read(7,*,err=89) mode
```

```
      call intergraphics(mode)
      call inqerr(113,ierr)
      if (ierr.ne.0) then
       write (output,*) 'error in initmode =', ierr
       stop
      end if
c** Initialize locator
      read(7,*,err=79) locator
      read(7,*,err=69) port
      call setlocator(locator,port)
      call inqerr(231,ierr)
      if (ierr.ne.0) then
       write (output,*) 'error detected in setting the locator: ', ierr
      end if
c** Stroke text
      read(7,*,err=59) font
      call setfont(font)
      call inqerr(147,ierr)
      if (ierr.ne.0) then
       write (output,*) 'error in setstroke= ', ierr
      end if
c** Printer driver
      read(7,*,err=49) printer
      call setprn(printer)
      call inqerr(304,ierr)
      if (ierr.ne.0) then
       write (output,*) 'error in setprn= ', ierr
      end if
c** Printing characteristics
      read(7,*,err=39) (prn(ii),ii=1,22)
```

```
      call setpattr(prn)
      call inqerr(305,ierr)
      if (ierr.ne.0) then
        write (output,*) 'error in setting printer attributes: ', ierr
      end if
      return
c
39    write(output,*) 'error in reading the printer parameters'
      stop
49    write(output,*) 'error in reading the printer driver'
      stop
59    write(output,*) 'error in reading the font file'
      stop
69    write(output,*) 'error in reading the port for the locator'
      stop
79    write(output,*) 'error in reading the locator driver'
      stop
89    write(output,*) 'error in reading the graphics mode'
      stop
99    write(output,*) 'error in reading the graphics device driver'
      stop
c
      end
```

1.5.1 Error Diagnostic

In the case where an error has taken place, for example, in setting device driver, or in entering a parameter in the "initializedevice" file, an error message is written in the output file "simex.out"

with an associated error function code. Following is a description of the possible errors and their error function codes:

1- Clipping, Coordinate out of range.

2- Parameter other than x, y coordinate out of range.

3- Function not initialized.

4- Display list capture buffer overflow.

5- Attempted change from world to device coordinate during display list capture.

9- Function not implemented on graphics device.

11- File not found.

12- Error closing file.

13- Error writing file.

14- Invalid filename

15- Premature end of file during read.

16- Not a HALO file wrong type.

Printer Error Codes

20- Device timeout.

21- I/O Error.

22- Paper out.

23- User abort.

30- Illegal width specified.

31- Illegal height specified.

32- Illegal DPI specified.

33- Illegal number of copies specified.

34- Illegal serial port specified.

35- Illegal parallel port specified.

36- Viewport exceeds maximum size.

Scanner Error Codes

40- Scanner not connected.

41- Timeout error.

42- I/O error.

43- Scanner overheat.

44- Nothing to scan

45- Scan beyond end of page.

46- User abort.

47- SCNBLCKN without STARTSCAN.

50- Bad mode.

51- Bad right/left margin.

52- Bad top/bottom margin.

53- Function not supported.

54- Bad DPI mode.